The Pennsylvania State University
APPLIED RESEARCH LABORATORY
P.O. Box 30
State College, PA 16804

ACOUSTIC DIAGNOSTICS OF AN AUTOMOTIVE HVAC SYSTEM

by

T. A. Brungart
G. C. Lauchle
J. Tichy

Technical Report No. TR 91-001
January 1991

Supported by:
Ford Motor Company

L.R. Hettche, Director
Applied Research Laboratory

ABSTRACT

The heating, ventilation, and air conditioning (HVAC) system of an automobile can be a source of acoustic annoyance, particularly when it is operated under maximum airflow conditions. In order to suggest possible design changes for the purpose of noise control, a systematic characterization of the acoustic sources and mechanisms must be conducted initially. This report addresses such a characterization for a typical automotive system. The approach is based on acoustic intensity measurements of the stand-alone HVAC system operating under maximum airflow conditions in the ARL Penn State flow-through anechoic chamber. The experimental data indicate that the centrifugal blower is the dominant low-frequency source of noise, while separation zones and the flow over sharp edges within the HVAC system ducting are secondary sources of noise that become increasingly dominant as the frequency exceeds 3 kHz. Qualification of these identified sources of sound is aided by detailed flow visualizations of the subject system. Recommendations for acoustic improvements to the system are provided.

TABLE OF CONTENTS

LIST OF FIGURES

LIST OF FIGURES (CONTINUED)

LIST OF FIGURES (CONTINUED)

LIST OF FIGURES (CONTINUED)

LIST OF TABLES

LIST OF SYMBOLS

AC	air conditioning
B	filter bandwidth
BPF	blade passage frequency
c	sonic velocity
FFT	fast Fourier transform
G_{11}, G_{22}	auto-spectral density for microphones 1 and 2 respectively
G_{21}	cross-spectral density between microphones 2 and 1
HVAC	heating, ventilation and air conditioning
I	active intensity vector component in the direction of the two microphone axis
INCE	Institute of Noise Control Engineering
I_c	complex acoustic intensity in the frequency domain as measured by a two microphone probe
I_T	true active intensity vector component in the direction of the two microphone axis
$\vec{I}$	active intensity vector
$\hat{I}$	estimated active intensity vector component in the direction of the two microphone axis
$\vec{I}_c$	complex intensity vector
$\hat{I}_i$	instantaneous intensity vector
$\vec{I}_j$	active intensity vector normal to the surface enclosing the sound source
k	acoustic wavenumber (ω/c)
p	acoustic pressure
P	acoustic pressure amplitude
Q	reactive intensity vector component in the direction of the two microphone axis
$\vec{Q}$	reactive intensity vector

LIST OF SYMBOLS (CONTINUED)

r	spatial coordinate
rpm	rotations per minute
T	data acquisition time
t	time
U	particle velocity amplitude
u	particle velocity vector component in the direction of the two microphone axis
$\vec{u}$	particle velocity vector
V_t	impeller tip speed
W	sound power
ΔP	pressure rise across the blower in the INCE box
Δr	microphone center to center separation distance
ΔS_j	incremental surface area enclosing sound source
δ	phase mismatch
ϵ	normalized bias error
λ	acoustic wavelength
ρ	fluid density
ϕ	phase angle
ψ	pressure coefficient
ω	circular frequency

ACKNOWLEDGEMENTS

This work has been supported by the Ford Motor Company under contract 747-8-G75483. The authors are grateful to Mr. Ronald E. Kretschmer, program monitor at Ford, for his interest and support of this work. Also acknowledged is the expert advice provided by Mr. Mark W. McBride of ARL Penn State and the efforts of Mr. Michael L. Sullivan in performing the acoustic intensity mapping.

CHAPTER 1

INTRODUCTION

The acoustic noise within the passenger compartment of an automobile can be attributed to several independent sources. Of particular concern is the noise generated by the heating, ventilation, and air conditioning (HVAC) system. In order to suggest and implement acoustic noise control measures, an acoustic evaluation of the system is required. Such an evaluation should identify the individual components responsible for noise production, and equally important, it should identify the predominant physical mechanisms within these components that produce acoustic energy. Once these mechanisms are understood, it is much easier to proceed with control concepts.

The HVAC system under consideration is typical of those used in automotive applications. The acoustic annoyance of this and all other similar systems tends to increase as the airflow is increased. Thus, it is known at the start that the predominant mechanism for noise generation is unsteady flow. A major objective of the current investigation is to identify the specific regions within the system where the flow has high unsteadiness and then to determine which of these regions produce radiated sound, and how much radiated sound. The part of the study directed toward flow measurements has been completed and documented by Denger et al. (1990). The part that is concerned with acoustic emissions and the correlation of these emissions with unsteady flow is reported here.

This study is experimental, as was the fluid mechanics investigation of Denger et al. (1990). The methodology selected is the

two-sensor acoustic intensity method which permits direct measurements of acoustic power flow from a source. By performing such measurements in the nearfield of a complex system, individual sources of noise can be identified. This approach was implemented in such a way that near-field intensity vectors were obtained in selected cross-sectional planes of the stand alone (removed from the automobile) HVAC system. The interpretation of these intensity "maps" is straightforward and key sources of noise are identified, and in some cases correlated directly to the unsteady flow fields measured previously in the same system.

Because the centrifugal blower used in the HVAC system was identified as the key source of noise, additional studies are discussed for the blower operating by itself in a specially designed acoustically transparent plenum box. This study provides information on the total power created by the blower and the dependence of this power on operational parameters such as head rise and wheel speed. Under low head conditions, the blower radiates sound at the blade passage frequency. A resonator concept was implemented to cancel this noise and is discussed in Appendix 1.

In another part of the study, the blower was removed from the HVAC system (as to eliminate this source of noise), and then air from a remote, quiet airflow source was pumped through the system. This enabled secondary sources of noise to be identified that are normally masked by the blower noise. Because passenger compartment register vents were identified as important contributors in this part of the investigation, a limited set of experimental data were acquired for register noise and is documented in Appendix 2.

The report concludes with recommendations for noise control. Prototype implementation of these recommendations is the subject of future investigation.

CHAPTER 2

ACOUSTIC INTENSITY TECHNIQUE

2.1 Background

The acoustic part of the research on identification of the sound generation, radiation and propagation was based on the recently developed intensity technique. This modern measurement and analytical tool turned out to be indispensable to measure the sound power generated by the blower, to determine the sound radiation from the ducts, and to reveal many details of the acoustical properties of the system. Therefore, conclusions could be made on the overall acoustical characteristics. The purpose of this section is to provide detailed information on the principles and relevant applications of this new and powerful tool.

Until recently the only acoustical quantity that could be measured with high precision was the sound pressure. Although, in principle, a complete knowledge of the sound pressure is sufficient to calculate other acoustical quantities of interest, the extent of scanning the sound field to secure a sufficient amount of data makes this approach impractical. Therefore the required acoustical quantities need to be measured directly.

The development of the Fast Fourier Transform analyzer, the introduction and perfection of digital electronic technology, and the improvement of electro-acoustic transducers has permitted the construction of a reliable acoustic intensity meter for both laboratory and field use. This permits a direct measurement of acoustic energy.

The ability to measure acoustic power flow substantially expands our capability to study details of sound radiation from complex structures, to obtain sound power radiated by acoustic sources into the farfield from the nearfield measurements, to study the qualitative and quantitative details of sound propagation in space with complex boundaries, to evaluate acoustic diffraction and dispersion, and to simplify or perfect the measurements of acoustical properties of materials and structures.

Signal processing, which was developed in conjunction with intensity measurements, can be easily extended to obtain sound pressure, particle velocity, potential and kinetic energy density and acoustic impedance. Using computational techniques, sound field maps of acoustic intensity vectors and wavefronts, which represent sound power propagation, can be constructed. Other sound field maps allow us to visualize the standing wave formation by means of the pressure magnitude gradient.

2.2 Sound Field Quantities

In most situations, we deal with sound fields that are steady over a sufficiently long period of time. Therefore, many useful mathematical formulations for intensity and other acoustical quantities can be based on the assumption of steady state and represented in the frequency domain.

Calculation of power progression in acoustic fields requires determination of two acoustical quantities. Acoustic intensity can be obtained from the sound pressure and particle velocity amplitudes and the phase between these quantities. While sound pressure can be

measured directly by small and precise microphones, there are no suitable transducers to directly measure particle velocity.

Because particle velocity is proportional to pressure gradient, the intensity probe approximates the gradient by the sound pressure difference obtained from two closely spaced microphones. In addition, we can also measure the acoustic pressure.

Assuming that both p and $\vec{u}$ can be obtained from field measurements, the relationships among the sound field quantities needed for extended applications of the intensity technique will be summarized.

2.3 Complex Acoustic Intensity

The power of the intensity technique is in its ability to provide comprehensive information on all acoustic quantities of interest thus permitting a complete analysis of sound radiation and propagation. Usually the sound field is described in terms of acoustic pressure which can, without loss of generality, be expressed at a point (r) by its amplitude P(r) and phase $\phi(r)$

$$p(r,t) = P(r)e^{-j\phi(r)}e^{j\omega t} \tag{1}$$

where both P(r) and $\phi(r)$ are real quantities.

The particle velocity, which can be obtained from Euler's equation,

$$\vec{u}(r,t) = \frac{-1}{j\omega\rho}\nabla p(r,t) = \frac{1}{\omega\rho}[P(r)\nabla\phi(r) + j\nabla P(r)]e^{-j\phi(r)}e^{j\omega t} \tag{2}$$

is thus expressed in terms of the pressure amplitude and phase gradient.

The instantaneous acoustic intensity, which describes the energy propagation through a point as a function of time, can be calculated from Equations (1) and (2)

$$\vec{I}_1(r,t) = Re\{p(r,t)\}.Re\{\vec{u}(r,t)\} = \frac{1}{2\omega\rho}P^2(r)\nabla\phi(r) \tag{3}$$

$$+ \frac{1}{2\omega\rho}P^2(r)\nabla\phi(r)\cos 2(\omega t - \phi(r)) - \frac{1}{2\omega\rho}P(r)\nabla P(r)\sin 2(\omega t - \phi(r)).$$

A quantity of greater practical interest is acoustic intensity, which describes the time-averaged power flux through a point, and can be obtained by time averaging the instantaneous intensity

$$\vec{I}(r) = \frac{1}{T}\int_0^T \vec{I}_1(t)\,dt = \frac{1}{2}\,Re[p(r).\vec{u}^*(r)] = \frac{1}{2\omega\rho}\,P^2(r)\nabla\phi(r). \tag{4}$$

As can be seen from Equation (4), the time-independent intensity vector $\vec{I}$ has a direction of the phase gradient $\nabla\phi(r)$. It is high in areas where $P^2(r)$ is large (high potential energy density) or where the wavefronts are compressed so that $\nabla\phi(r)$ is large.

It should be emphasized that the intensity vector $\vec{I}(r)$, which depends on r, only describes the power associated with a sound wave at a field point. The intensity vector is time independent and does not propagate with the sound field.

The concept of acoustic intensity can be extended by using the complex intensity defined as

$$\vec{I}_c(r) = \vec{I}(r) + j\vec{Q}(r) = \frac{p(r).\vec{u}^*(r)}{2} = \frac{1}{2\omega\rho}[P^2(r)\nabla\phi(r) - jP(r)\nabla P(r)]. \tag{5}$$

The first term in Equation (5) is intensity $\vec{I}$ as defined by Equation (4), which can be alternatively calculated from $1/2\ Re[p(r).\vec{u}^*(r)]$.

The imaginary part of the complex intensity $\vec{I}_c(r)$ is called reactive intensity $\vec{Q}(r)$ and can be further expressed as

$$\vec{Q}(r) = \frac{1}{2} Im[p(r).\vec{u}^{*}(r)] = -\frac{1}{2\omega\rho} P(r)\nabla P(r) = -\frac{1}{4\omega\rho}\nabla P^{2}(r) \qquad (6)$$

Similarly to $\vec{I}(r)$, $\vec{Q}(r)$ is time-independent and depends on coordinates only.

An example of the sound field representation in the vicinity of sound radiators is shown in Figure 1. The sources generate a sound pressure field, characterized by surfaces of constant pressure amplitude P(r) and constant phase ϕ(r). The constant phase surfaces are the wavefronts and, as shown in Equation (4), the $\vec{I}$ magnitude is proportional to the phase gradient, and vector $\vec{I}$ is, therefore, perpendicular to the wavefronts (Figure 1). Knowledge of the wavefronts is very useful in determining the source behavior. The wavefronts, which are not measured directly, can be obtained by reconstructing the phase from the $\vec{I}$ map.

As Equation (6) reveals, the reactive intensity vector is proportional to the pressure square gradient and, therefore, once a $\vec{Q}$ field map is plotted, areas of constant P(r) can be constructed.

At a given point, both intensity vectors $\vec{I}$ *and* $\vec{Q}$ have a different direction and, therefore, the surfaces of constant P(r) and ϕ(r) mutually intersect, as shown in Figure 1. These vectors have the same direction only in the case of one-dimensional fields of plane waves or spherical waves. In spherical waves, areas of constant P(r) and ϕ(r) are concentric spheres.

The vector $\vec{Q}$ as defined in Equation (6), is proportional to the gradient of squared pressure amplitude. Because the gradient is equal to zero at the pressure maxima or minima, the reactive intensity vector

aims toward the minima and is pointed away from the maxima. These pressure extremes are sources and sinks of $\vec{Q}$.

Both vectors $\vec{I}$ *and* $\vec{Q}$ are particularly useful for investigation of sound sources and sound radiation in general. As mentioned above, the intensity vector $\vec{I}$ describes the sound power at a point which of course includes the surface of vibrating objects. Most surface vibrations consist of modes representing the standing transverse waves. A classical example are plates and shells which constitute the constructional elements of many machine parts. The duct walls of the HVAC system vibrate like plates.

Vector $\vec{I}$ is an invaluable tool to reveal the relationship between the vibration and sound power radiation. The sound power radiation from plates depends on the ratio of the wavelengths of the bending wave on the radiator to the wave in the air. The maps of vector $\vec{I}$ reveal that if the wavelengths of the mechanical waves on the radiator are shorter than in the air, areas of sound power radiation alternate with areas of sound power absorption. The total radiated power is given by the algebraic sum of both powers.

The reactive intensity vector $\vec{Q}$, which is proportional to the pressure square gradient, reveals on the surface of radiators the areas of vibration which set the surrounding air into motion. The larger the vibration amplitude, the higher is the sound pressure at the radiator surface. However, the radiated sound power depends also on the phase shift between the pressure and particle velocity and, therefore, areas of high pressure are not generally associated with large sound power radiation.

While hard wall vibrators are marked by high values of vector $\vec{Q}$, openings such as duct terminations or leaks which radiate acoustic power have high $\vec{I}$ and low $\vec{Q}$. This means that although acoustic pressure is low, sound power is radiated due to the large in-phase particle velocity component with sound pressure. This brief description of radiator properties shows the importance of both vectors $\vec{I}$ and $\vec{Q}$.

2.4 Measurement Technique

As mentioned earlier, the measurement of intensity is based on direct or indirect determination of p and $\vec{u}$.

A measurement probe consists of two pressure microphones which are closely spaced to obtain the sound pressure from the average, and the particle velocity from the difference of the two measured sound pressures. In the frequency domain, the complex intensity can be expressed in terms of the auto-spectra and cross-spectra between the two microphones

$$I_c(\omega) = I(\omega) + jQ(\omega) = \frac{1}{2j\omega\rho\Delta r}[G_{22}(\omega) - G_{11}(\omega) - j2Im(G_{21}(\omega))] \quad (7)$$

where $G_{11}(\omega)$ and $G_{22}(\omega)$ are the pressure auto-spectral densities at the microphone locations, $G_{21}(\omega)$ is the complex cross-spectral density, and Δr is the distance between the microphones. Both intensity estimates can be obtained from

$$I(\omega) = Re[I_c(\omega)] = \frac{-1}{\omega\rho\Delta r} Im[G_{21}(\omega)] \quad (8)$$

and

$$Q(\omega) = Im[I_c(\omega)] = \frac{-1}{2\omega\rho\Delta r}[G_{22}(\omega) - G_{11}(\omega)]. \quad (9)$$

The sound pressure amplitude is obtained as the average of the two pressures

$$p(r,t) = P(r)e^{-j\phi(r)}e^{j\omega t} = \frac{1}{2}[P_1(r)e^{-j\phi_1(r)} + P_2(r)e^{-j\phi_2(r)}]e^{j\omega t} \quad (10)$$

as

$$P^2(\omega) = \frac{1}{4}[G_{11}(\omega) + G_{22}(\omega) + 2Re(G_{21}(\omega))] \quad (11)$$

The particle velocity is obtained from the pressure gradient approximated by the pressure difference

$$\vec{u}(r,t)) = \frac{-1}{j\omega\rho}|\nabla p(r,t)| = \frac{-1}{j\omega\rho\Delta r}[P_2e^{-j\phi_2(r)} - P_1e^{-j\phi_1(r)}]e^{j\omega t} \quad (12)$$

and the velocity amplitude is written as shown in Equation (13)

$$U^2(\omega) = \frac{1}{4\omega^2\rho^2(\Delta r)^2}[G_{11}(\omega) + G_{22}(\omega) - 2Re(G_{21}(\omega))]. \quad (13)$$

2.5 Measurement Precision

The precision of intensity measurements depends on many more factors than relatively simple sound pressure measurements. Besides the quality and precision of the transducers and associated electronics, errors can be caused by unsuitable transducer configuration which includes their distance, size and associated diffraction effects. In addition, the measurement precision depends on the field properties which are, of course, not known prior to their measurement. However, both the theoretical analysis of the errors and an intensive effort of the manufactures to develop new transducers and electronics resulted in

the construction of an intensity meter which satisfies the demands of noise control engineers.

The principal systematic errors, when using intensity probes, are caused by the finite physical distance and response mismatch of the two microphones and associated electronics. An intensity probe consists of two transducers with Δr separation of their centers. The sound pressure is determined from the pressure average, and the particle velocity from the pressure difference which approximates the pressure gradient. In a plane wave, the estimated intensity f depends on the true intensity I_T and Δr, and is given by

$$f = I_T \frac{\sin(k\Delta r)}{k\Delta r}, \tag{14}$$

where k is the acoustic wavenumber. The error affects the upper frequency limit of the probe and, therefore, a sufficiently small Δr has to be chosen. In nonuniform fields, such as those created by monopoles, multipoles, and other complex sources, the error is larger, particularly for measurements taken close to the sources.

Both the amplitude, and particularly the phase difference of the response of the two probe channels measured by exposing them to an identical sound field, cause another bias error. The response magnitude can usually be adjusted, while the phase mismatch depends on the actual hardware used. The normalized bias error for equalized magnitude response and phase mismatch δ between the microphone channels is

$$e = \frac{\hat{I} - I_T}{I_T} \approx \frac{\delta}{\phi_{12}} \approx \delta \frac{P^2}{I_T} \qquad (15)$$

where ϕ_{12} is the phase difference in the measured wave which depends on the measured sound field. For plane propagating waves $\phi_{12} = k\Delta r$, while in perfect standing waves $\phi_{12} = 0$. For the same δ, the error can be decreased by choosing sufficiently large Δr which, however, limits the upper frequency limit as given by Equation (14). The error depends on the mixture of propagating and standing waves which, as shown in Equation (15), can be expressed in terms of P^2/I_T. This ratio varies from point to point in the field. The error affects the low frequency limit of the probe due to the small value of $\phi_{12} = 2\pi\Delta r/\lambda$, where λ is the acoustic wavelength.

Although microphone pairs with $\delta = 0.05°$ are available today, it is safe to use $\delta = 0.3°$ as an overall value, for the practical choices of Δr to keep the high frequency bias error low.

Depending on the type of source signal and the goals of the intensity measurements, an FFT broadband analyzer can be used for the data processing. Alternatively, great flexibility may be achieved by acquiring and processing the data by a computer. In any case, the random error, which depends on the BT product of the filter bandwidth B and the data acquisition time T, has to be minimized by selecting sufficiently large BT. In addition, when synthesizing 1/3 or 1/1 octave data from line spectra obtained from an FFT analyzer, the frequency range of the analyzers has to be selected for a minimum of 10 lines in the bandwidth. When taking broadband measurements, a true band analyzer could be a better choice than an FFT analyzer.

The above formulations for I, Q and u are valid for a component of a particular vector having the direction of the two microphone axis. Therefore, in order to obtain the entire vector, three measurements with orthogonal microphone axes are needed. Similarly, the kinetic energy density is obtained (see Equation (9)) from a dot product of two vectors with three orthogonal components.

A practical measurement arrangement consists of two microphone pairs with perpendicular axis so that the vector quantities in a plane are obtained. Such measurement is very efficient in sound fields which, for reasons of symmetry, become two-dimensional.

The above Equations (8) - (13) show that all quantities of interest can be obtained from auto- and cross-spectral densities between two closely spaced pressure sensors. Therefore, once these are calculated and stored in a computer, extensive information on the sound field can be obtained with only moderate additional computational effort. Figure 2 shows the block diagram of a universal measurement technique which provides all acoustic quantities of interest. A variety of available FFT and other analyzers have internal postprocessing circuitry which usually calculates the active intensity and sound pressure level.

2.6 Applications

The main incentive leading to the development of the intensity technique was the need to develop a better tool for sound power measurements than the techniques based on calculating sound power from the squared pressure data. Once a reliable sound power measurement technique was developed, the applications have escalated rapidly and the new technique has been adopted in practically all measurement techniques based on sound power, such as transmission loss, sound absorption

coefficient and radiation efficiency measurement. In addition to improving the laboratory procedures, the intensity meter is irreplaceable for field measurements because of its ability to directly measure the sound power. The growing interest in near-field data linked to sound radiation and source identification provides the necessary data base to develop new prediction techniques. Finally, the ability of the intensity technique to measure sound power flux in addition to the sound pressure and particle velocity, makes it a perfect tool for complete studies of diffraction, reflection and other field studies linked to wave propagation.

2.7 Sound Power Measurements

Precise knowledge of sound power radiated from a source is needed for its characterization and labeling, and as the input parameter for environmental design. The extensively researched reverberation room technique, which has the needed precision to measure the radiated power, requires large and costly reverberation rooms. In addition, it is usable for small sources only. The in-situ sound measurement of large sources is based on determining the sound power flux over an enclosed surface around the source. The use of intensity, instead of pressure, eliminates up to 10 dB of error which arises from the substitution of $p^2/\rho c$ for intensity when measuring in the nearfield of sources.

The sound power measurement procedure consists of selecting a surface enclosing the source. Sound intensity is measured at a sufficient number of points and the sound power W is calculated as a sum of partial power contributions from small areas ΔS_j associated with each intensity vector $\vec{I}_j$, normal to the surface.

$$W = \sum_{j=1}^{n} \vec{I}_j \, \Delta S_j \qquad (16)$$

The principal advantage of the intensity technique is the ability to measure the power flow in the farfield as well as in the nearfield. As a consequence, the power radiated by large sources located in a highly reverberant environment can, for the first time, be measured with sufficient precision. Measurement procedures are provided in the drafted standards: International ISO DIS9614, "Determination of the Sound Power Levels of Noise Sources Using Sound Intensity Measurement at Discrete Points," and U.S. Standard ANSI S 12.12, "Engineering Method for the Determination of Sound Power Levels of Noise Sources Using Sound Intensity." Work is also in progress on an international IEC Standard, "Instruments for the Measurement of Sound Intensity" and on its U. S. ANSI counterpart.

These standards define the optimum number and location of the measurement points, the steps determining the desired measurement distance from the source surface, and the procedures for the verification of the measurement precision.

The intensity technique permits measurement of the sound power of a source in the presence of other noise sources operating simultaneously. If no sound energy is absorbed inside the volume circumscribed by the measurement surface, the sound power flux from external sources penetrates and eventually exits the measurement areas so that the total net flow is zero. This strategy can be applied to measure the sound power output of parts of larger systems which cannot be separated mechanically and measured in parts. The presence of reflectors, or the proximity of hard walls, as well as highly reverberant environments,

results in the formation of standing waves. These environments require careful selection of measurement locations, sufficiently large number of measurement points. and a carefully calibrated system. The precision of the measurements has been the subject of intensive research and, as a result, indicators were formulated to verify the precision of the measurements. The mentioned Standard drafts provide details on the use of these indicators. In general, the overall precision of the intensity technique equals the precision of sound power measurements in reverberation rooms and other reflecting environments.

2.8 Sound Source Identification

Detailed measurements and mapping of sound pressure and acoustic intensity in the nearfield of a radiator lead to both qualitative and quantitative evaluation of the sound radiation from a source. The maps of intensity vectors reveal the areas of sound power emission and their propagation into the farfield. They are essential in determining the radiation pattern of a source and in deciding on noise control strategies.

First, examples of the nearfield of typical radiators will be shown. The vibration of plates, beams, or machine surfaces can be expressed in terms of modes. Each vibrational mode on the source surface is characterized by areas which are separated by nodal lines and vibrate with 180° phase shift. If the distance between the centers of the adjacent areas is smaller than one-half wavelength of the radiated sound, a substantial amount of the radiated energy is returned back into the source and usually only a small fraction propagates into the farfield.

This "shortcircuiting" of the acoustical power flux is due to the coupling. Its effect will be shown first on a field of three sources, separated by one-tenth of the wavelength (Figure 3). The center source vibrates with 180° phase shift relative to the two outer sources. As the intensity field reveals, the outer sources radiate sound power which sinks partially into the center source and only a fraction of the radiated power propagates into the farfield. The solid lines in this figure are wavefronts reconstructed by the computer as lines normal to the intensity vectors (see Equation 4). Figure 4 shows the pressure distribution represented by circles proportional to P^2 amplitude. This figure reveals that the pressure measurement cannot provide any information on actual energy flow from one source into another; it is the result of the wave interference in the nearfield. The overall reduction of the energy propagating into the farfield is caused by the strong source coupling. As shown in Figure 5, when the source distance is increased (1.35 wavelength), the coupling has substantially decreased and all three sound sources radiate sound power into the farfield.

The "shortcircuiting" of acoustic energy is characteristic of radiation from vibrational modes at frequencies lower than the critical frequency for which the distance of the adjacent "source centers" is smaller than one-half wavelength. Figure 6 shows the active intensity in the nearfield of a circular membrane in a baffle which is excited to its (0,3) mode. Again, sound power radiated by the source areas partially sinks into the adjacent areas. Figure 7 shows the pressure distribution which is fairly uniform and does not provide any information on the actual source behavior. We can now show the usefulness of reactive intensity $\vec{Q}$, which is proportional to the P^2

gradient as revealed in Equation 6. Figure 8 shows that the vibrating portions of the hard surface are sources of $\vec{Q}$, because the sound pressure has maxima at these surfaces.

CHAPTER 3

EXPERIMENTAL PROCEDURES FOR THE HVAC SYSTEM

3.1 Acoustic Intensity Mapping

The acoustic measurements were performed in the ARL Penn State Flow-Through Anechoic Chamber. Figure 9 shows the construction and dimensions of this chamber; it has a low-frequency cutoff of 70 Hz. The stand alone HVAC system was positioned near the floor at the center of the chamber. It was attached to a simple wooden frame for support above the floor. Acoustically absorbing foam was draped over support members during the tests. Figure 10 shows a photograph of the setup in the anechoic chamber. The metallic structure seen in this view is part of a large 3-D microphone positioning apparatus (scanner). Figure 11 shows an isometric drawing of the scanner which is typically 8 feet on a side. A computer controlled stepping motor powers each of the three independent carriages.

Two (2) pairs of phased-matched 1/4-inch microphones were remotely positioned by the scanner. The microphone pairs were oriented 90° to each other so that two orthogonal components of the intensity vector could be measured at each measurement point in space. Thus, a measurement plane was selected, measurement locations were programmed into the computer (these required detailed physical measurements of the HVAC system), and the scanner moved the intensity probes to the points selected. Once set into operation the scanner moves the probes and then pauses for a sufficiently long period of time so that mechanical vibrations dampen out, and then the acoustic data acquisition is performed. Once the signals are in computer memory, the computer

directs the scanner to move to the next position and repeat the data acquisition. Based on the several hundred measurement points required, it was not uncommon for a typical scan (over one plane) to take two hours. Data acquisition and post-processing of the acoustic intensity quantities were performed by a MASSCOMP computer.

3.2 INCE Plenum Box

In 1985, the Institute of Noise Control Engineering (INCE) adopted a standard practice for the measurement of sound power from small air-moving devices. This practice is commonly referred to as the INCE Plenum Box Method and is documented as Recommended Practice 1-85 (INCE Publication TG-CBE 1-85). The fundamental feature of the method is that a simple frame box has walls covered with acoustically transparent mylar sheets. The fan or blower under consideration is mounted in one wall as depicted in Figure 12; the box thus provides a pressure chamber that allows the fan to be tested under various conditions of back pressure. The back pressure (head rise) is varied by a sliding door opening in one wall, and the static pressure is measured by a piezometer. Microphones can be positioned around the box and are sensitive to the emissions from the fan because the mylar is transparent; furthermore, the box prevents extraneous flow noise from acting on the microphones. The box fabricated for the current project was made slightly smaller than the recommended dimensions. A photograph of this box with the production blower mounted is shown in Figure 13. The box was used to measure the sound power of the blower over a range of pressures and wheel speeds.

CHAPTER 4

EXPERIMENTAL RESULTS

4.1 Nearfield Acoustic Intensity Maps of the HVAC System

The computer controlled, three axis traverser described in the previous section positioned the intensity probe for nearfield acoustic intensity mapping. The data were acquired with the HVAC system operating in its maximum AC configuration with a volumetric flow rate equivalent to the maximum AC throughput. Two dimensional, acoustic intensity vector measurements were performed at numerous locations in five planes for up to five one-third octave frequency bands. The measurement planes are described with the data. In planes 1, 2, and 3, data were taken both with the blower installed in the system and with the blower located in an acoustically isolated box. The same air flow rate was maintained to the system at all times. Data in Plane 4 were acquired only with the blower installed and data in Plane 5 were acquired only with the blower removed.

Figures 14 through 48 present the intensity maps in a format designed to orient the reader so that he/she can easily relate the intensity to features on the HVAC system. Each map consists of a three dimensional figure of the HVAC system with the corresponding measurement plane in the upper left corner of the page, one-third octave band active intensity levels appear at top right, active intensity vectors at bottom right, and reactive intensity vectors at bottom left. Photos of the HVAC system were taken at the appropriate angles and were modified for placement in the blank spaces of the intensity maps representing the surface in the measurement plane.

4.1.1 Measurement Plane 1

Intensity vector maps taken in measurement Plane 1 are presented in Figures 14 through 22. For comparison purposes, at a given frequency, the data are first presented with the blower installed in the system, and then with equivalent airflow being supplied by a fan in an acoustically isolated box.

At 250 Hz, with the blower installed, Figure 14 clearly shows that the blower dominates the field; radiating sound through the inlet and recirculating door. With the blower removed, the strongest source region is, as shown in Figure 15, the top of the evaporator core; the intensity vectors fan out radially from that location. Although the source at the top of the evaporator core contributes locally to the sound field, it is a secondary source in terms of the integrated intensity (i.e. sound power) radiated by the HVAC system in Plane 1 at 250 Hz; the blower being the primary source.

Figure 16 shows that at 500 Hz the blower is the dominant noise source in Plane 1. The blower radiates sound predominantly through the inlet although there is a substantial amount transmitted through the recirculating door. Figure 17 reveals that, with the blower removed, the exit of the evaporator is the strongest source region. However, compared to the fan, the evaporator exit source contributes only a small amount of acoustic energy to the field (comparisons of the maximum level indicated on all of these figures aids in such conclusions).

At 1000 Hz in Plane 1, Figure 18 shows that the blower is again the dominant noise source although there is a local contribution from the area at the evaporator exit. With the blower removed, Figure 19 shows that the area at the evaporator exit is the strongest source region,

and, compared to the fan, contributes equal energy to the sound field at that location. However, in terms of the total sound power radiated by the system, the contribution from the evaporator exit source is small.

Figure 20 also shows that the blower is the dominant noise source for 2000 Hz in measurement Plane 1. The blower radiates sound primarily through the inlet and recirculating doors. There is, however, a local contribution from a source at the evaporator exit. Figure 21 is a repeat of the active intensity shown in Figure 20, but color has been applied to aid in hot spot identification. The red indicates an acoustic hot spot. Figure 22 shows that, in measurement Plane 1 with the fan removed, the area at the evaporator exit is the strongest source region at 2000 Hz. Again, in terms of the total sound power radiated by the system, the contribution from the evaporator exit source is small.

Figures 14 through 22 clearly show that the blower is by far the dominant noise source measured in Plane 1 at frequencies ranging from 250 to 2000 Hz. Two additional flow noise source locations have been identified though; the top of the evaporator at 250 Hz and the exit of the evaporator at frequencies ranging from 500 to 2000 Hz. These flow noise sources contribute to the sound field only locally. If the intensity is measured a short distance away from either flow noise source region, the sound field would be dominated by the fan. Locally, flow noise can contribute equally to the sound field (relative to the local contribution from the fan), but in terms of the overall sound power radiated by the HVAC system (in Plane 1), the flow noise sources are secondary contributors.

4.1.2 Measurement Plane 2

Figures 23 through 30 present intensity vector maps measured in Plane 2. As in Plane 1, the data taken with the blower installed in the system are presented first, and then, for comparison purposes, the intensity vector map taken with the air moving device located in an acoustically isolated box is presented.

Figures 23 and 24 show that in Plane 2 at 250 Hz (even with the blower installed in the HVAC system) the middle vents contribute significant energy to the field; the active intensities being high in front of them. There is also a substantial, if not dominant, contribution from the blower in that area of the measurement plane ranging from the middle vents to the edge. The passenger's side vent ranks third out of the four vents in terms of sound generation with the driver's side vent contributing the least amount of energy to the field. Figure 25 shows that with the blower removed the middle vents contribute most of the acoustic energy to the field. The passenger's side vent ranks third out of the four vents in terms of noise radiation with the driver's side vent contributing the least amount of energy to the field. With the blower removed, the active intensity is reduced only approximately 3 dB in front of the middle vents and passenger's side vent. This indicates that flow noise contributes a significant amount of energy to the field. Locally, register flow noise contributes up to 50% of the acoustic energy with the remaining 50% coming from the fan. Near the blower, however, the sound field is dominated by the blower.

At 500 Hz in Plane 2, Figure 26 shows the active intensity to be greatest between the middle vents and the passenger's side vent and to the side of the passenger's side vent. The active intensity is also

fairly high in front of the middle vents. The intensity to the side of the passenger's side vent is thought to be high due to the proximity of the measurement location to the fan. The fan also contributes to the measured intensities between the middle vents and the passenger's side vent and in front of the middle vents, but to a lesser extent. As one would expect, the influence of the fan is inversely proportional to distance from the fan and decreases as other sound sources are approached. With the blower removed from the system, Figure 27, like Figure 25, shows that the active intensity is greatest over the middle vents. The passenger's side vent contributes a lesser amount of energy to the field and the driver's side vent contributes the least amount of energy. Locally, the middle vents contribute most of the acoustic energy to the field compared to the fan. Overall, flow noise is a significant contributor to the measured sound field.

Figure 28 shows that in Plane 2 at 1000 Hz with the blower installed in the system, the active intensity is greatest in the area between the middle vents and the passenger side vent. This is due to the proximity of the measurement location to the fan. The middle vents contribute to the sound field as well but to a lesser extent. The driver's side vent contributes only a small amount of energy to the field.

In Plane 2 at 2000 Hz with the blower installed, the active intensity is seen in Figure 29 to be greatest in that portion of the measurement plane located to the side of the passenger's side vent. The active intensity is also fairly high between the middle vents and the passenger's side vent and over the middle vents. The contribution of the blower to the local sound field appears to decrease with distance

away from it, with flow noise sources dominating locally. Figure 30 shows that with the blower removed from the system the middle vents are the dominant sources of sound. The passenger's side vent and the driver's side vent contribute approximately equal amounts of energy to the field. Comparing the active intensity levels measured with the blower in place to the levels measured with the blower removed indicates that flow noise is a very important source of sound in Plane 2 at this frequency.

Figures 23 through 30 show that both the fan and register flow noise are significant contributors to the intensities measured in Plane 2. With the blower installed, the active intensities tend to be highest between the middle vents and the passenger's side vent and in that area of the measurement plane located to the side of the passenger's side vent. This is undoubtedly due to the proximity of the measurement location to the fan. With the blower installed, the middle vents are also primary contributors to the sound field, but, in general, to a lesser extent. The driver's side vent contributes little energy to the field.

With the blower removed from the system, the high active intensity levels between the middle vents and the passenger's side vent disappear as do the high active intensity levels in that area of the measurement plane located to the side of the passenger's side vent. In this configuration, the middle vents are the dominant sound source. The passenger's side vent contributes to the sound field as well, but to a lesser extent. Of all four vents, the driver's side vent contributes the least amount of energy to the field.

4.1.3 Measurement Plane 3

Figures 31 through 38 present intensity vector maps taken in Plane 3. As in measurement planes 1 and 2, maps taken with the blower in place are presented first and then, for comparison purposes, maps taken with the airflow supplied by an acoustically isolated source are shown.

In Plane 3 at 250 Hz, Figure 31 shows the intensities to be greatest at the fan inlet. There is a substantial contribution also from the area at the back of the fan. Fan noise may be leaking through the gap at the juncture of the two sections of the casing. With the blower removed, Figure 32 fails to reveal a single dominant sound source region. Sound is radiating from the surface enclosed by Plane 3 in a fairly uniform fashion. Slightly higher active intensity levels were measured at the inlet, at the back of the fan, and between the blower and the duct. In general, however, the flow noise measured in this plane at this frequency is negligible and by comparing the maximum active intensity level measured with the blower in place to the level measured with the blower removed, it is obvious that the blower is totally dominant at 250 Hz in Plane 3.

Figure 33 shows that at 500 Hz the fan inlet is the dominant sound generating region. As at a frequency of 250 Hz, fan noise appears to be leaking through the gap at the juncture of the two sections of the casing. Figure 34 shows the fan inlet to be the dominant noise source region even though the blower is removed from the system. However, its maximum value is 54.3 dB; some 12.5 dB lower than the maximum intensity value measured with the blower in place. Obviously, the fan is the dominant noise source at 500 Hz in Plane 3.

At 1000 Hz, the fan inlet is again identified in Figure 35 as the dominant source region. As at 250 and 500 Hz, sound leaks are thought to be present at the casing juncture. With the blower removed, Figure 36 still shows the most intense sound to be radiating from the fan inlet. The magnitude of the intensity at the inlet is 13.2 dB lower than with the blower installed. Obviously, at this location and frequency, flow noise is negligible compared to the noise generated by the fan.

Figure 37 shows that at 2000 Hz the intensity is highest at the lower part of the fan inlet and at a corresponding location behind the fan. Figure 38 also shows that with the blower removed the intensities are greatest at the fan inlet and at a corresponding location behind the fan. However, with the blower removed, the active intensity is reduced by 5.5 dB.

Figures 31 through 38 show that the blower is the dominant noise source in Plane 3. Unlike in Planes 1 and 2, distinct secondary flow noise sources were not identified. The source at the fan inlet which appears in the measurements performed with the blower removed is probably due to the delivery of air to the system.

4.1.4 Measurement Plane 4

Figures 39 through 43 are intensity vector maps of measurement Plane 4. All data were taken with the blower installed in the system.

At 125 Hz (Figure 39) the intensities are largest at the entrance to the plenum. The active intensity fans out radially from that location. The measurements performed at the back (opposite the area where the flow enters the plenum) indicate that the noise emanates from

the area where the flow enters the plenum. It is noted that the intensity values measured in this plane probably contain contributions from the fan.

Figure 40 (250 Hz) indicates that the intensities are greatest at the area where the flow enters the plenum. The measurements taken at the back of the plenum also indicate that this area is a source region.

Figure 41 (500 Hz) reveals that the active intensities are fairly uniform over the measurement plane. The sound from the fan is affecting the measured intensities considerably.

At 1000 Hz the intensities are shown in Figure 42. They are greatest over a relatively large area at the back of the plenum at the location of the door used to control the flow to the floor vents. The fan appears to contribute less to the measured intensities at this frequency than at 500 Hz.

The intensity vectors farthest from the HVAC system in Figure 43 indicate that at 2000 Hz sound is emanating from the back of the plenum at the location of the floor vent door. Some blower noise is contributing to this frequency band, however.

The intensity maps presented in Figures 39 through 43 appear to be influenced by fan noise, particularly at 500 Hz and above. At the lower measurement frequencies, the dominant source region is the area where the flow enters the plenum. At 500 Hz, the area where the flow enters the plenum is contributing approximately as much energy to the field as is the area at the back of the plenum. Above 500 Hz, the dominant source region is the area at the back of the plenum at the location of the floor vent door.

4.1.5 Measurement Plane 5

Figures 44 through 48 present intensity vector maps taken in Plane 5. All measurements were performed with the blower removed from the system; the air being supplied by a fan in an acoustically isolated box.

At 250 Hz (Figure 44), the intensities are greatest in the area between the plenum and the exit of the evaporator. The active intensities fan out radially from that location.

Figure 45 (500 Hz) reveals the notch between the plenum and the exit of the evaporator to be the dominant source region. The active intensities are greatest at this location and fan out radially from it.

Figure 46 again shows the notch between the plenum and the exit of the evaporator to be the dominant source region with the 1000 Hz active intensity vectors fanning out radially from it. An additional source near the location of the air entrance contributes to the acoustic field as well. The color representation of Figure 47 shows this second source as a yellow region at the top of the figure.

At 2000 Hz, Figure 48 shows the active intensity to fan out radially from the area between the plenum and the exit of the evaporator; this is a source region.

Figures 44 through 48 indicate that the area between the plenum and the exit of the evaporator is the dominant source region in Plane 5 with the blower removed. A source at the location where the air is delivered to the system may contribute at some frequencies, however, this source is probably due to the experimental set-up (i.e. the flow from the ducting impinging on the motor backplate). In any case, the plenum/evaporator exit source dominates the field.

4.2 Sound Power Measurements of the HVAC System

The sound power radiated by the HVAC system was measured by the method described in a previous section on applications of the acoustic intensity technique. The system was operating in its maximum AC mode during these measurements. This operating condition has been defined as the "standard" condition. For comparison purposes, the sound power was also measured with airflow only through the system. The mass flow rate of air through the system was identical in both cases since the static pressures at the evaporator exit were matched. Air was supplied to the system through a 30 ft. long section of dryer hose connected to a quiet airflow facility that is used in related studies of the aeroacoustics of flow separations. Initially, the discharge from the dryer hose was perpendicular to the motor backplate (the wheel was removed). This resulted in a "jet impinging on a solid surface" and was diagnosed as being a possible noise source. As a precaution against generating unwanted noise, the discharge from the dryer hose was subsequently turned gradually into the scroll using a flexible duct. Broadband five point sound power measurements confirmed that the resulting noise was reduced by approximately 2 dB.

Figure 49 shows the sound power spectrum radiated by the HVAC system operating in the "standard" configuration and with "airflow only" through the system. The sound power results confirm that the blower is the dominant noise source, although the data also show that the sound power radiated by the blower decreases with increasing frequency and that secondary flow noise sources become more important as the frequency increases. These results were verified through five point farfield sound power measurements performed using an octave band sound pressure

level meter and 20 point sound power measurements performed using the intensity measurement system.

4.3 INCE Plenum Box Measurements

Five point sound power measurements were performed for the standard blower mounted in the INCE plenum box, see Figure 50 for a schematic. The pressure rise across the blower, ΔP, ranged between 0 and 1.72 inches of water in these tests, while the blower speed ranged from approximately 1700 to 2900 rpm.

Figures 51 through 54 summarize the INCE box sound power measurements performed. Each figure is for a constant blower speed and for various total pressure rises across the unit. It is clear that a line component at the blade passage frequency (BPF) appears in the lightly-loaded cases. A means of reducing this line component is discussed in Appendix 1. As the pressure rise increases, wheel blades are prone to separation (stall) and turbulence noise and turbulence-turbulence interaction mechanisms begin to mask the time-invariant mechanisms that govern BPF noise generation. When the blower is installed in the HVAC system, pressure rises in excess of 1.5 inches of water are present and as a result, the BPF noise is reduced somewhat compared to the lightly-loaded cases.

One may use the data shown in the previous figures to establish a blower speed scaling law. As an example, and because the spectra are broadband in nature, we choose 500 and 1500 Hz for the analysis. The pressure coefficient is defined as:

$$\psi = 2P_{tot}/\rho V_t^2, \qquad (17)$$

where P_{tot} = total pressure rise across the fan,

V_t = impeller tip speed,

and ρ = air density.

Figure 55 is a cross plot of sound power level versus wheel speed at constant Ψ. These may or may not correspond to the HVAC system operating points, but that is irrelevant because the sound power increases as the fifth power of wheel speed, regardless of the pressure coefficient.

CHAPTER 5

CONCLUSIONS

The blower is the dominant noise source in the HVAC system, particularly at lower frequencies. In general, the sound power radiated by the blower decreases with increasing frequency and the secondary flow noise sources (which are broadband in nature) become more dominant at higher frequencies. At 250 Hz, the blower is contributing approximately 10 times more energy to the acoustic field than is flow noise; however, at 3 kHz, the blower and flow noise contribute nearly equally to the acoustic field.

Specific flow (or flow-induced) noise source locations identified by the intensity vector maps include the region between the evaporator core and plenum, the inlet to the evaporator core, and the dash board registers, particularly the middle ones. Denger et al. (1990), document dye injection flow visualization through all of these regions. Figure 56 shows the quantitative flow path in the blower exit region. Because the diffuser angle is large (greater than 7°), separated flow regions exist and these are believed to contribute to the secondary flow noise. Perhaps more important is the contracted flow on the downstream side of the evaporator core. Figure 57 shows the detailed flow path, the dynamics of which are lost here, but real-time flow visualization confirms that there is a great deal of chaotic flow in this contraction. A gusset is in the flow path and it is capable of creating significant edge noise. The flow visualization shows considerable unsteady vorticity at this edge; such vorticity is an efficient generator of

aerodynamic sound. Furthermore, a pair of freon supply pipes cross the flow path as indicated in Figure 58. The vorticity in the wakes of these pipes is another acoustic mechanism.

Flows impinging on non-rigid surfaces can also result in sound radiation due to structural vibration and subsequent re-radiation. The diagnosis of this mechanism was beyond the scope of the present investigation, but will be the subject of future work.

The dash board registers also were found to be sources of sound with the middle registers radiating the most noise, followed by the passenger's side vent and then the driver's side vent. The strength of the acoustic emission from a register appears to be proportional to the airflow velocity through it. Also, in general, the active intensity level measured in front of the middle registers decreased by less than 3 dB when the fan was removed from the system and equivalent airflow was supplied by the acoustically isolated blower. This indicates that blower noise is not being transmitted through the ductwork and radiating from the vents. It appears that high-velocity airflow over the louvers in these registers is the primary cause for the sound. A preliminary investigation of this type of noise was conducted and the results are given in Appendix 2. The noise appears to depend on the trailing edge configuration of the louvers since the levels are observed to increase as the louver angle of attack is increased. Although the blower is the dominant contributor to the sound power radiated by the HVAC system, the registers are important local contributors to the acoustic energy field. Due to their proximity to the vehicle occupants, and due to the fact that the dash helps shield the occupants from the blower, register noise warrants further attention.

Identifying particular noise sources within the blower itself was not within the capability or scope of the current project. In general, however, Denger's results indicate that inlet distortions and the circumferential variation in blade stall may contribute to sound generation by the blower. Local separation zones on the volute wall may also produce significant broadband noise, as will the convection of boundary layer turbulence off the trailing edges of the fan blades. Basically, there are several noise generating mechanisms that will contribute to the overall sound produced by the standard HVAC system blower and only additional research will enable one to establish a rank ordering of these sources and implement effective noise control measures.

CHAPTER 6

RECOMMENDATIONS FOR QUIETING

It is obvious that in order to quiet the subject HVAC system, the noise generated by the blower must be reduced. However, as shown by the results for equivalent airflow being supplied by a quiet external source, blower noise reductions of 10 dB at 250 Hz and only 3 dB at 3 kHz will result in a total system noise emission dominated by flow noise created by other system components and ducts. Flow noise in the present system results from poor flow quality, i.e., flow separation, flow impingement on solid surfaces, obstructions jutting into the flow path, high fluid velocity over edges, etc. The poor flow quality results in severe pressure losses necessitating a given blower to run faster to overcome these losses and achieve a given mass flow rate. Figure 55 shows that the faster the blower runs, the more noise it will produce. Thus, the quality of the flow through the HVAC system and the noise generated by a given blower are coupled.

In general, improved flow quality and reduced noise can be achieved if the following features are avoided:

1) sharp corners and bends (to avoid flow separation and pressure losses)
2) edges conducive to the generation of trailing edge noise
3) sudden area expansions (to avoid flow separation)
4) sudden area contractions (to avoid fluid impingement and accelerating flow)
5) small cross sectional area ducts (to reduce flow velocity)
6) obstructions jutting into the flow path (to avoid edge tones)

7) structures prone to vibration (loose doors, etc.)

8) air leaks (to avoid edge tones)

Following the above recommendations will reduce flow noise and pressure losses. Reduced pressure losses will enable a given blower to run slower. A 25% reduction in blower speed alone will result in more than a 75% reduction in the sound power radiated by the system. Obviously, a quieter blower design will reduce the noise radiated by the system even further.

REFERENCES

[1] Denger, G. R., M. W. McBride, G. C. Lauchle. An Experimental Evaluation of the Internal Flow Field of an Automotive Heating, Ventilation, and Air Conditioning System. ARL Penn State Technical Report TR 90-011 (July 1990).

[2] Neise, W., G. H. Koopmann. Reduction of Blower Noise by Resonators. J. Sound Vib. 73:297 (1980).

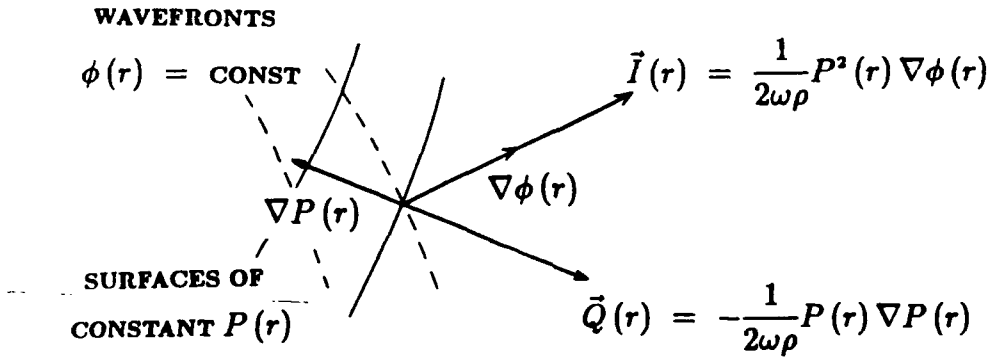

Figure 1. Intensity Vectors, Wavefronts and Contours of Constant Pressure

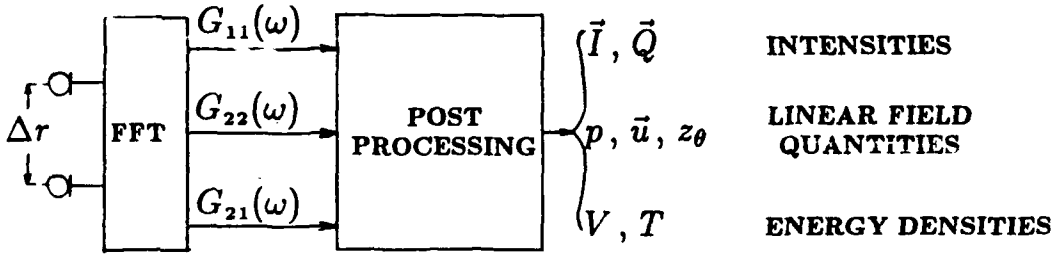

Figure 2. Block Diagram of Measurement Technique

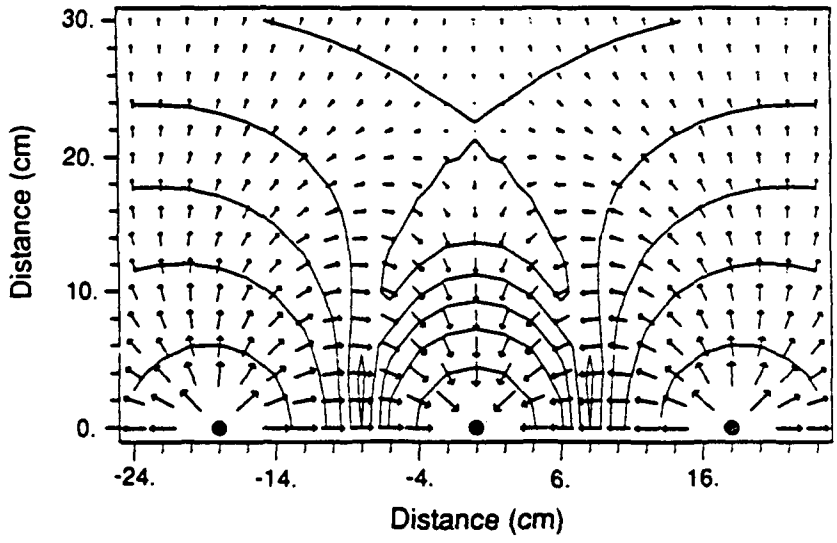

Figure 3. Intensity Field and Wavefronts of Three Sources Separated by 1/10 Wavelength

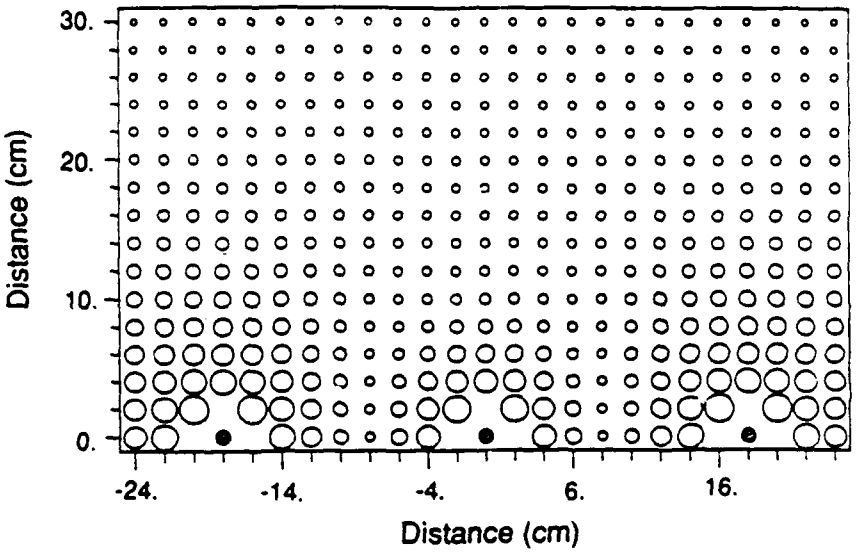

Figure 4. Sound Pressure Field of Three Sources Separated by 1/10 Wavelength

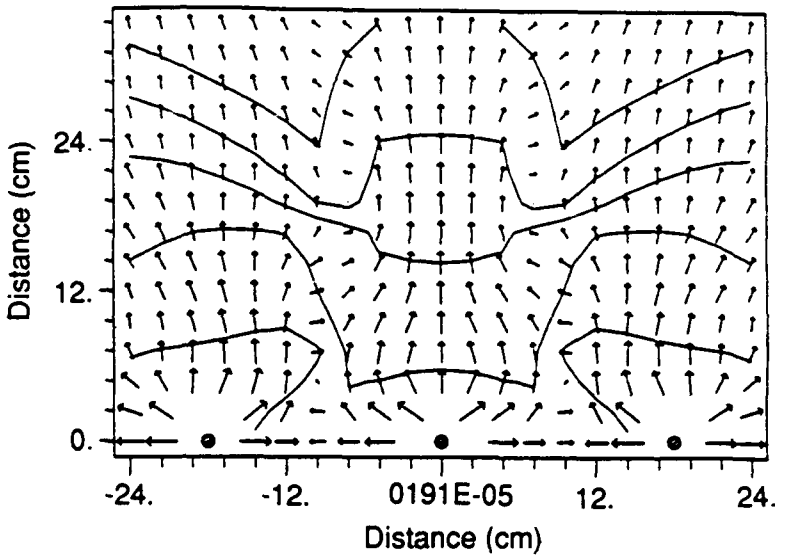

Figure 5. Intensity Field and Wavefronts of Three Sources Separated by 1.35 Wavelength

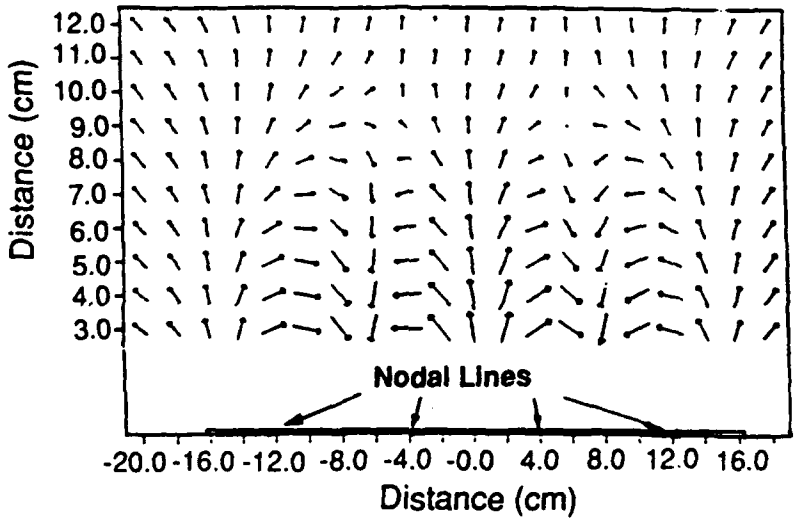

Figure 6. Active Intensity in Nearfield of Circular Membrane Excited to (0,3) Mode

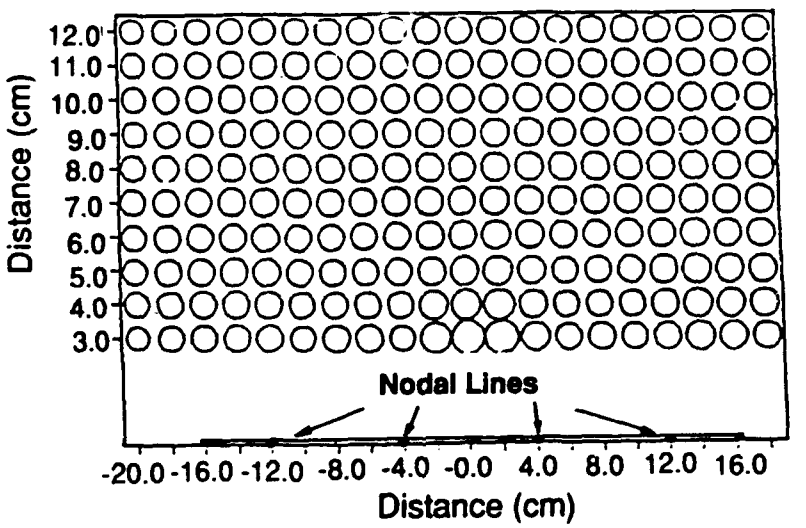

Figure 7. Potential Energy for Configuration of Figure 6

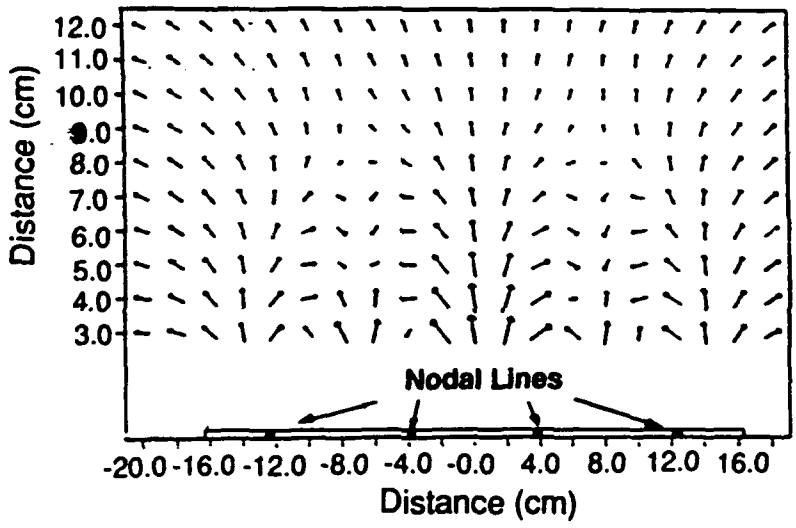

Figure 8. Reactive Intensity for Configuration of Figure 6

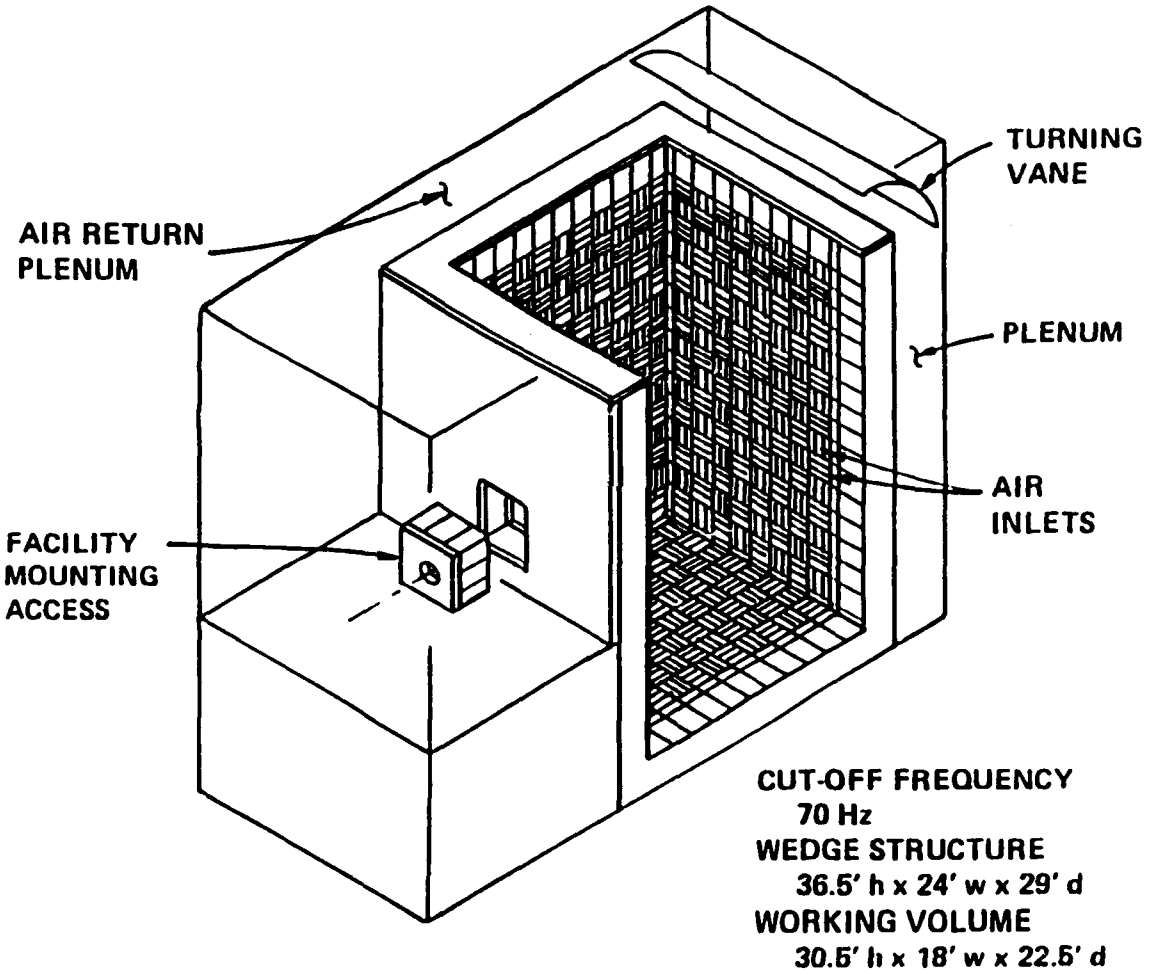

Figure 9. The ARL Penn State Flow-Through Anechoic Chamber

Figure 10. The HVAC System Situated in the Anechoic Chamber

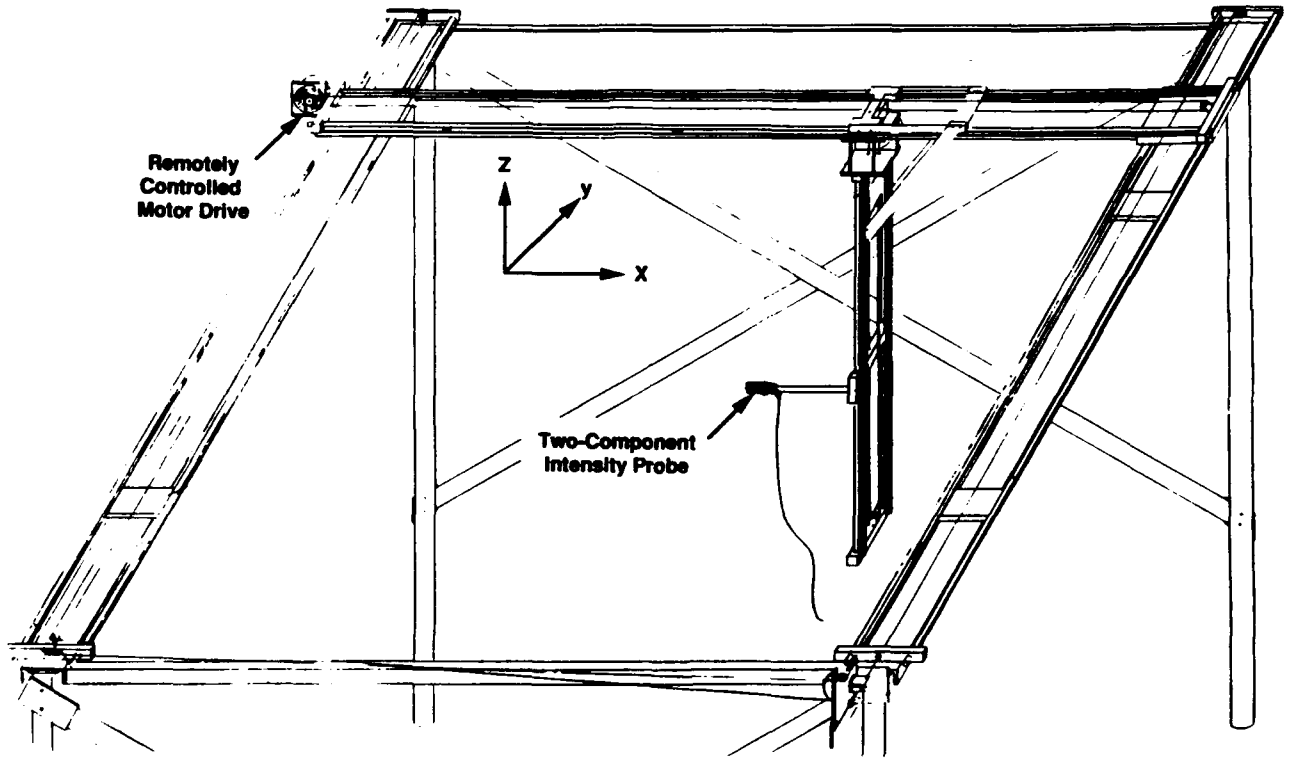

Figure 11. Schematic Diagram of the 3-D Acoustic Scanner

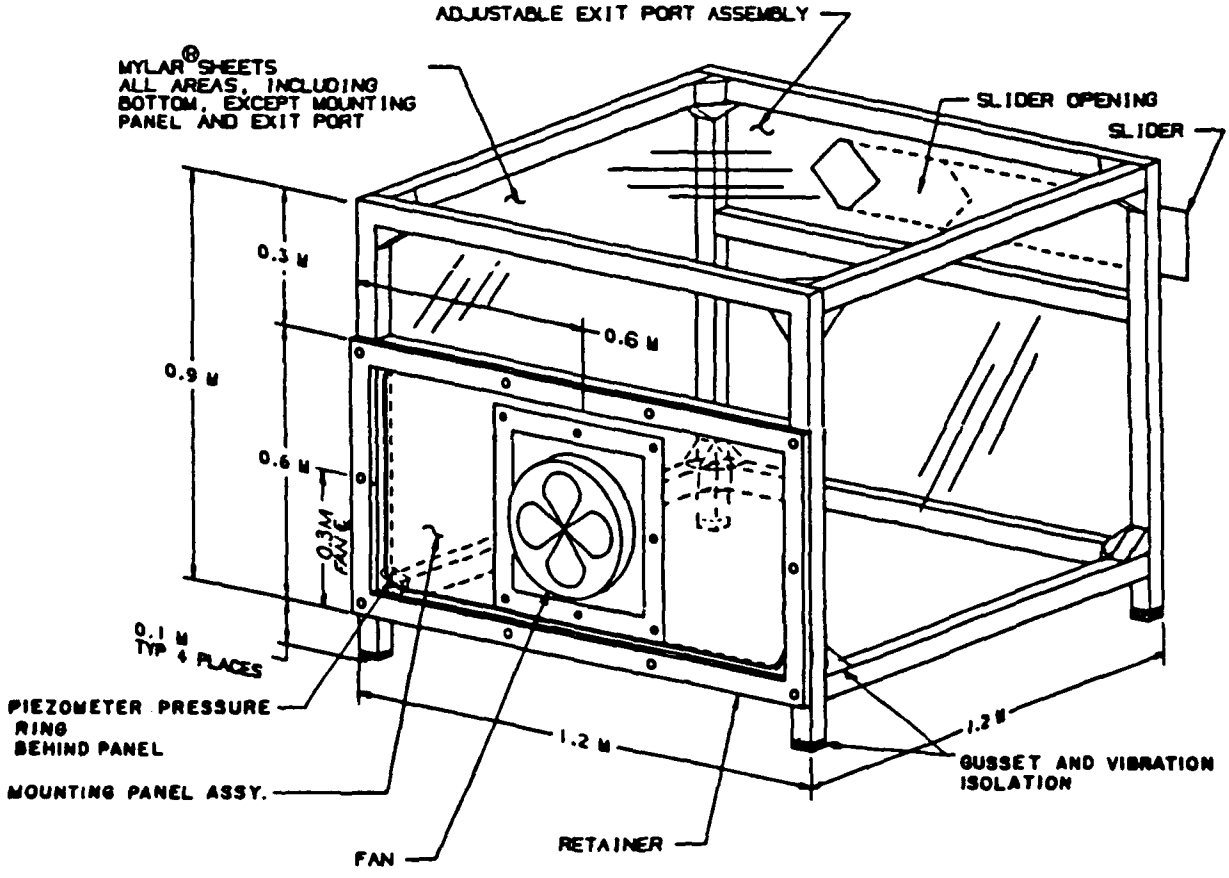

Figure 12. Construction Notes for INCE Plenum Box

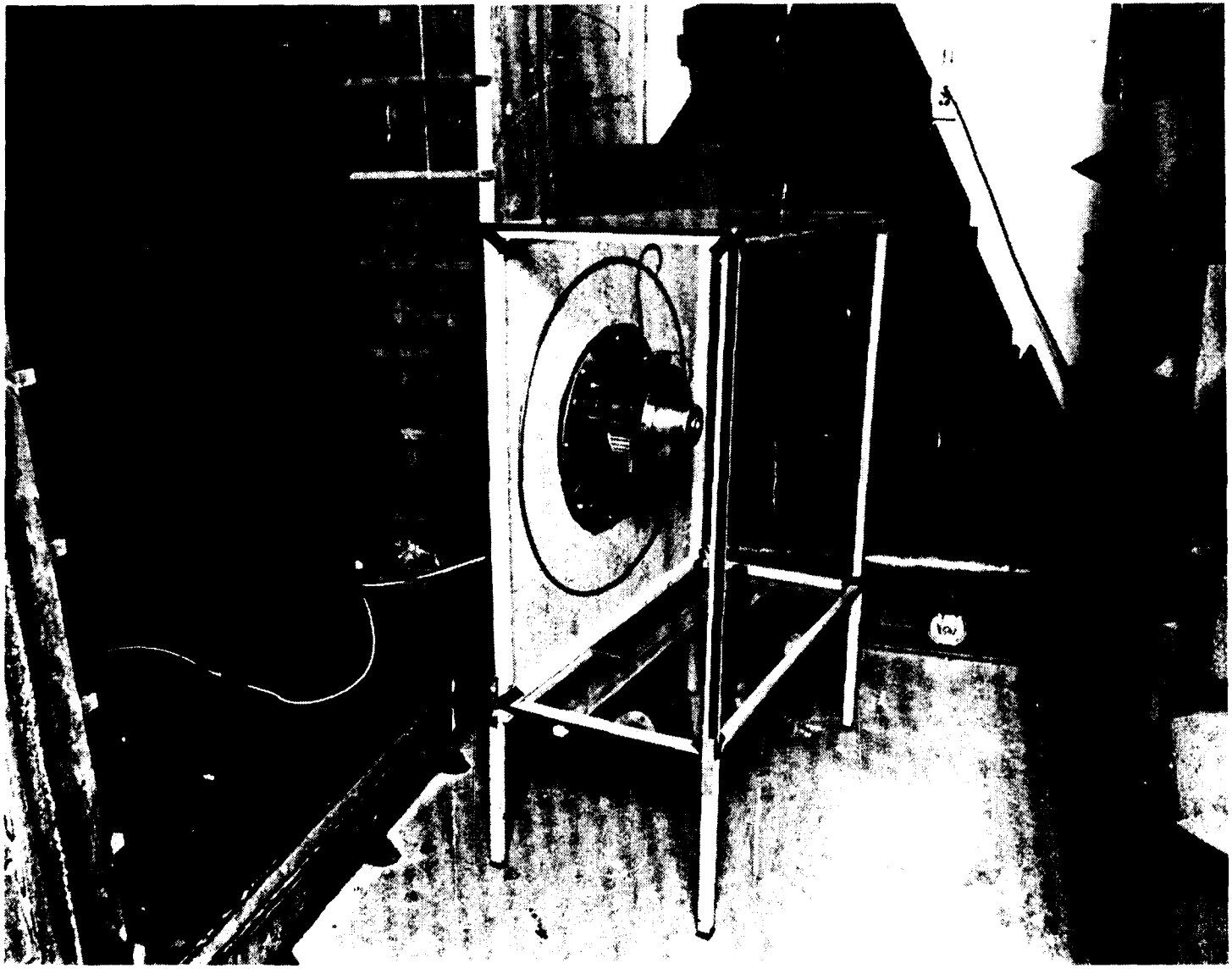

Figure 13. INCE Plenum Box Used in Production Blower Sound Power Measurements

3-D VIEW

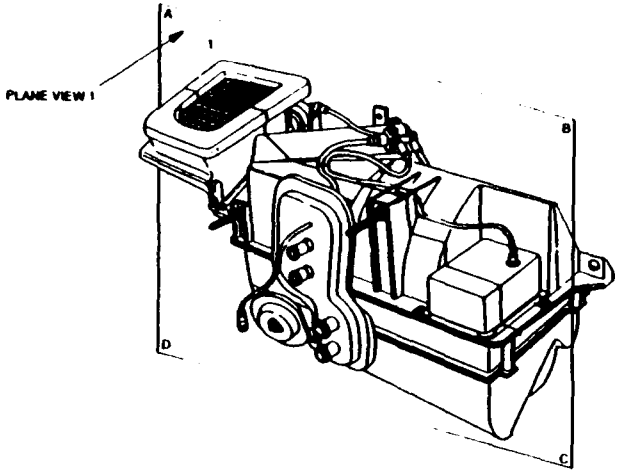

ACTIVE INTENSITY LEVELS AT 250 Hz IN PLANE 1
Maximum Level: 66.9 dB re 1 x 10^{-12} W/m^2

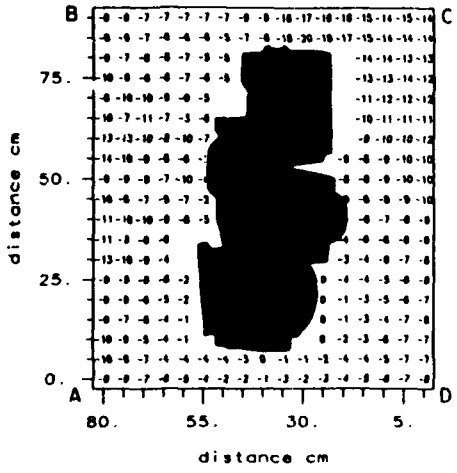

REACTIVE INTENSITY VECTORS AT 250 Hz IN PLANE 1
Maximum Level: 71.2 dB re 1 x 10^{-12} W/m^2

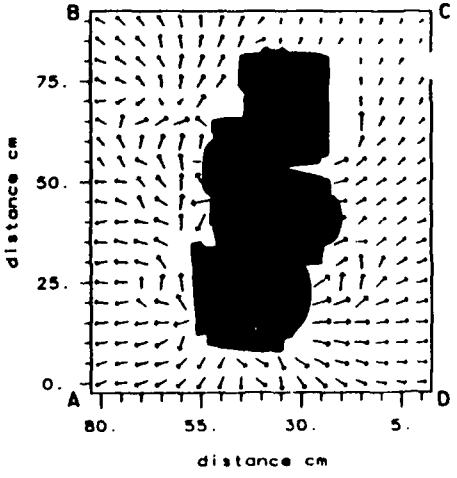

ACTIVE INTENSITY VECTORS AT 250 Hz IN PLANE 1
Maximum Level: 66.9 dB re 1 x 10^{-12} W/m^2

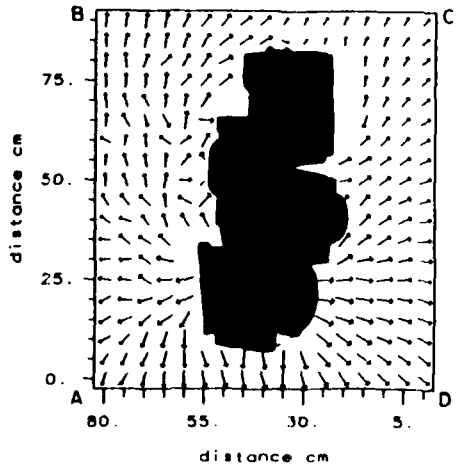

Figure 14. Measurement Plane 1 Intensity Vector Map, 250 Hz, Blower In

3-D VIEW

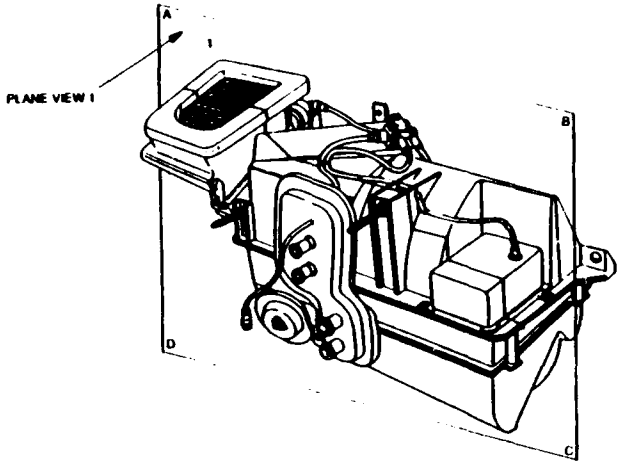

ACTIVE INTENSITY LEVELS AT 250 Hz IN PLANE 1
Maximum Level: 56.4 dB re 1 x 10^{-12} W/m^2

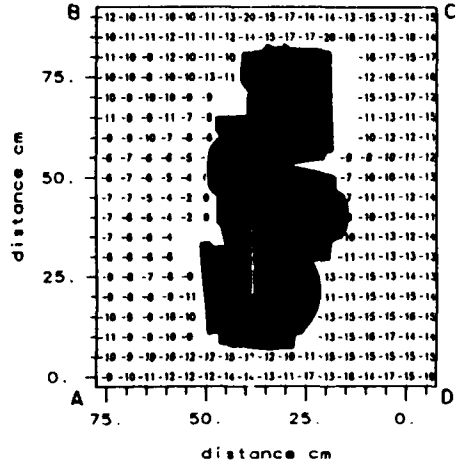

REACTIVE INTENSITY VECTORS AT 250 Hz IN PLANE 1
Maximum Level: 63.0 dB re 1 x 10^{-12} W/m^2

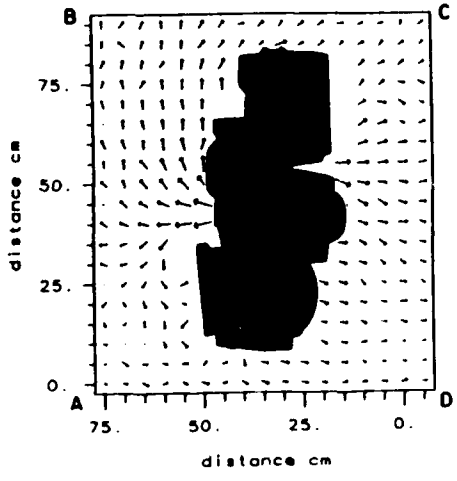

ACTIVE INTENSITY VECTORS AT 250 Hz IN PLANE 1
Maximum Level: 56.4 dB re 1 x 10^{-12} W/m^2

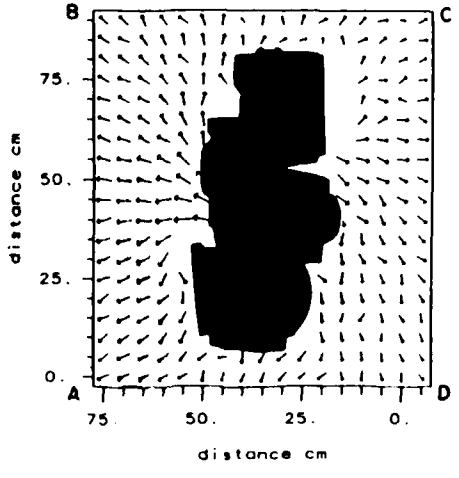

Figure 15. Measurement Plane 1 Intensity Vector Map, 250 Hz, Blower Out

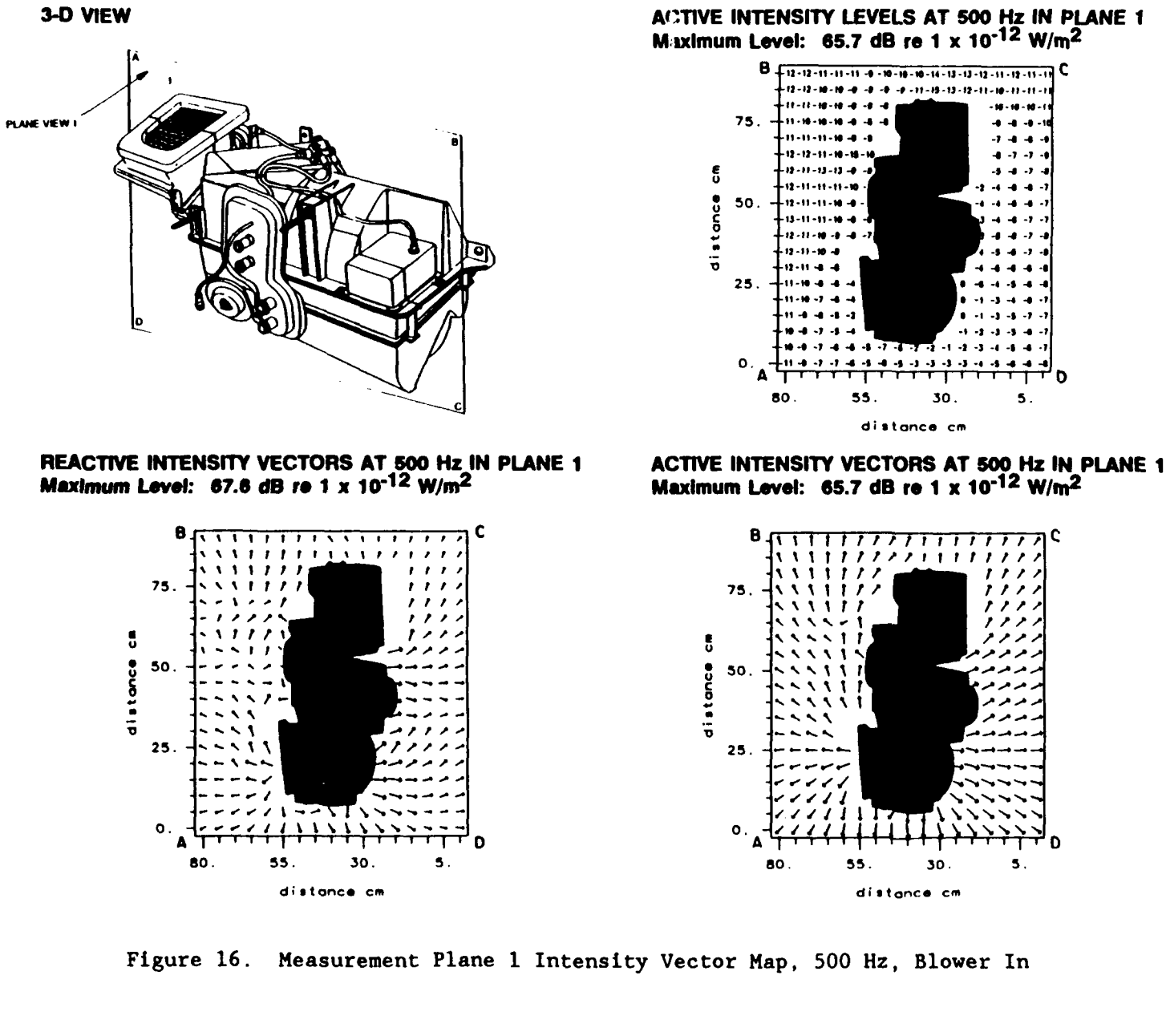

Figure 16. Measurement Plane 1 Intensity Vector Map, 500 Hz, Blower In

3-D VIEW

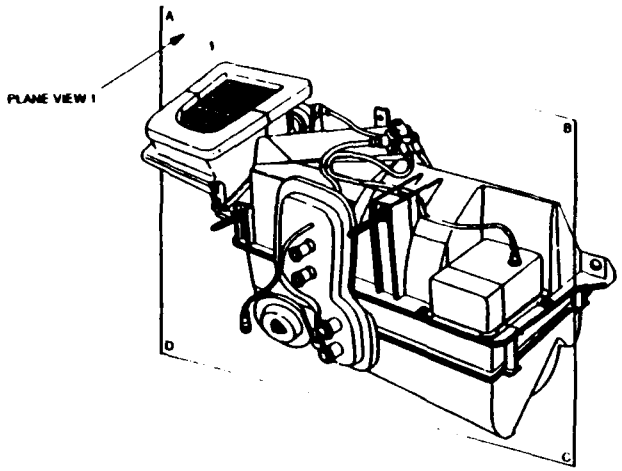

ACTIVE INTENSITY LEVELS AT 500 Hz IN PLANE 1
Maximum Level: 48.7 dB re 1 x 10^{-12} W/m^2

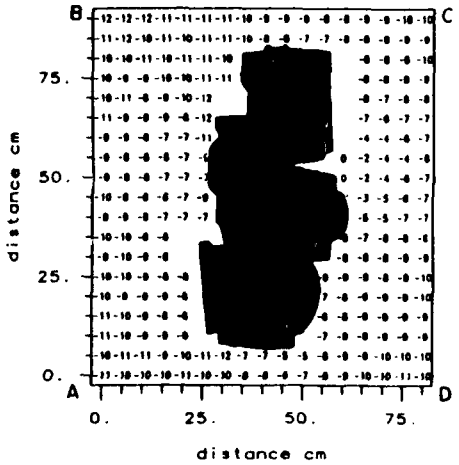

REACTIVE INTENSITY VECTORS AT 500 Hz IN PLANE 1
Maximum Level: 51.3 dB re 1 x 10^{-12} W/m^2

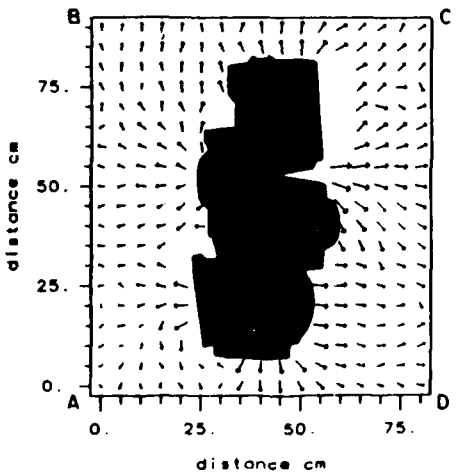

ACTIVE INTENSITY VECTORS AT 500 Hz IN PLANE 1
Maximum Level: 48.7 dB re 1 x 10^{-12} W/m^2

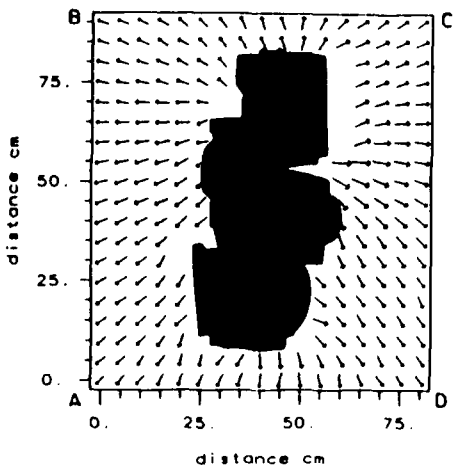

Figure 17. Measurement Plane 1 Intensity Vector Map, 500 Hz, Blower Out

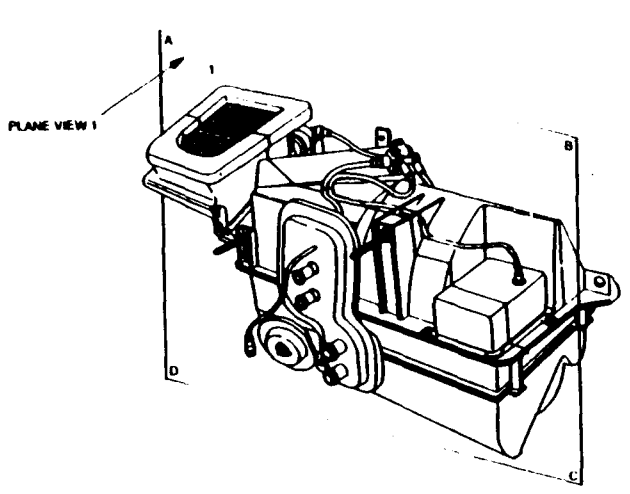

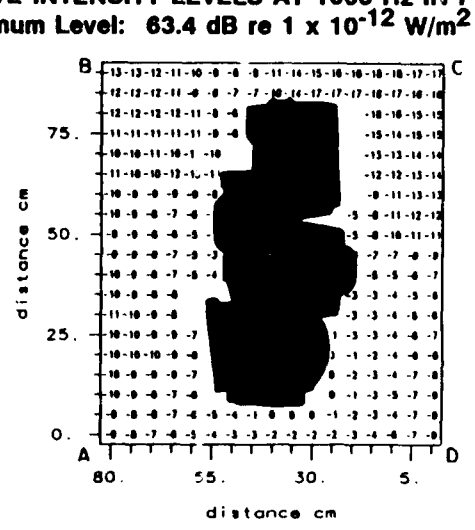

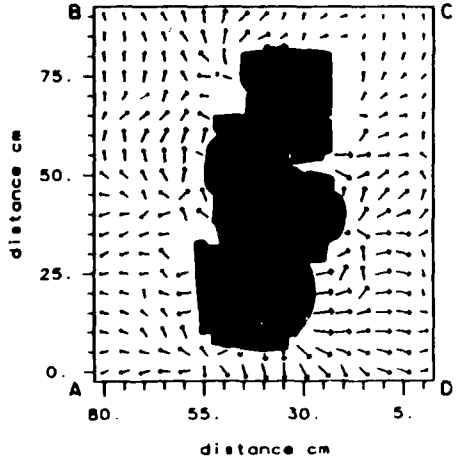

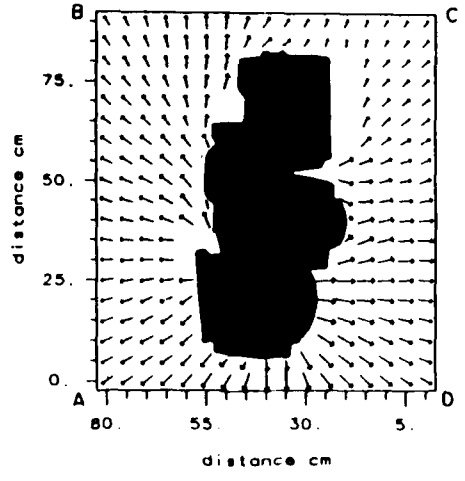

Figure 18. Measurement Plane 1 Intensity Vector Map, 1 kHz, Blower Out

3-D VIEW

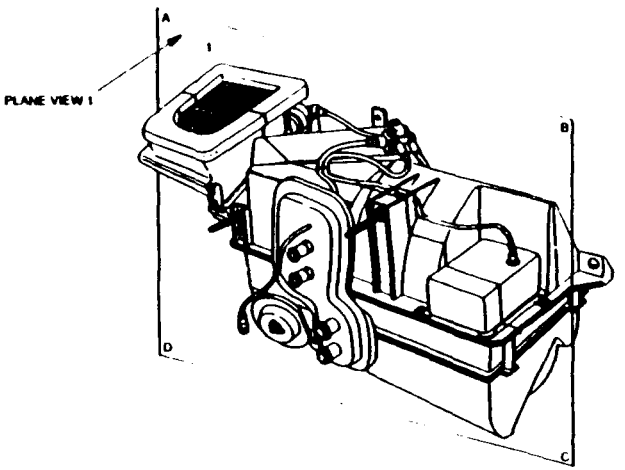

ACTIVE INTENSITY LEVELS AT 1000 Hz IN PLANE 1
Maximum Level: 55.1 dB re 1 x 10^{-12} W/m^2

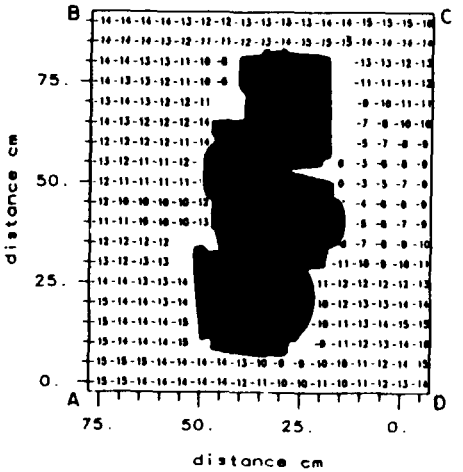

REACTIVE INTENSITY VECTORS AT 1000 Hz IN PLANE 1
Maximum Level: 54.5 dB re 1 x 10^{-12} W/m^2

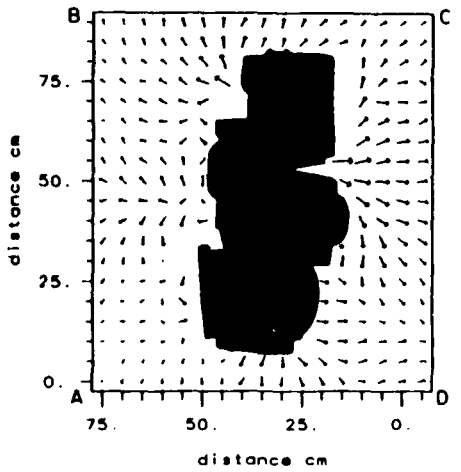

ACTIVE INTENSITY VECTORS AT 1000 Hz IN PLANE 1
Maximum Level: 55.1 dB re 1 x 10^{-12} W/m^2

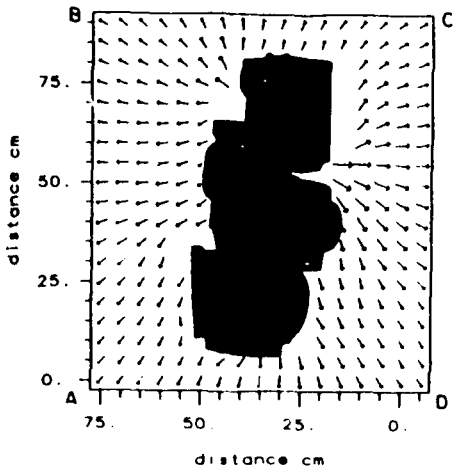

Figure 19. Measurement Plane 1 Intensity Vector Map, 1 kHz, Blower In

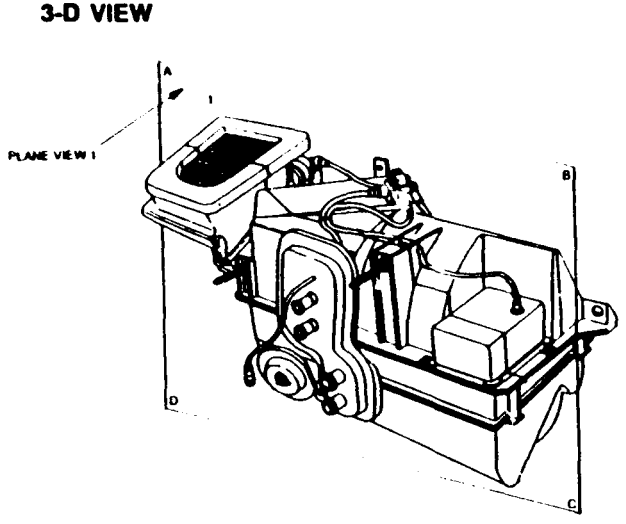

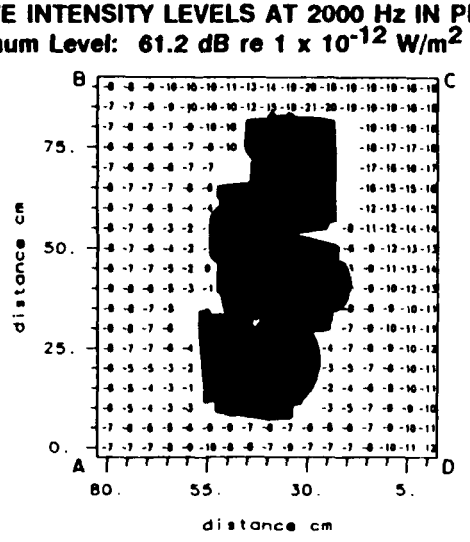

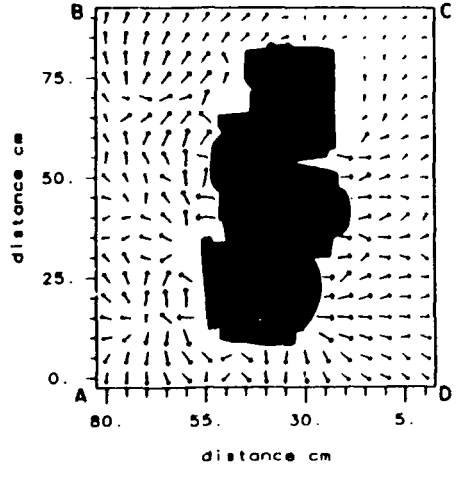

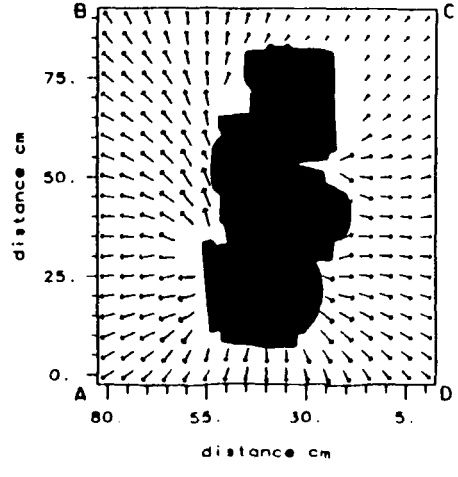

Figure 20. Measurement Plane 1 Intensity Vector Map, 2 kHz, Blower In

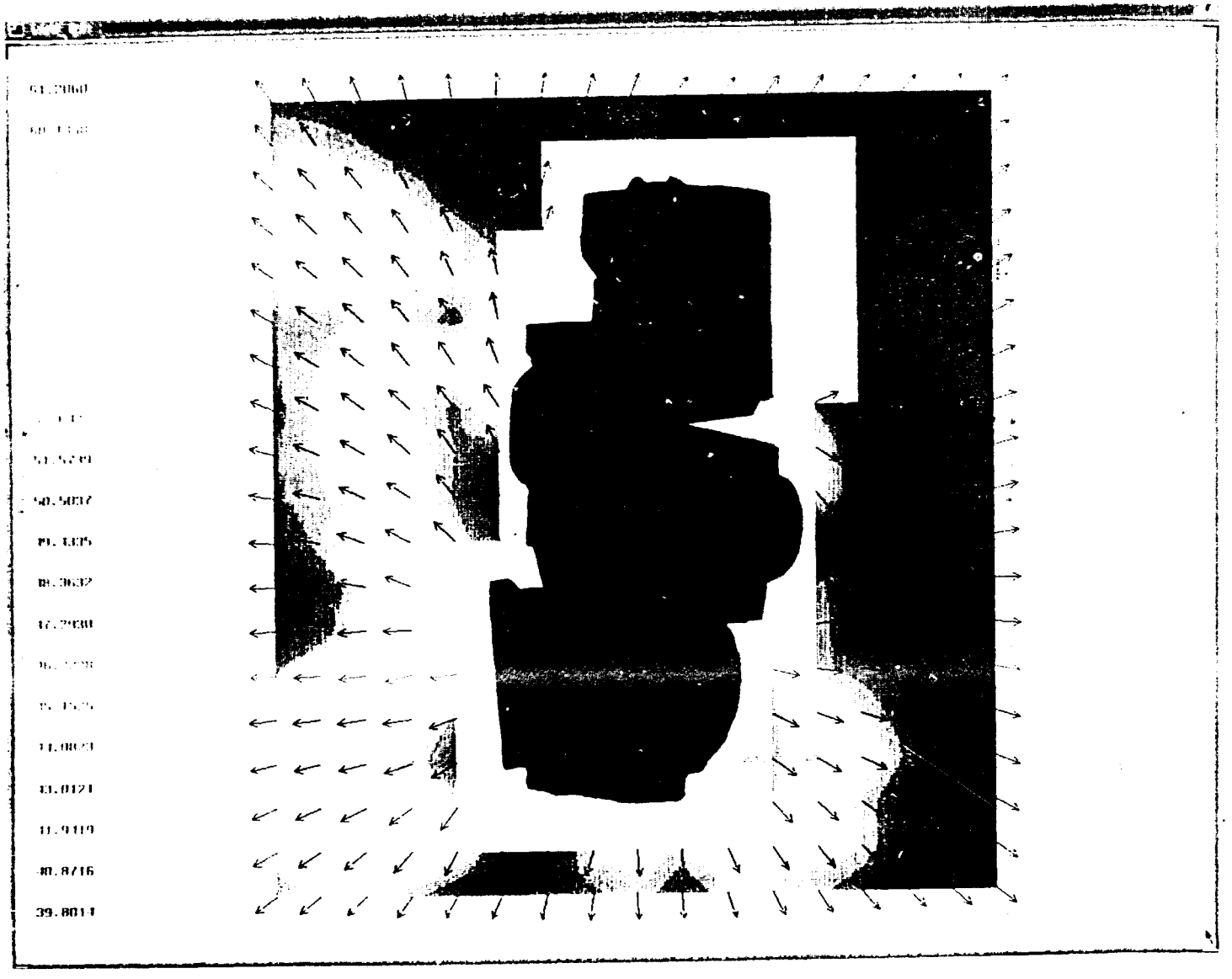

Figure 21. Active Intensity Data of Figure 20 with Color Applied to the Levels

3-D VIEW

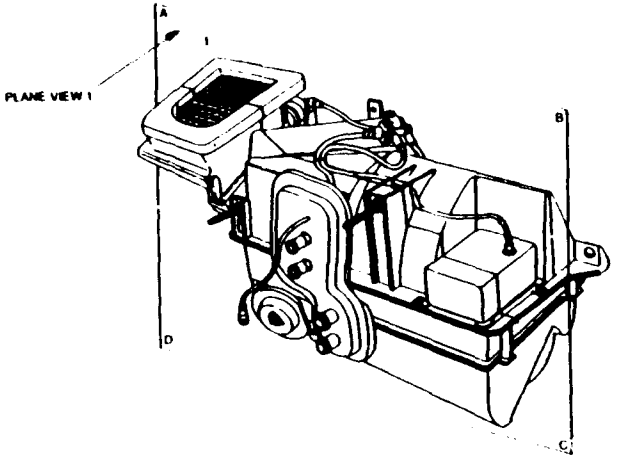

ACTIVE INTENSITY LEVELS AT 2000 Hz IN PLANE 1
Maximum Level: 49.8 dB re 1 x 10^{-12} W/m^2

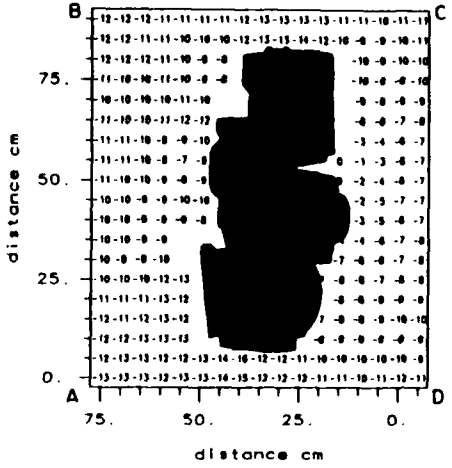

REACTIVE INTENSITY VECTORS AT 2000 Hz IN PLANE 1
Maximum Level: 46.2 dB re 1 x 10^{-12} W/m^2

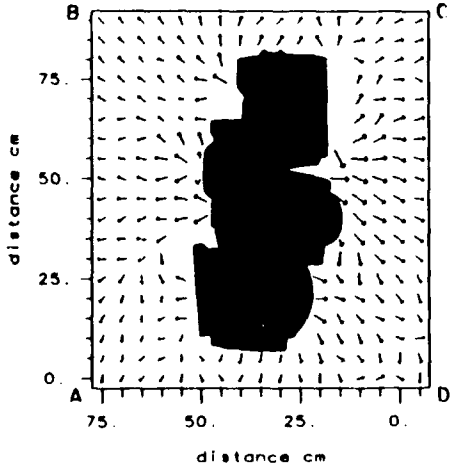

ACTIVE INTENSITY VECTORS AT 2000 Hz IN PLANE 1
Maximum Level: 49.8 dB re 1 x 10^{-12} W/m^2

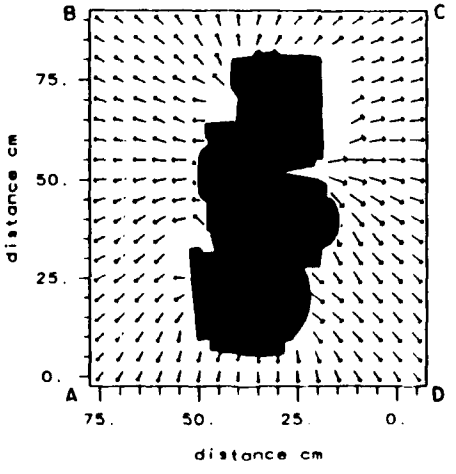

Figure 22. Measurement Plane 1 Intensity Vector Map, 2 kHz, Blower Out

3-D VIEW

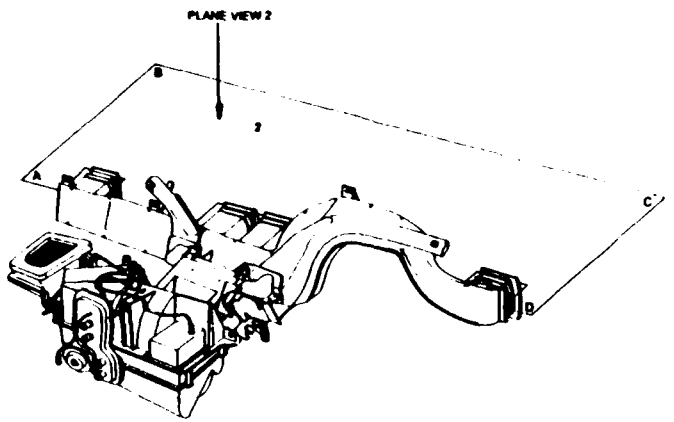

ACTIVE INTENSITY LEVELS AT 250 Hz IN PLANE 2
Maximum Level: 58.0 dB re 1 x 10^{-12} W/m^2

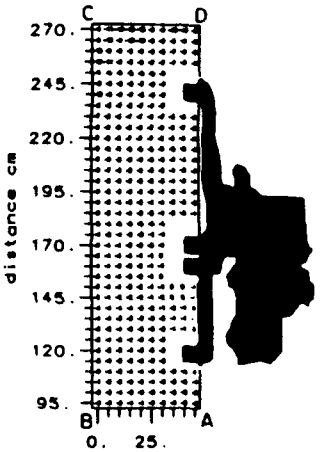

REACTIVE INTENSITY VECTORS AT 250 Hz IN PLANE 2
Maximum Level: 63.3 dB re 1 x 10^{-12} W/m^2

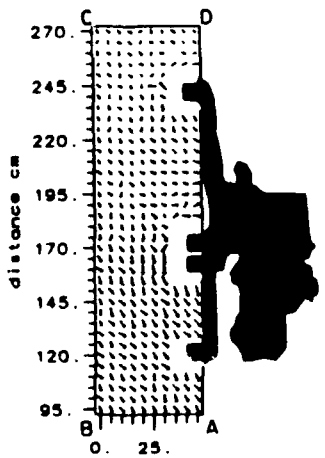

ACTIVE INTENSITY VECTORS AT 250 Hz IN PLANE 2
Maximum Level: 58.0 dB re 1 x 10^{-12} W/m^2

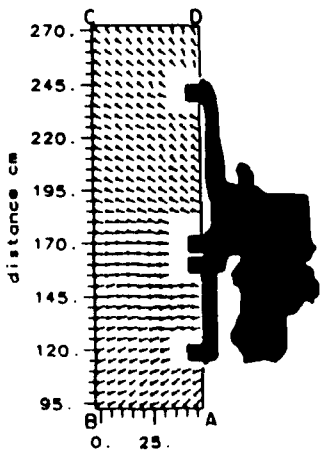

Figure 23. Measurement Plane 2 Intensity Vector Map, 250 Hz, Blower In

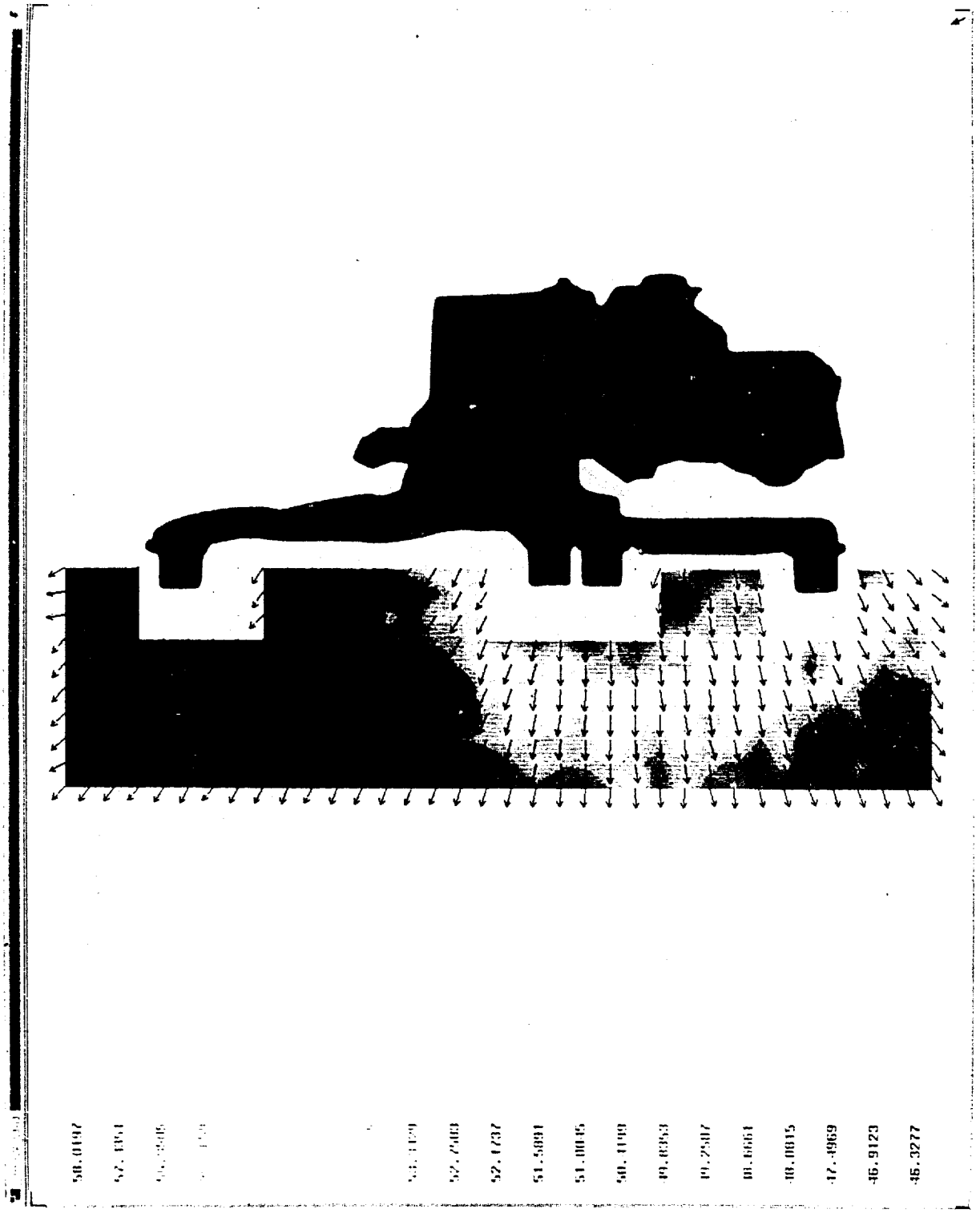

Figure 24. Active Intensity Data of Figure 23 with Color Applied to the Levels

3-D VIEW

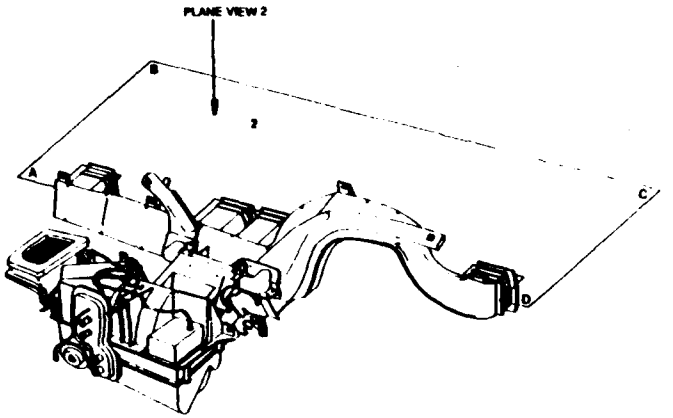

ACTIVE INTENSITY LEVELS AT 500 Hz IN PLANE 2
Maximum Level: 53.4 dB re 1 x 10^{-12} W/m^2

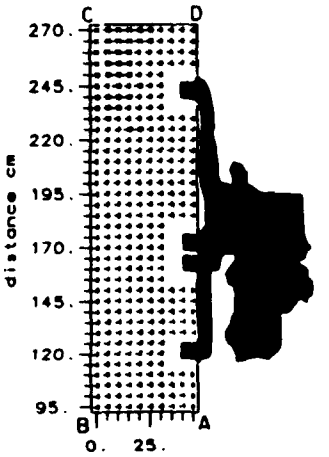

REACTIVE INTENSITY VECTORS AT 500 Hz IN PLANE 2
Maximum Level: 55.4 dB re 1 x 10^{-12} W/m^2

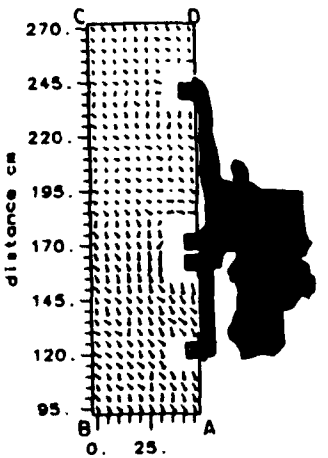

ACTIVE INTENSITY VECTORS AT 500 Hz IN PLANE 2
Maximum Level: 53.4 dB re 1 x 10^{-12} W/m^2

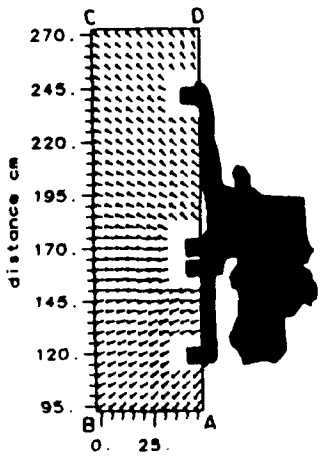

Figure 25. Measurement Plane 2 Intensity Vector Map, 250 Hz, Blower Out

3-D VIEW

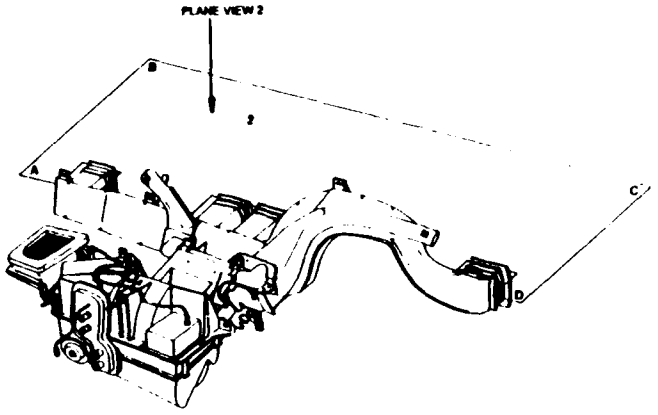

ACTIVE INTENSITY LEVELS AT 250 Hz IN PLANE 2
Maximum Level: 54.6 dB re 1 x 10^{-12} W/m^2

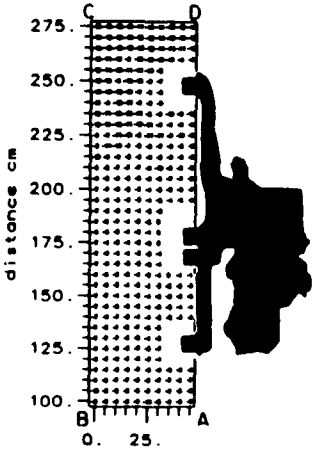

REACTIVE INTENSITY VECTORS AT 250 Hz IN PLANE 2
Maximum Level: 55.9 dB re 1 x 10^{-12} W/m^2

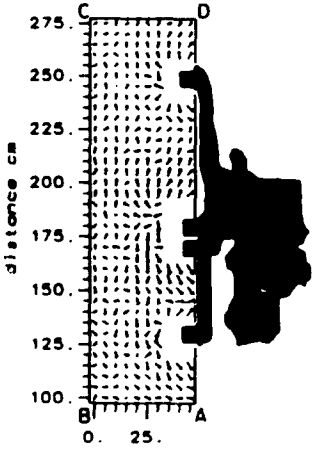

ACTIVE INTENSITY VECTORS AT 250 Hz IN PLANE 2
Maximum Level: 54.6 dB re 1 x 10^{-12} W/m^2

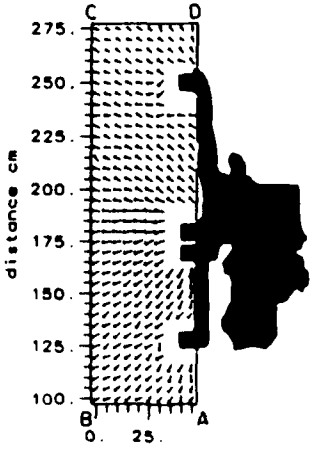

Figure 26. Measurement Plane 2 Intensity Vector Map, 500 Hz, Blower In

3-D VIEW

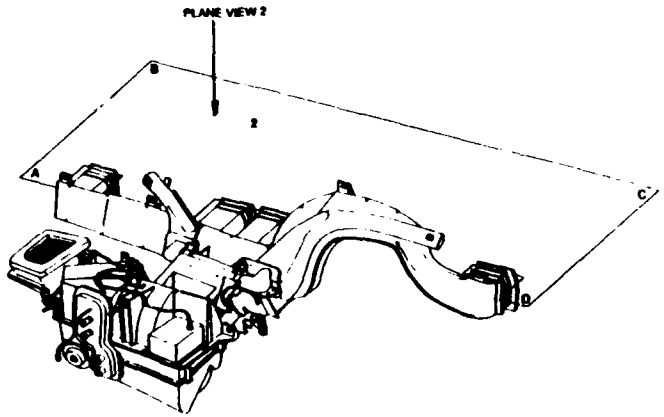

ACTIVE INTENSITY LEVELS AT 500 Hz IN PLANE 2
Maximum Level: 50.3 dB re 1 x 10^{-12} W/m^2

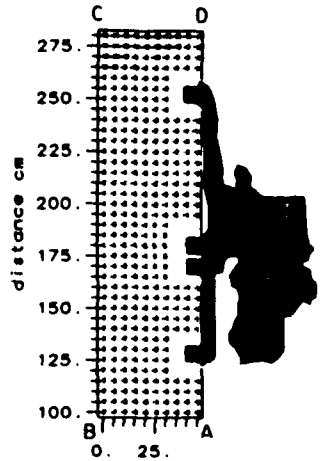

REACTIVE INTENSITY VECTORS AT 500 Hz IN PLANE 2
Maximum Level: 49.5 dB re 1 x 10^{-12} W/m^2

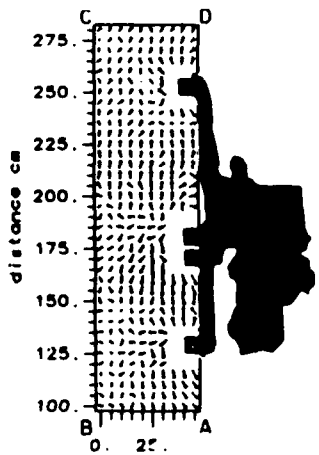

ACTIVE INTENSITY VECTORS AT 500 Hz IN PLANE 2
Maximum Level: 50.3 dB re 1 x 10^{-12} W/m^2

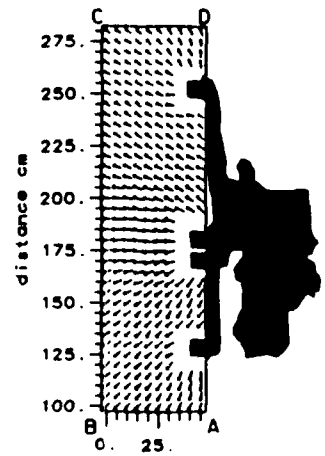

Figure 27. Measurement Plane 2 Intensity Vector Map, 500 Hz, Blower Out

3-D VIEW

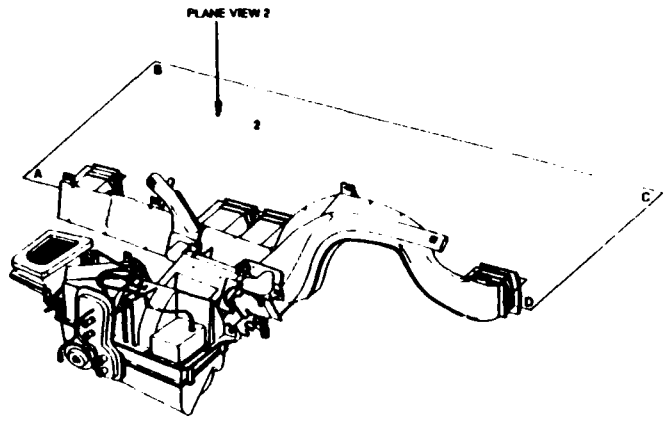

ACTIVE INTENSITY LEVELS AT 1000 Hz IN PLANE 2
Maximum Level: 53.9 dB re 1 x 10^{-12} W/m^2

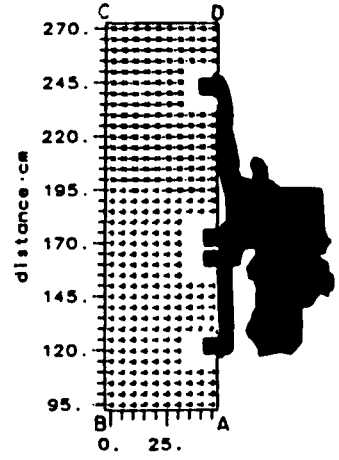

REACTIVE INTENSITY VECTORS AT 1000 Hz IN PLANE 2
Maximum Level: 52.7 dB re 1 x 10^{-12} W/m^2

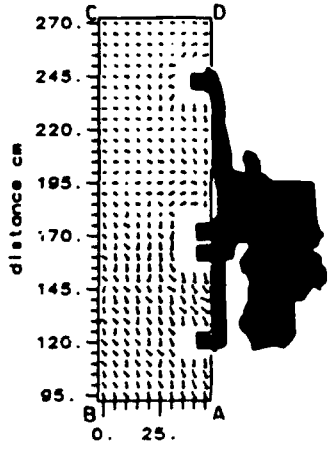

ACTIVE INTENSITY VECTORS AT 1000 Hz IN PLANE 2
Maximum Level: 53.9 dB re 1 x 10^{-12} W/m^2

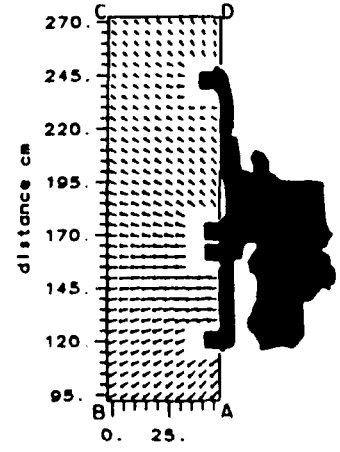

Figure 28. Measurement Plane 2 Intensity Vector Map, 1 kHz, Blower In

3-D VIEW

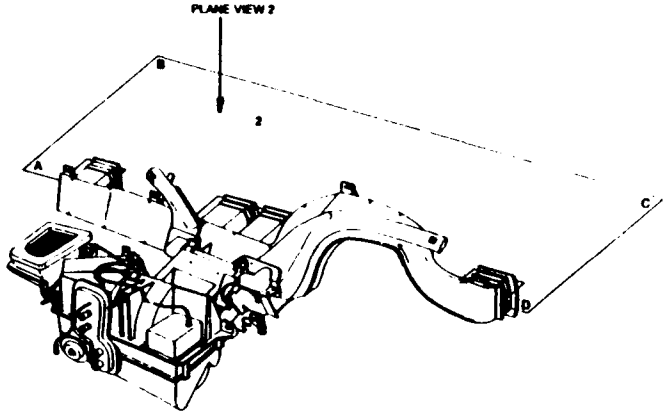

ACTIVE INTENSITY LEVELS AT 2000 Hz IN PLANE 2
Maximum Level: 47.9 dB re 1 x 10^{-12} W/m^2

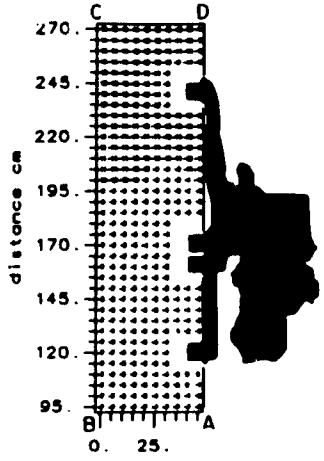

REACTIVE INTENSITY VECTORS AT 2000 Hz IN PLANE 2
Maximum Level: 42.2 dB re 1 x 10^{-12} W/m^2

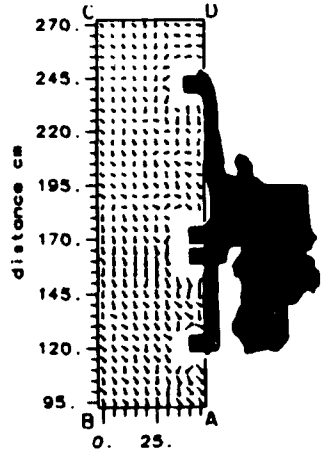

ACTIVE INTENSITY VECTORS AT 2000 Hz IN PLANE 2
Maximum Level: 47.9 dB re 1 x 10^{-12} W/m^2

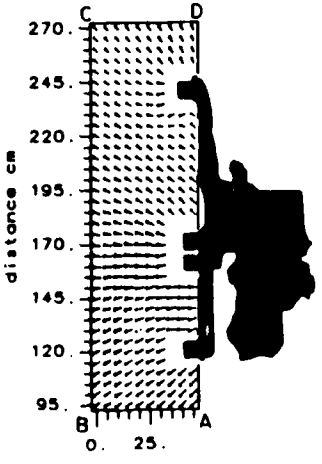

Figure 29. Measurement Plane 2 Intensity Vector Map, 2 kHz, Blower In

3-D VIEW

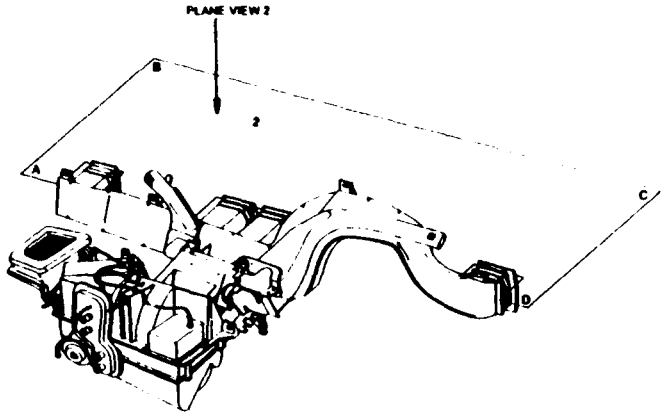

ACTIVE INTENSITY LEVELS AT 2000 Hz IN PLANE 2
Maximum Level: 44.4 dB re 1 x 10^{-12} W/m^2

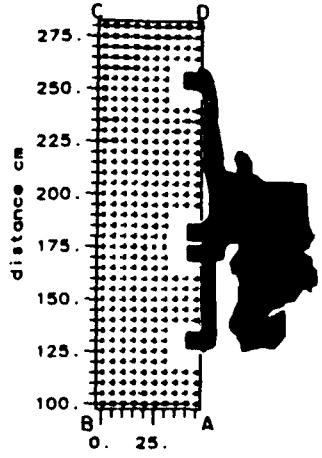

REACTIVE INTENSITY VECTORS AT 2000 Hz IN PLANE 2
Maximum Level: 36.5 dB re 1 x 10^{-12} W/m^2

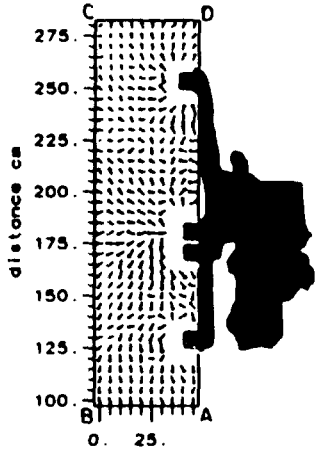

ACTIVE INTENSITY VECTORS AT 2000 Hz IN PLANE 2
Maximum Level: 44.4 dB re 1 x 10^{-12} W/m^2

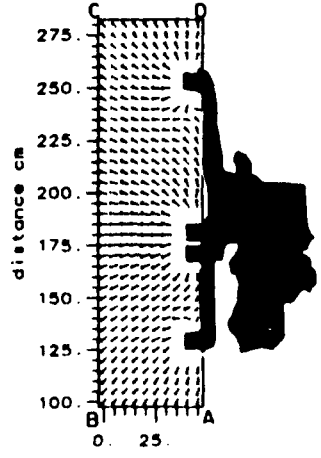

Figure 30. Measurement Plane 2 Intensity Vector Map, 2 kHz, Blower Out

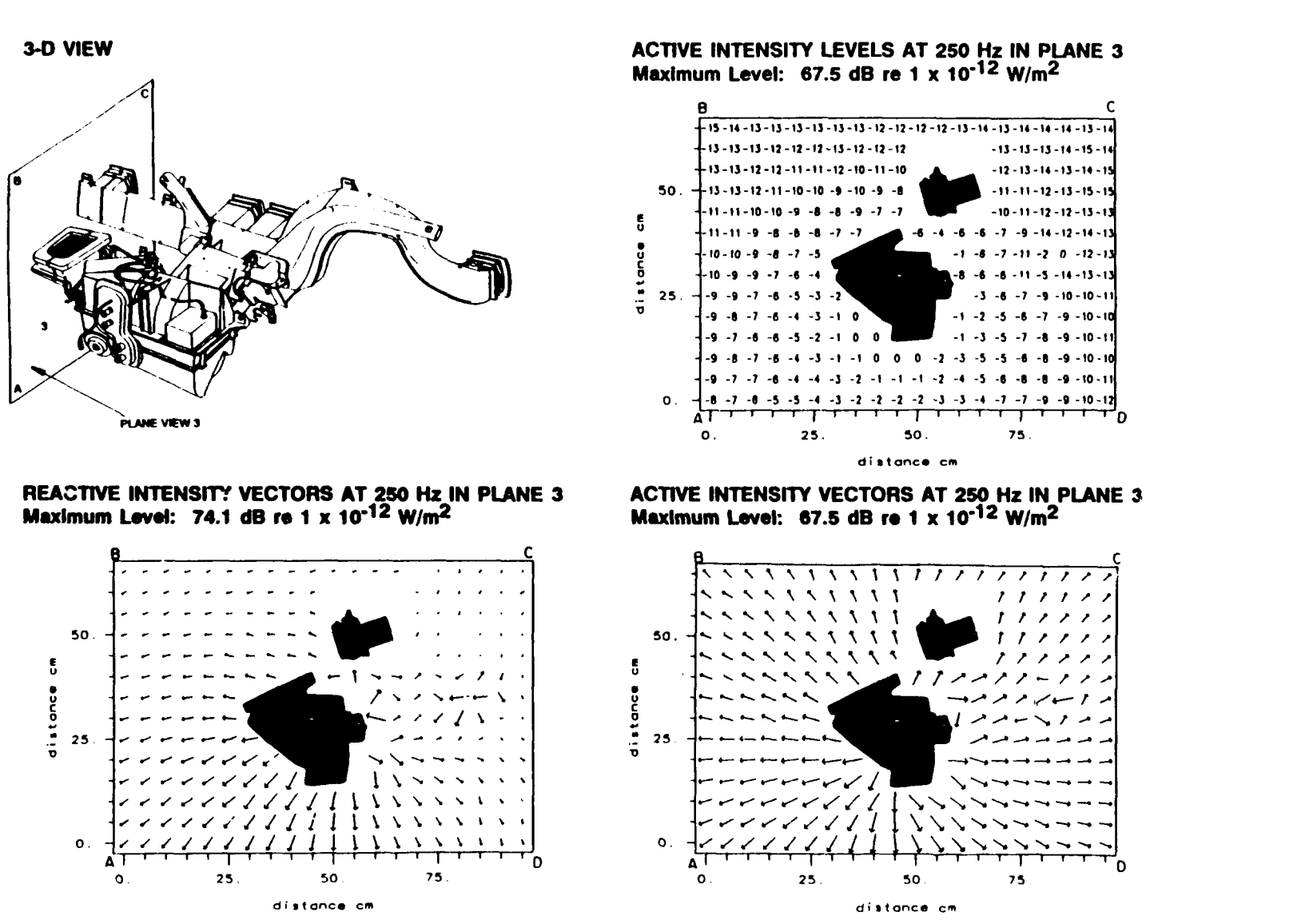

Figure 31. Measurement Plane 3 Intensity Vector Map, 250 Hz, Blower In

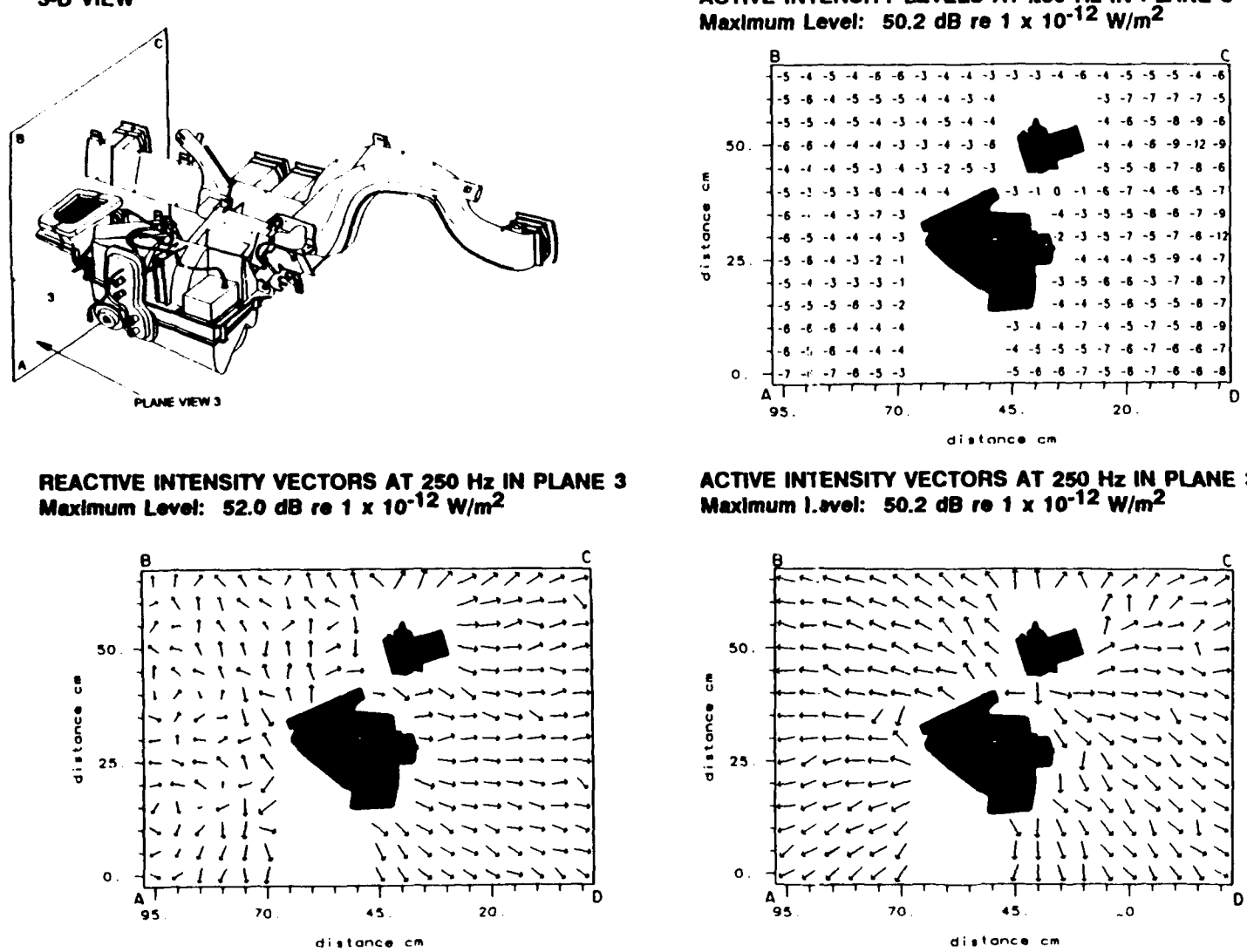

Figure 32. Measurement Plane 3 Intensity Vector Map, 250 Hz, Blower Out

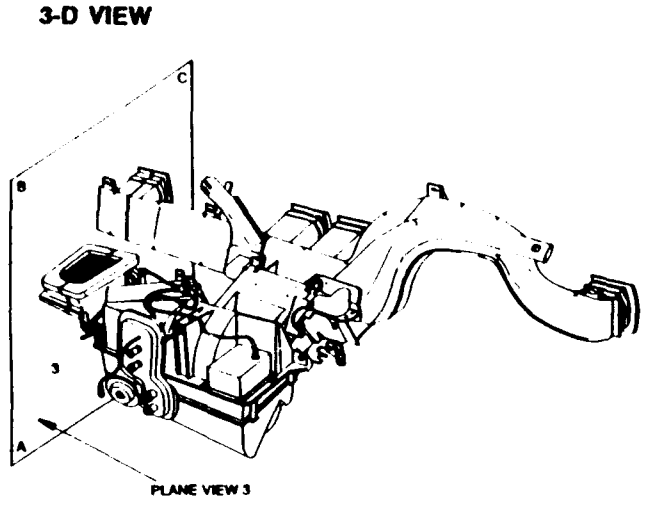

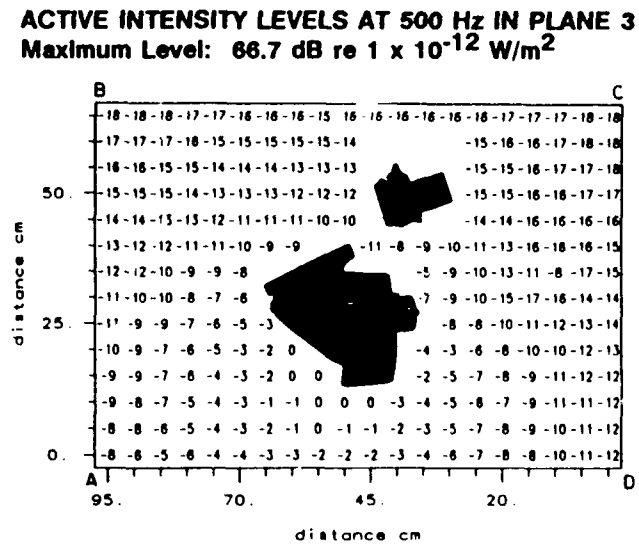

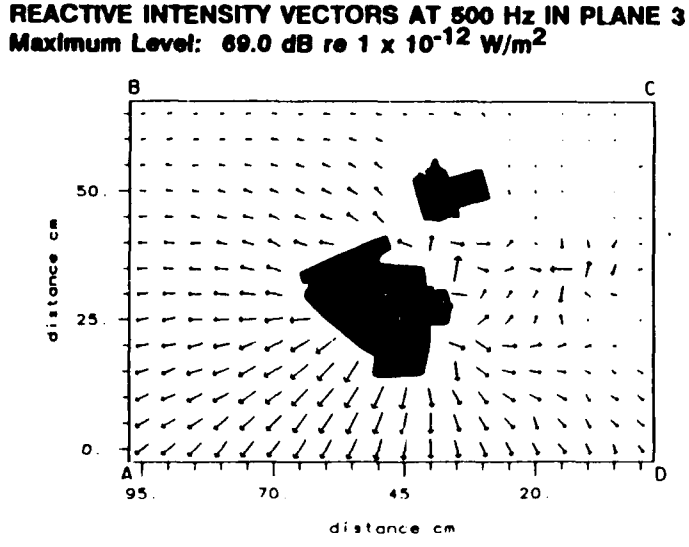

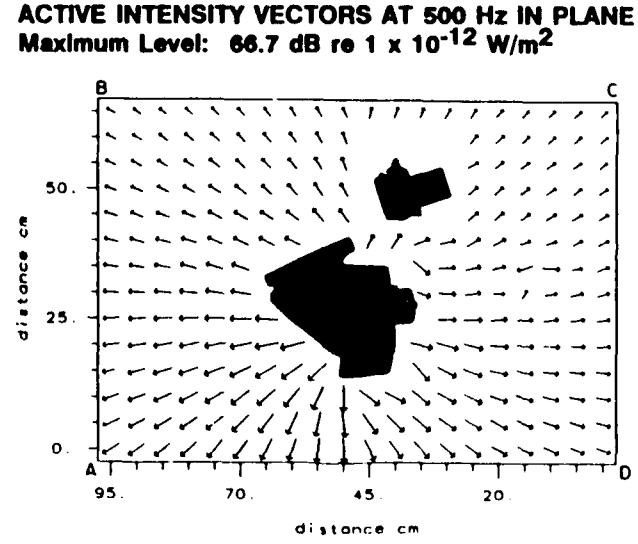

Figure 33. Measurement Plane 3 Intensity Vector Map, 500 Hz, Blower In

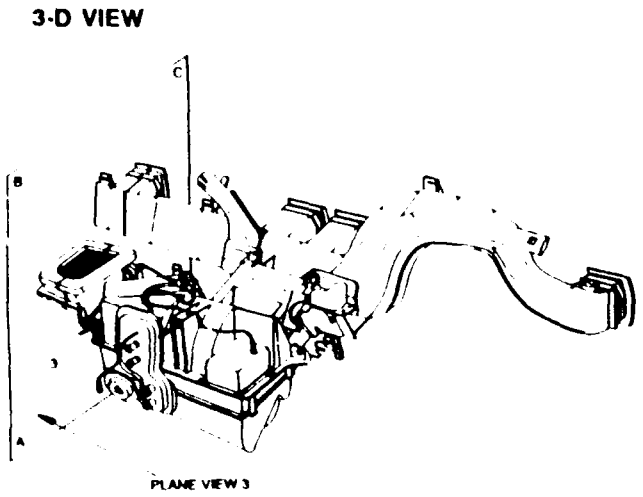

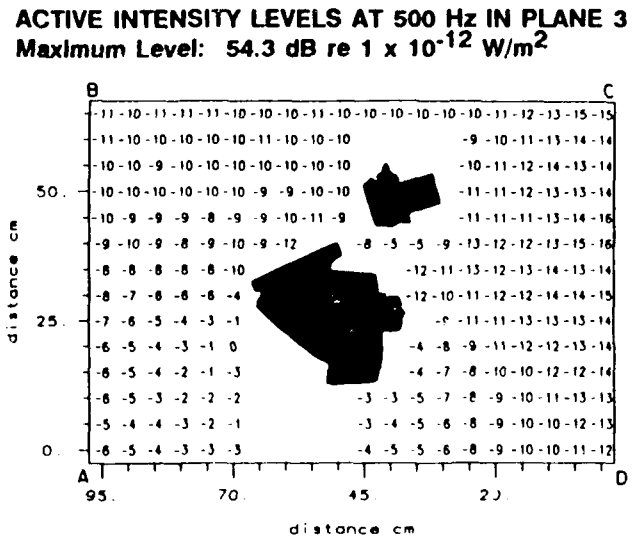

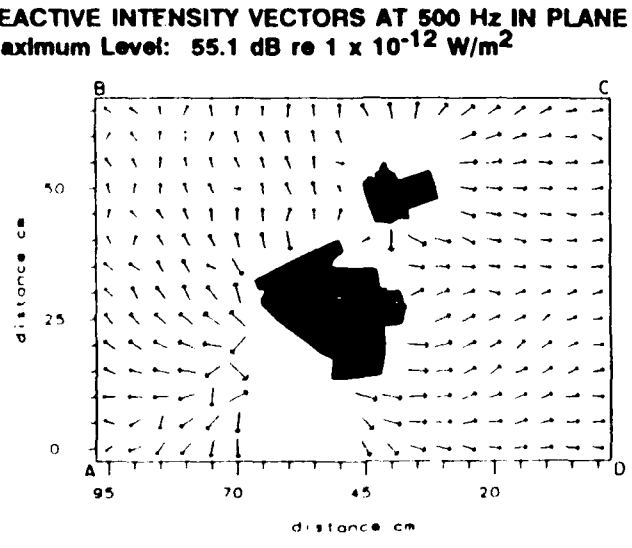

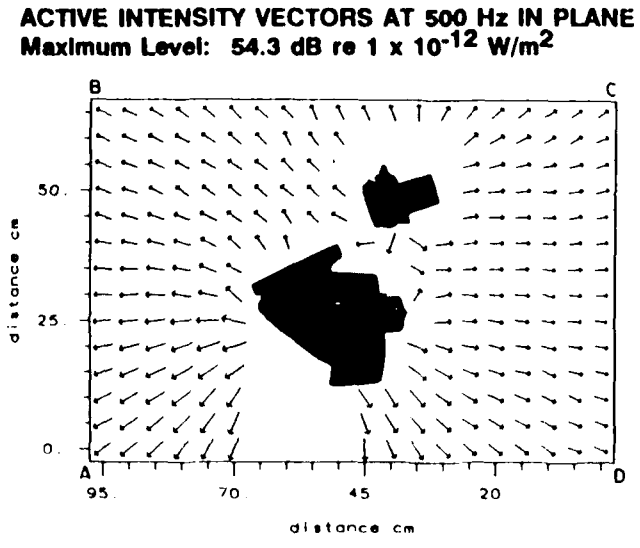

Figure 34. Measurement Plane 3 Intensity Vector Map, 500 Hz, Blower Out

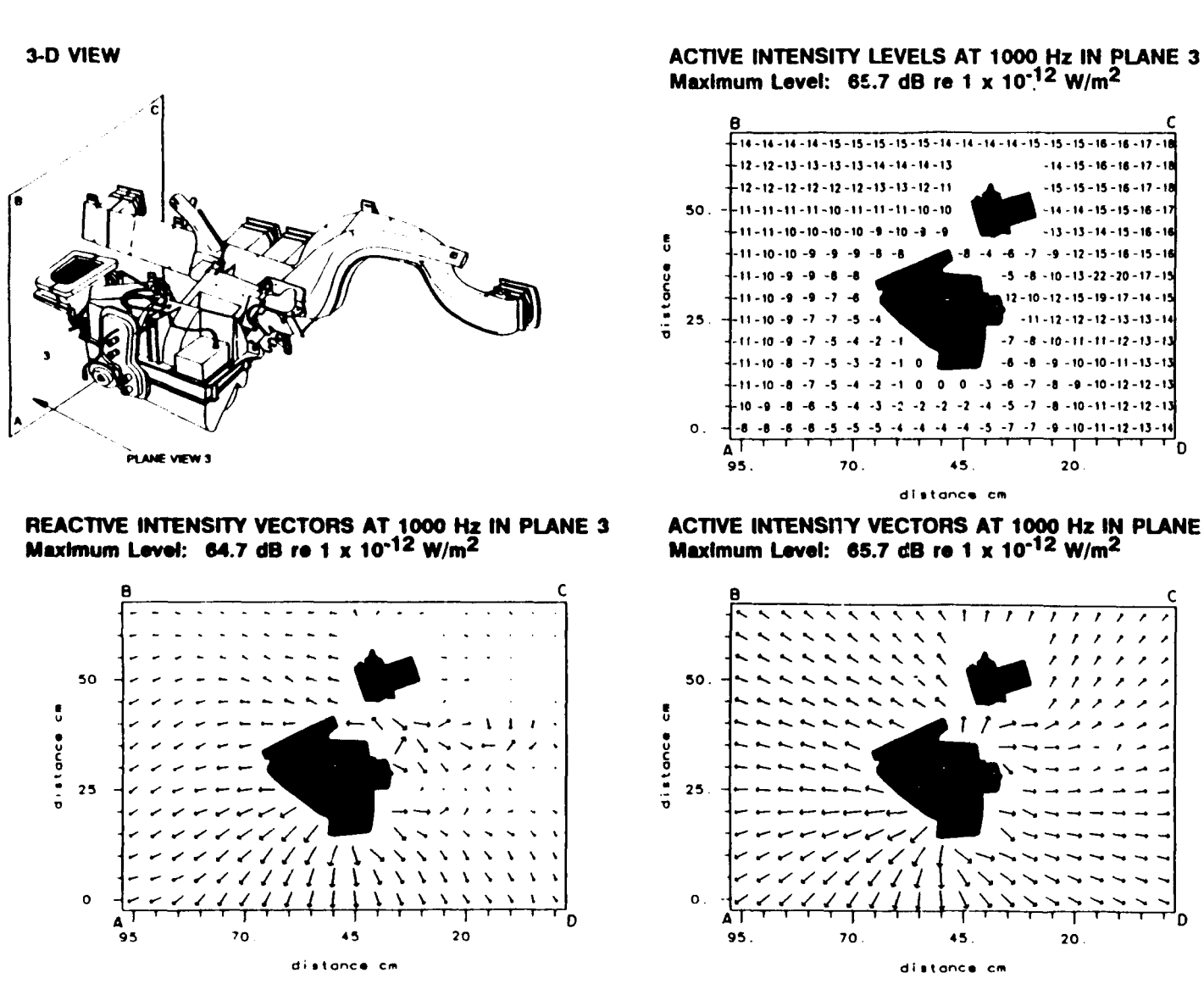

Figure 35. Measurement Plane 3 Intensity Vector Map, 1 kHz, Blower In

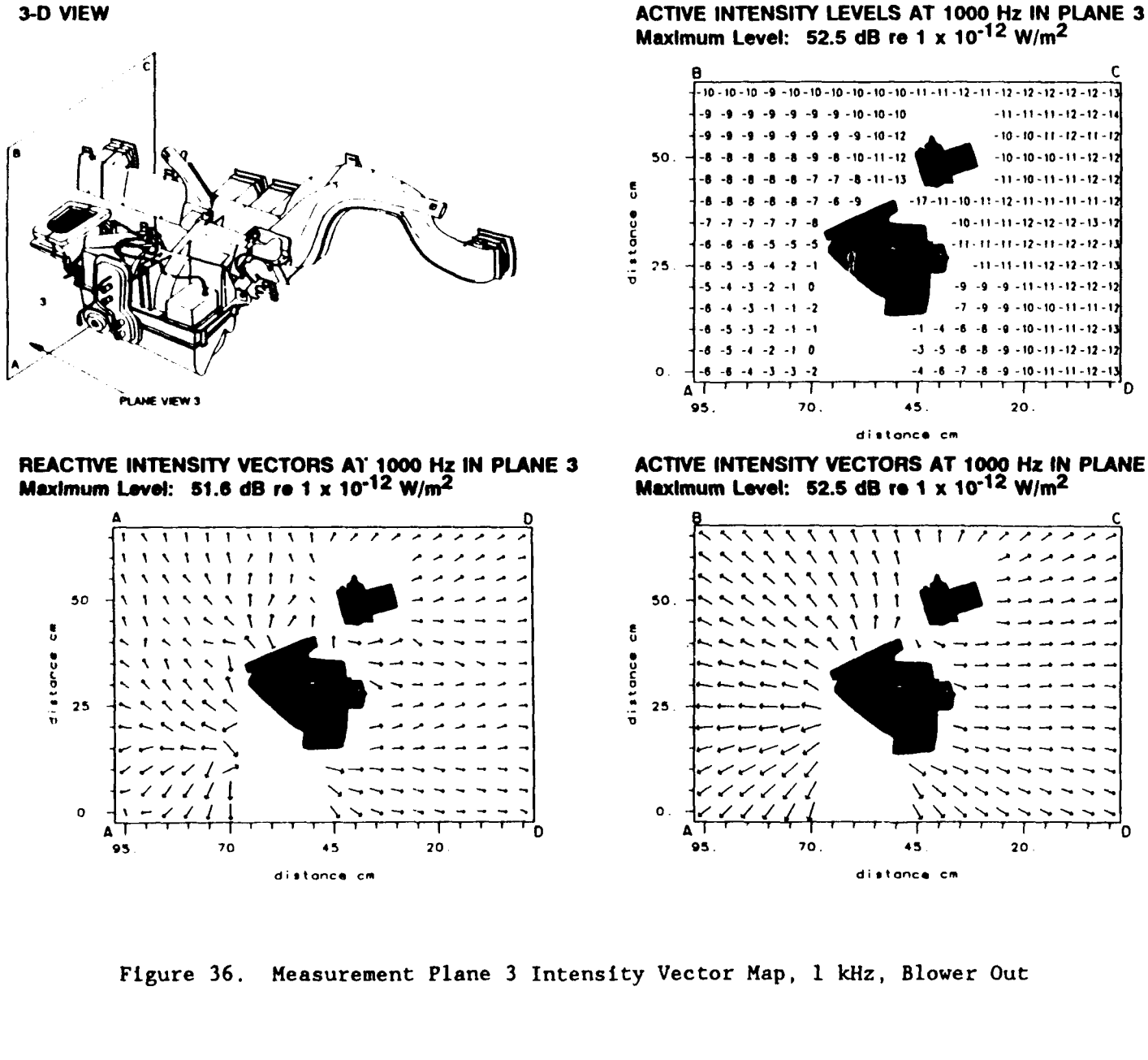

Figure 36. Measurement Plane 3 Intensity Vector Map, 1 kHz, Blower Out

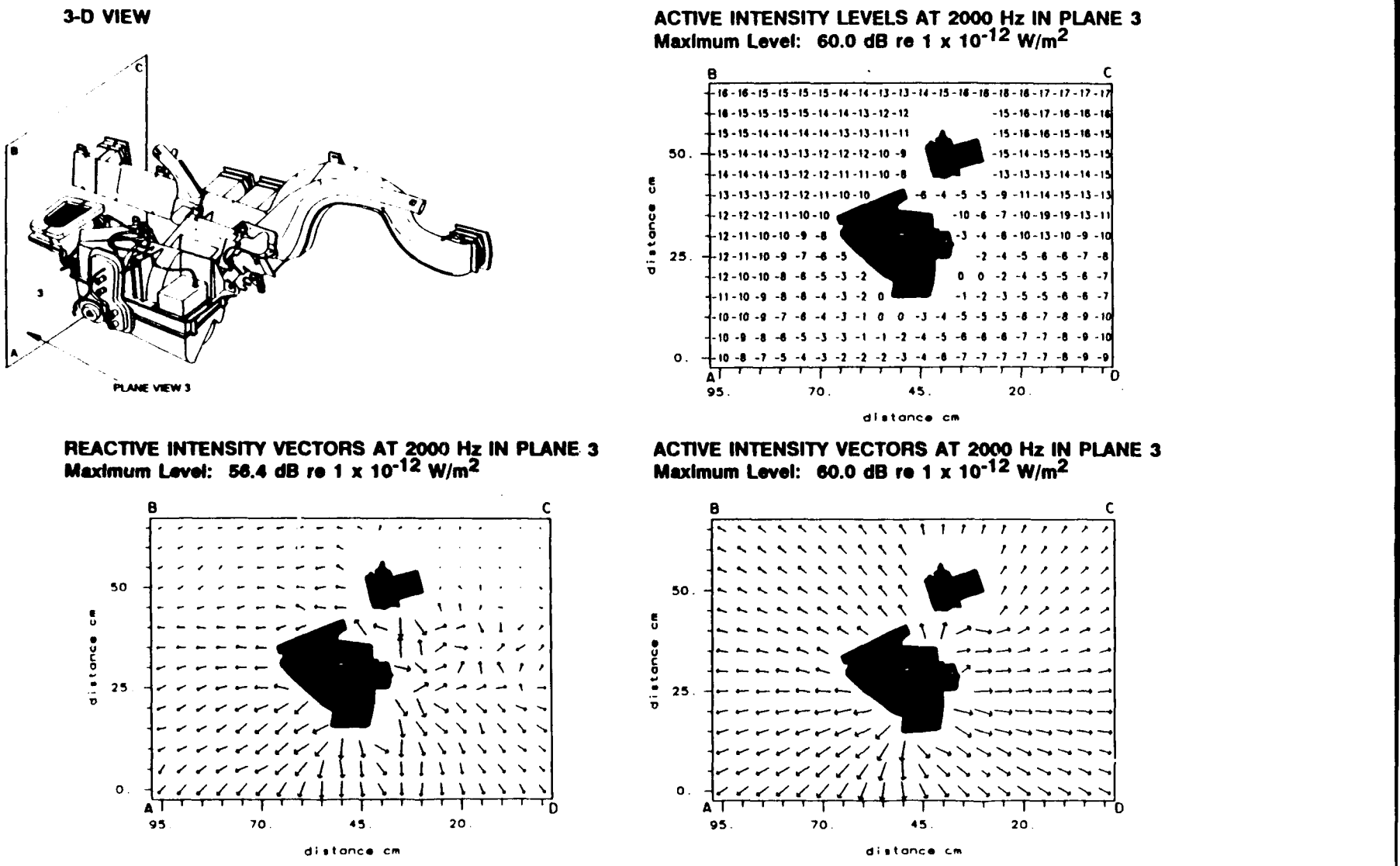

Figure 37. Measurement Plane 3 Intensity Vector Map, 2 kHz, Blower In

3-D VIEW

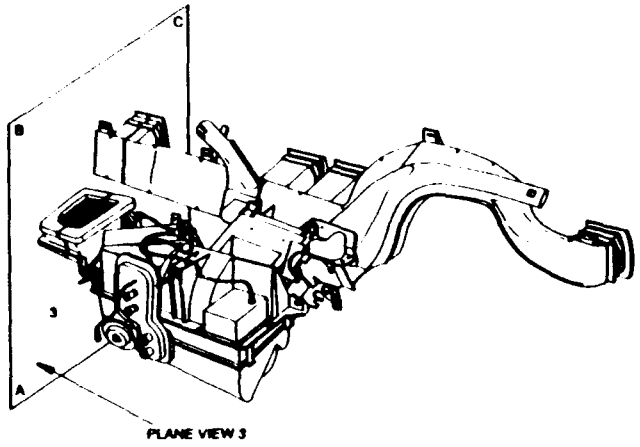

ACTIVE INTENSITY LEVELS AT 2000 Hz IN PLANE 3
Maximum Level: 54.5 dB re 1 x 10^{-12} W/m^2

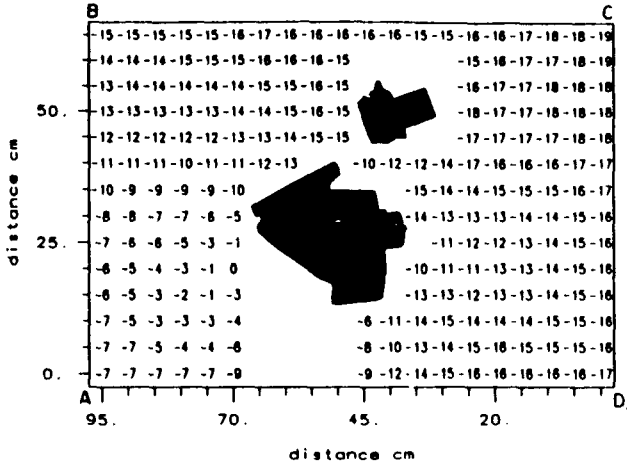

REACTIVE INTENSITY VECTORS AT 2000 Hz IN PLANE 3
Maximum Level: 49.6 dB re 1 x 10^{-12} W/m^2

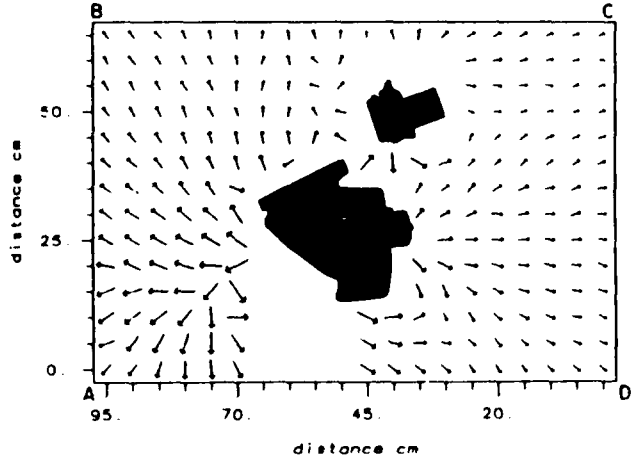

ACTIVE INTENSITY VECTORS AT 2000 Hz IN PLANE 3
Maximum Level: 54.5 dB re 1 x 10^{-12} W/m^2

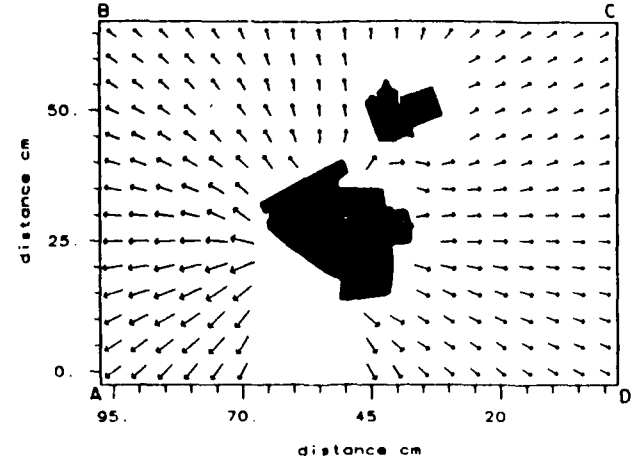

Figure 38. Measurement Plane 3 Intensity Vector Map, 2 kHz, Blower Out

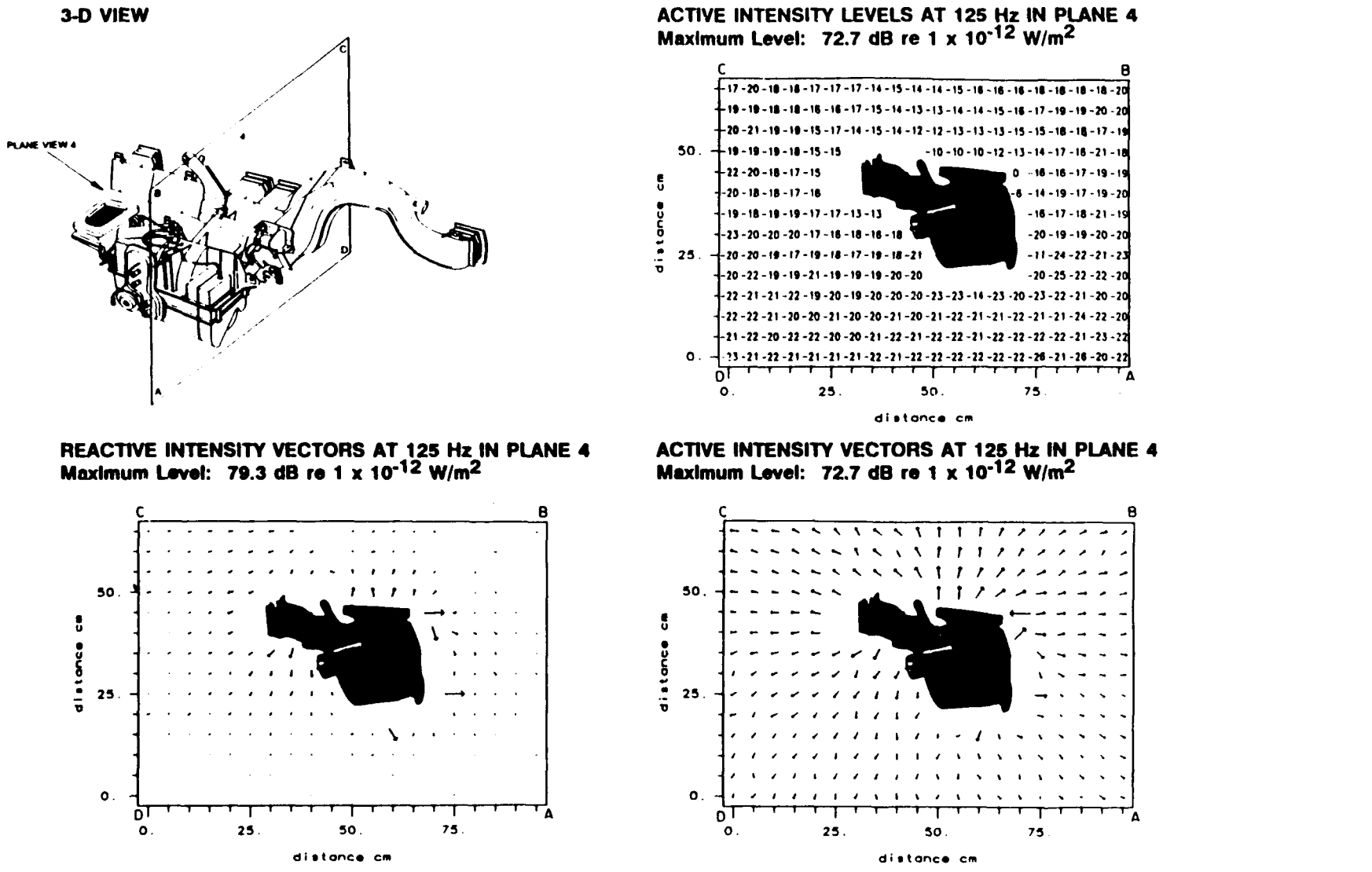

Figure 39. Measurement Plane 4 Intensity Vector Map, 125 Hz

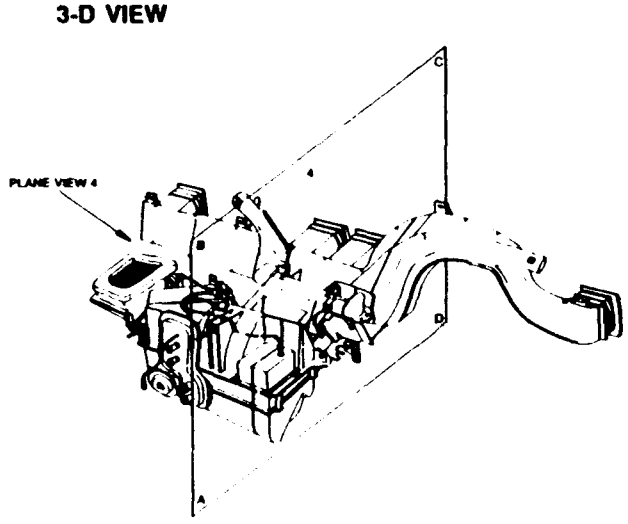

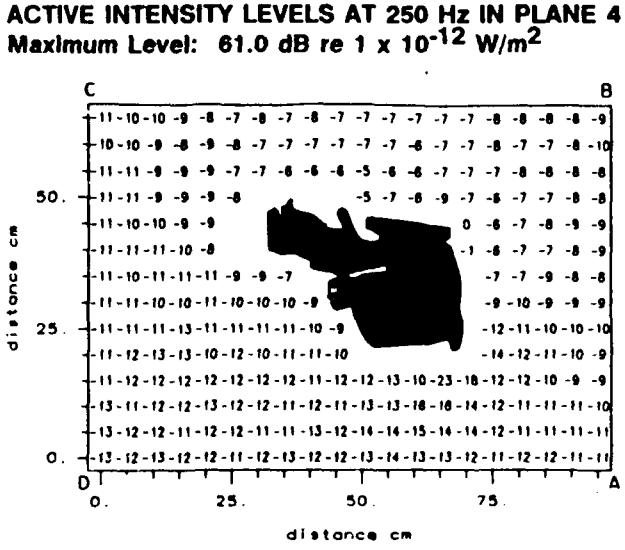

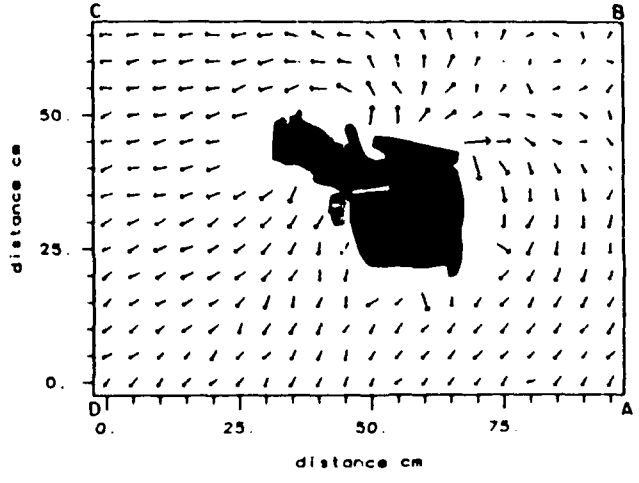

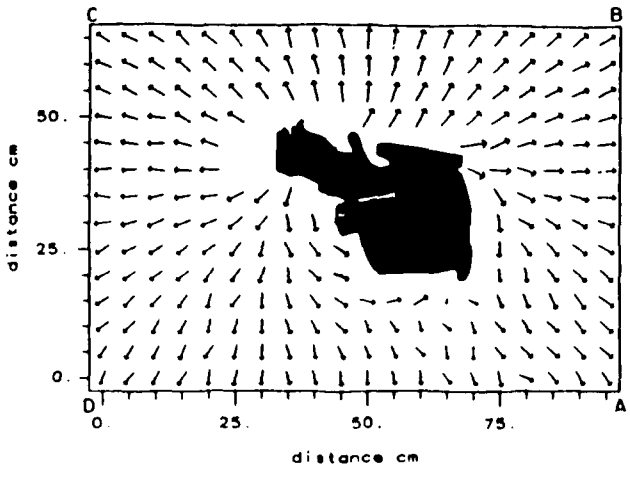

Figure 40. Measurement Plane 4 Intensity Vector Map, 250 Hz

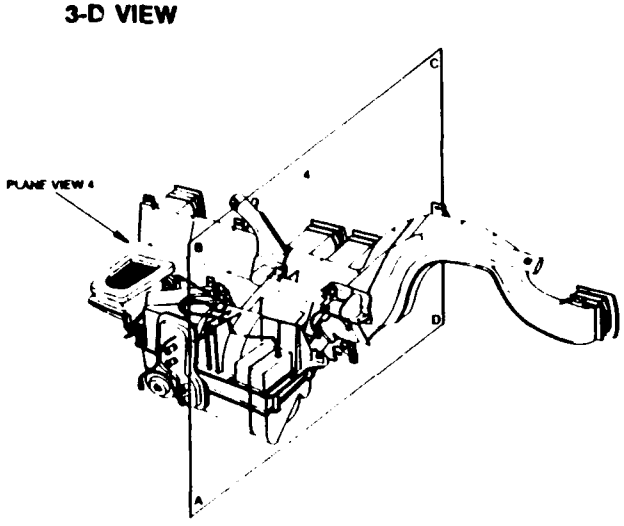

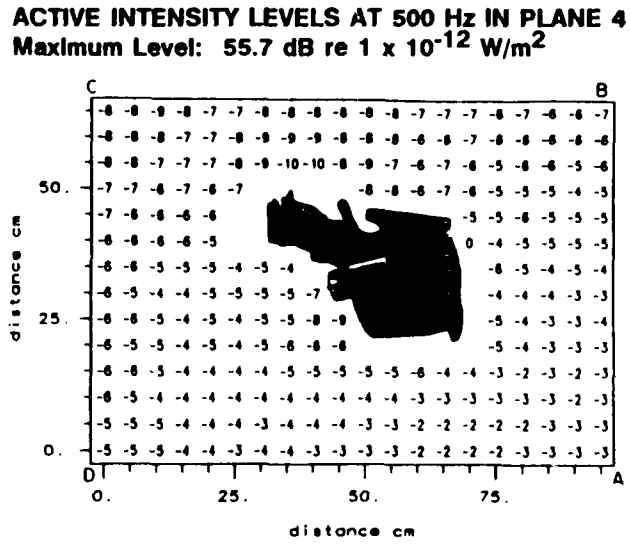

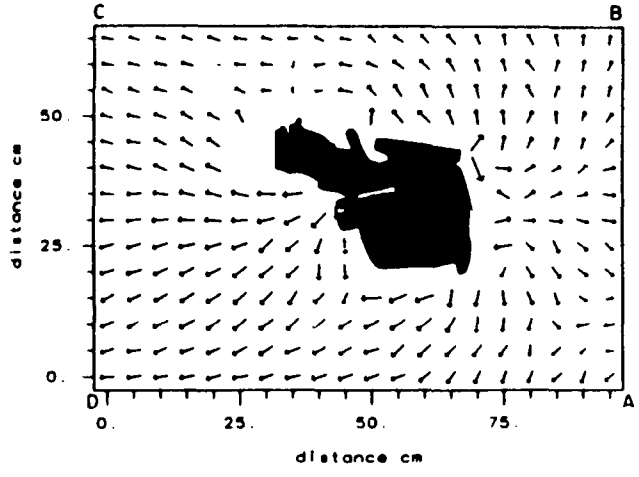

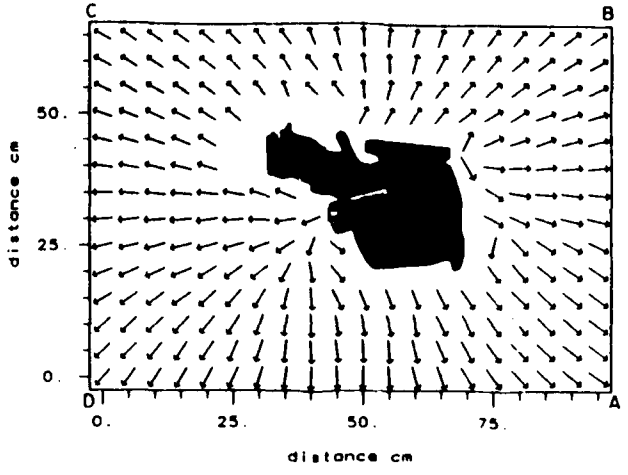

Figure 41. Measurement Plane 4 Intensity Vector Map, 500 Hz

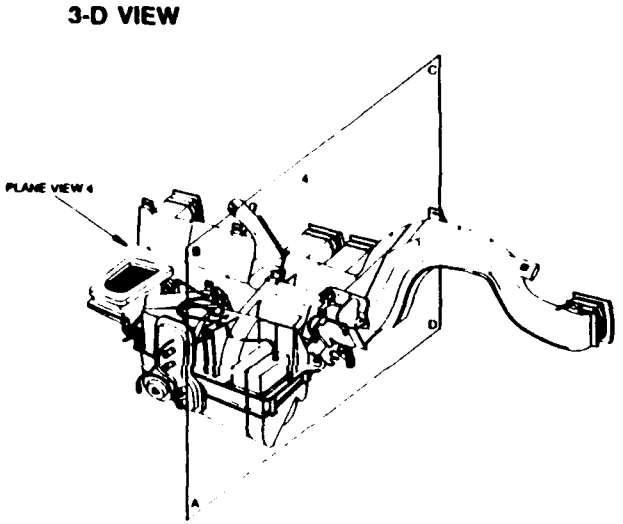

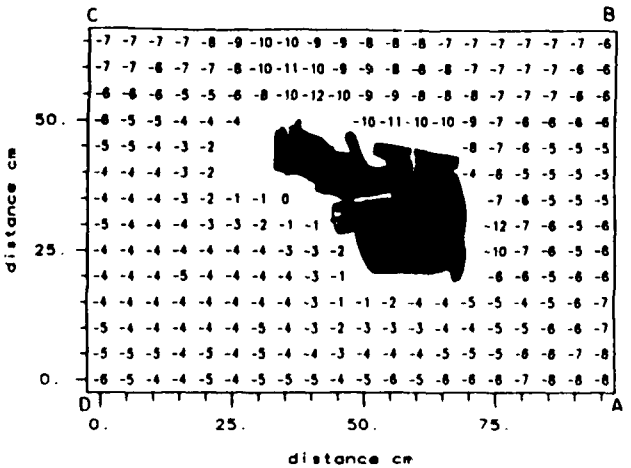

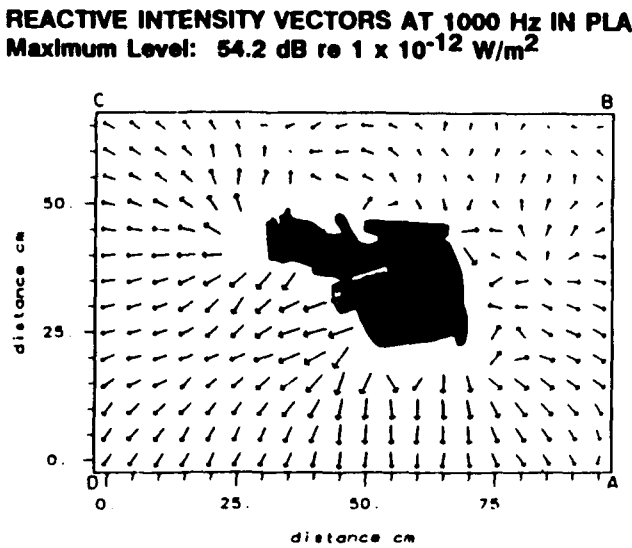

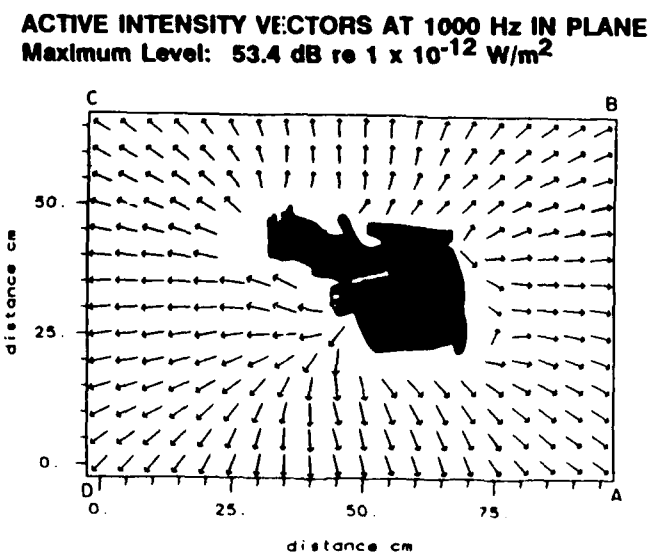

Figure 42. Measurement Plane 4 Intensity Vector Map, 1 kHz

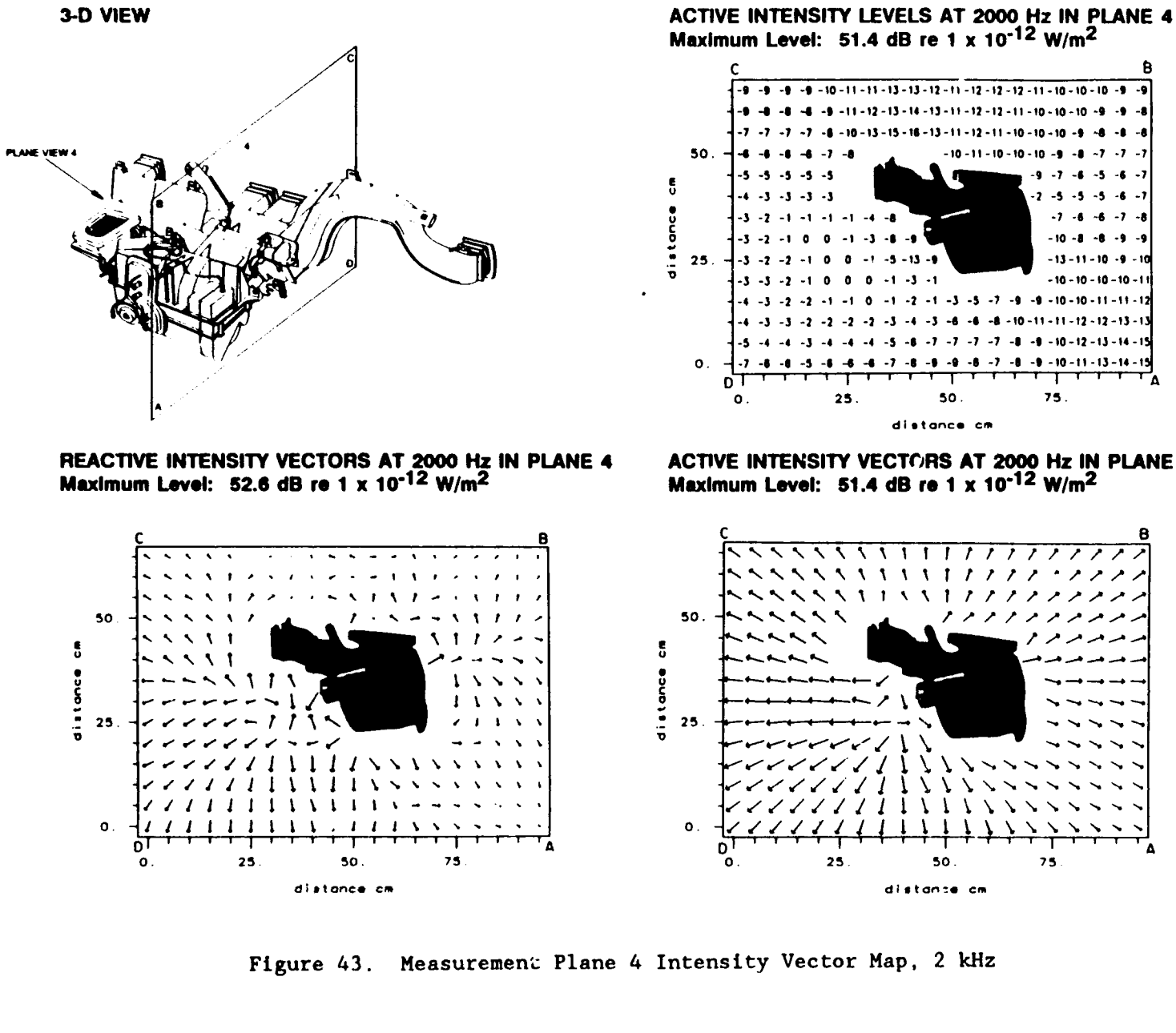

Figure 43. Measurement Plane 4 Intensity Vector Map, 2 kHz

3-D VIEW

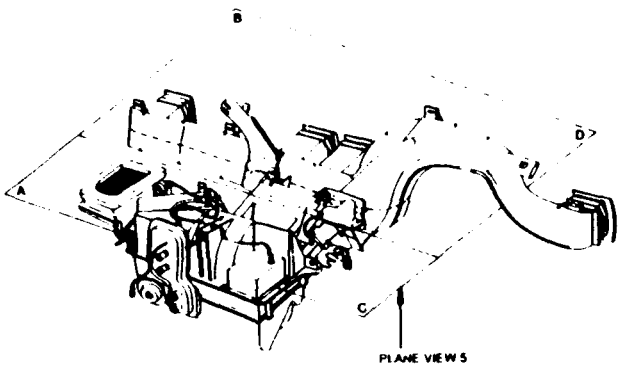

ACTIVE INTENSITY LEVELS AT 250 Hz IN PLANE 5
Maximum Level: 60.2 dB re 1 x 10^{-12} W/m^2

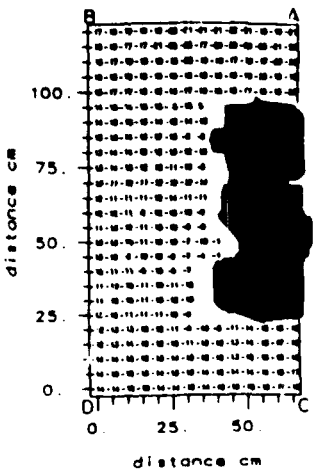

REACTIVE INTENSITY VECTORS AT 250 Hz IN PLANE 5
Maximum Level: 70.5 dB re 1 x 10^{-12} W/m^2

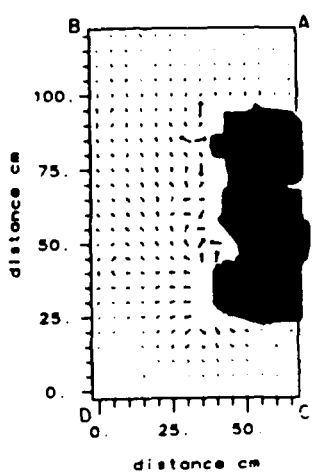

ACTIVE INTENSITY VECTORS AT 250 Hz IN PLANE 5
Maximum Level: 60.2 dB re 1 x 10^{-12} W/m^2

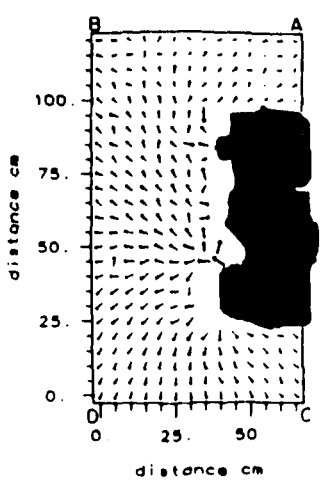

Figure 44. Measurement Plane 5 Intensity Vector Map, 250 Hz

3-D VIEW

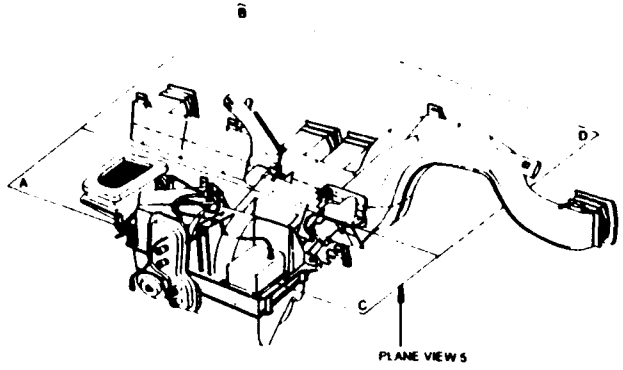

ACTIVE INTENSITY LEVELS AT 500 Hz IN PLANE 5
Maximum Level: 54.1 dB re 1 x 10^{-12} W/m^2

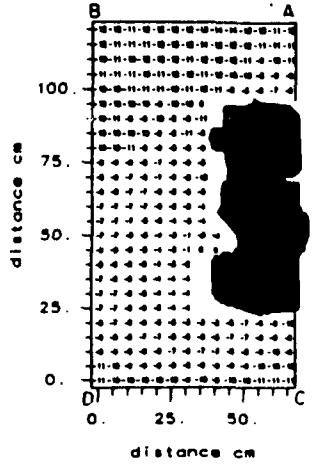

REACTIVE INTENSITY VECTORS AT 500 Hz IN PLANE 5
Maximum Level: 62.9 dB re 1 x 10^{-12} W/m^2

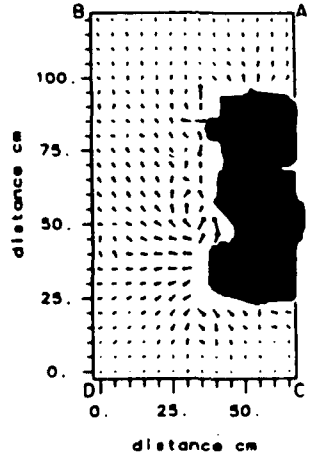

ACTIVE INTENSITY VECTORS AT 500 Hz IN PLANE 5
Maximum Level: 54.1 dB re 1 x 10^{-12} W/m^2

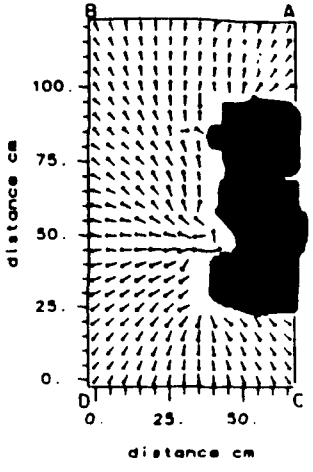

Figure 45. Measurement Plane 5 Intensity Vector Map, 500 Hz

3-D VIEW

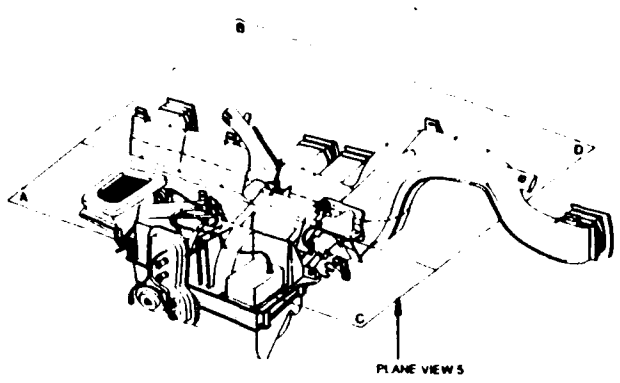

ACTIVE INTENSITY LEVELS AT 1000 Hz IN PLANE 5
Maximum Level: 53.3 dB re 1 x 10^{-12} W/m^2

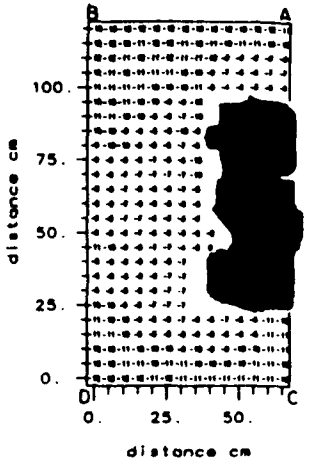

REACTIVE INTENSITY VECTORS AT 1000 Hz IN PLANE 5
Maximum Level: 56.5 dB re 1 x 10^{-12} W/m^2

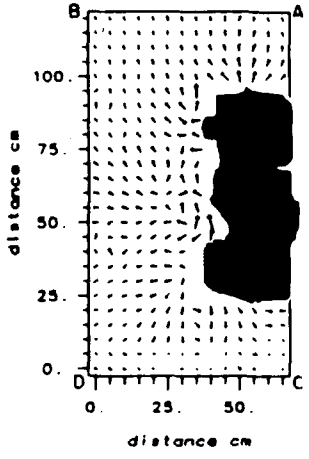

ACTIVE INTENSITY VECTORS AT 1000 Hz IN PLANE 5
Maximum Level: 53.3 dB re 1 x 10^{-12} W/m^2

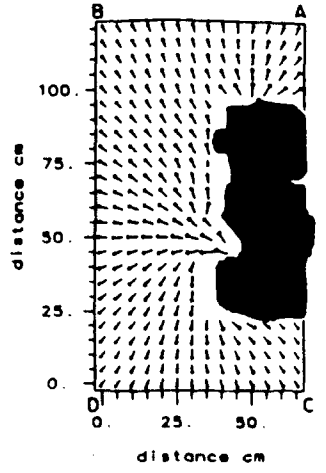

Figure 46. Measurement Plane 5 Intensity Vector Map, 1 kHz

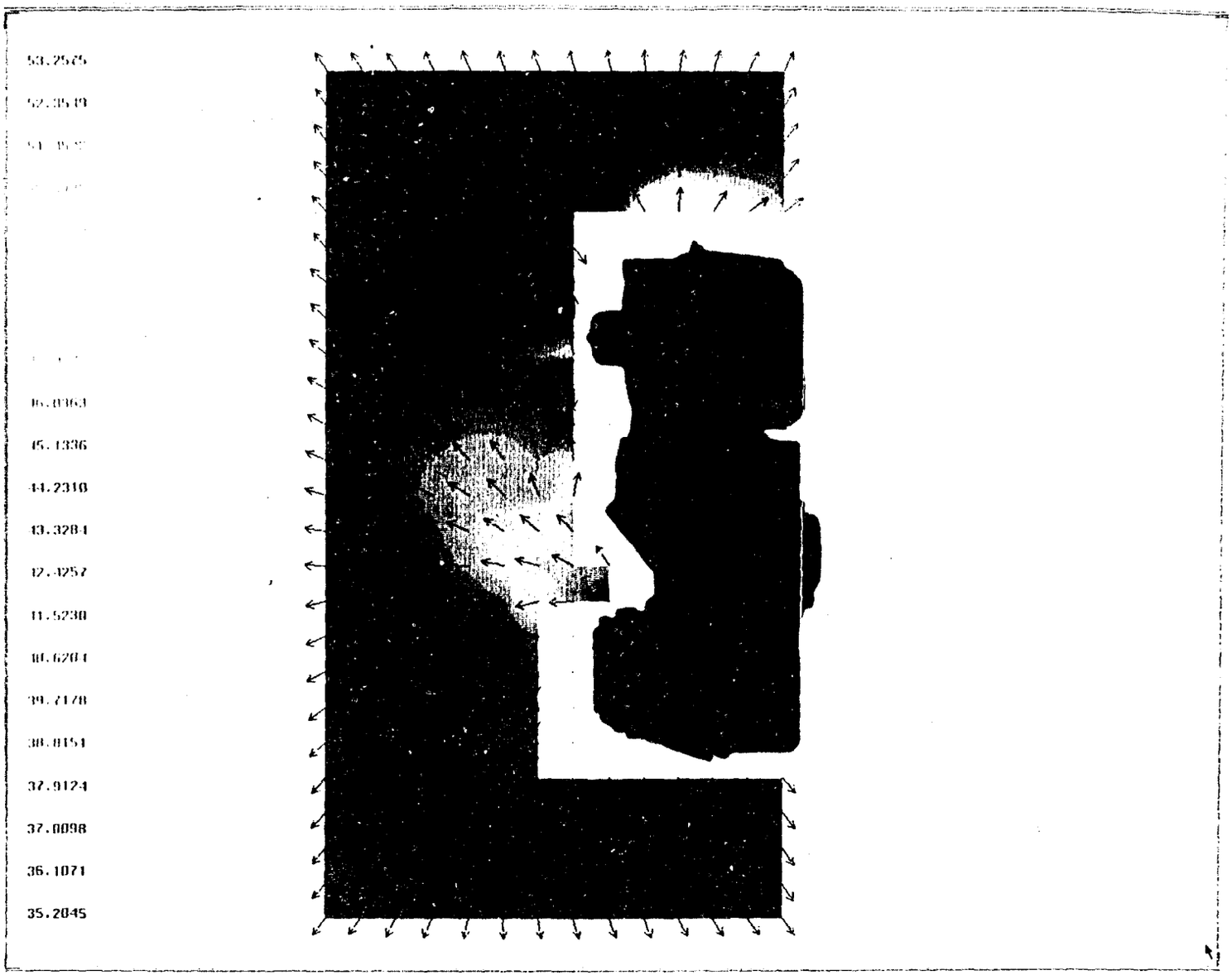

Figure 47. Active Intensity Data of Figure 46 with Color Applied to the Levels

3-D VIEW

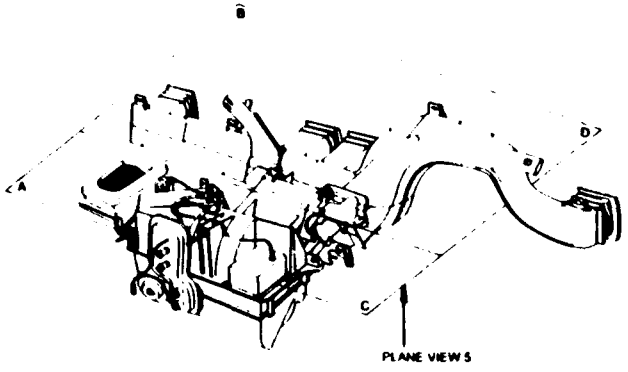

ACTIVE INTENSITY LEVELS AT 2000 Hz IN PLANE 5
Maximum Level: 48.4 dB re 1 x 10^{-12} W/m^2

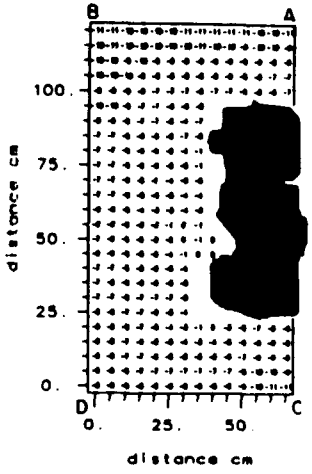

REACTIVE INTENSITY VECTORS AT 2000 Hz IN PLANE 5
Maximum Level: 50.9 dB re 1 x 10^{-12} W/m^2

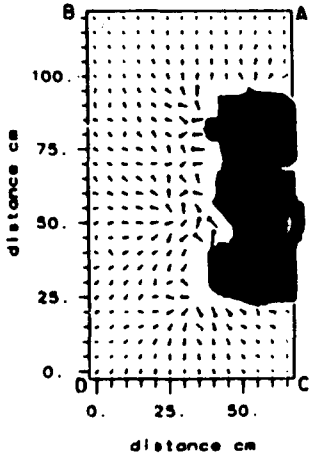

ACTIVE INTENSITY VECTORS AT 2000 Hz IN PLANE 5
Maximum Level: 46.4 dB re 1 x 10^{-12} W/m^2

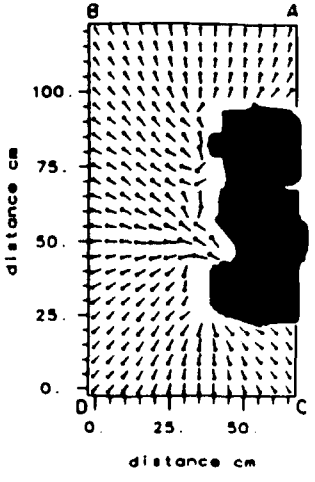

Figure 48. Measurement Plane 5 Intensity Vector Map, 2 kHz

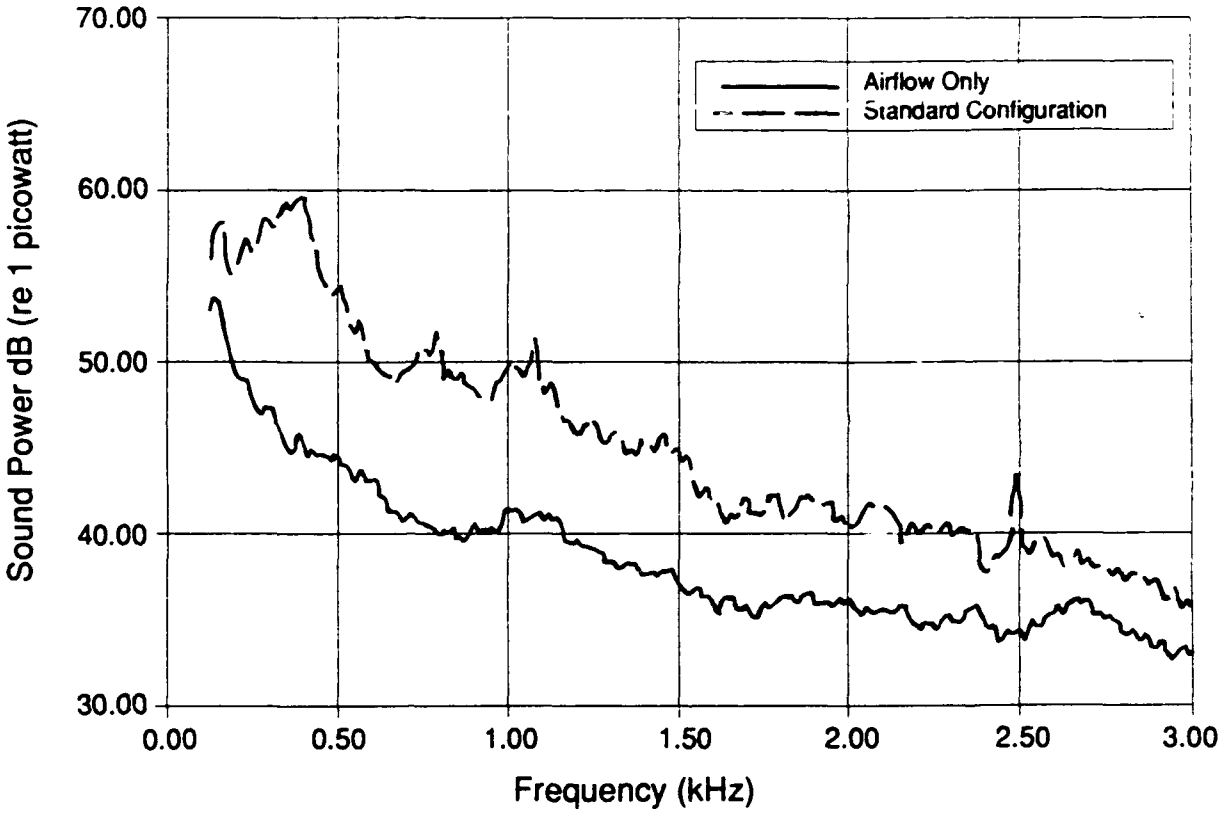

Figure 49. Sound Power Radiated by the HVAC System Operating in its "Standard" Condition and With Airflow Only

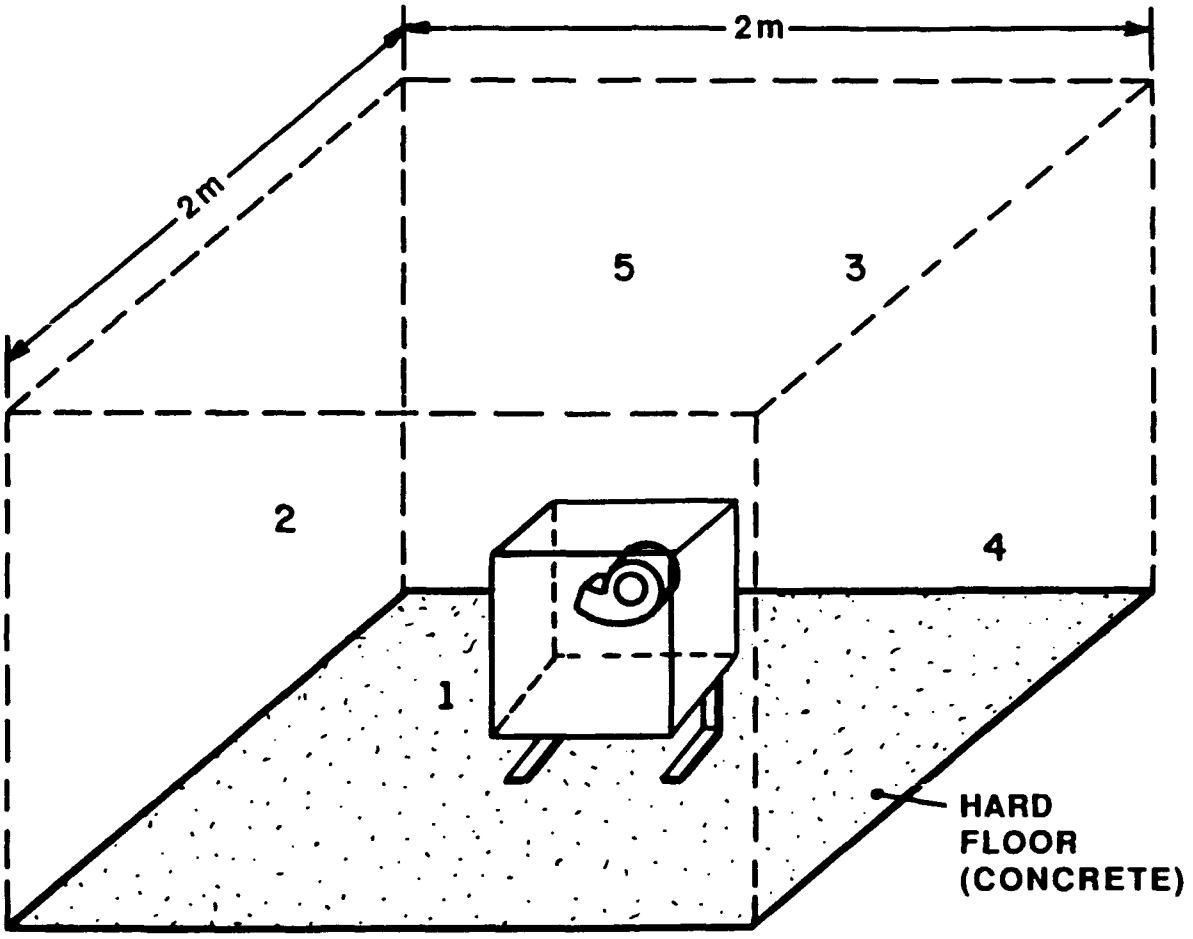

FIVE POINT POWER MEASUREMENT

INTENSITY MEASURED AT 5 PTS.

$\Delta S = 4\ M^2$

Figure 50. Measurement Positions Used in INCE Plenum Box Sound Power Measurements

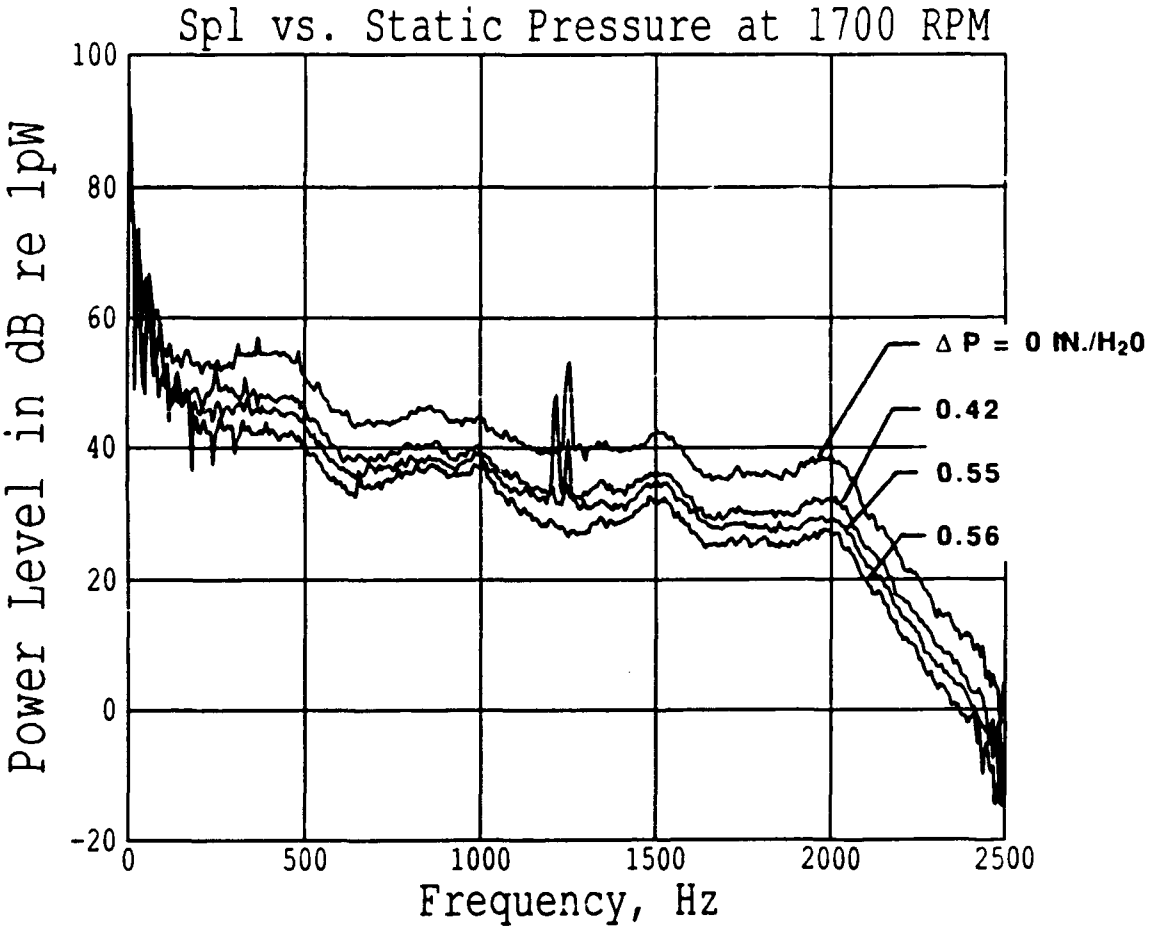

Figure 51. Sound Power Measurements of the Blower at 1700 RPM

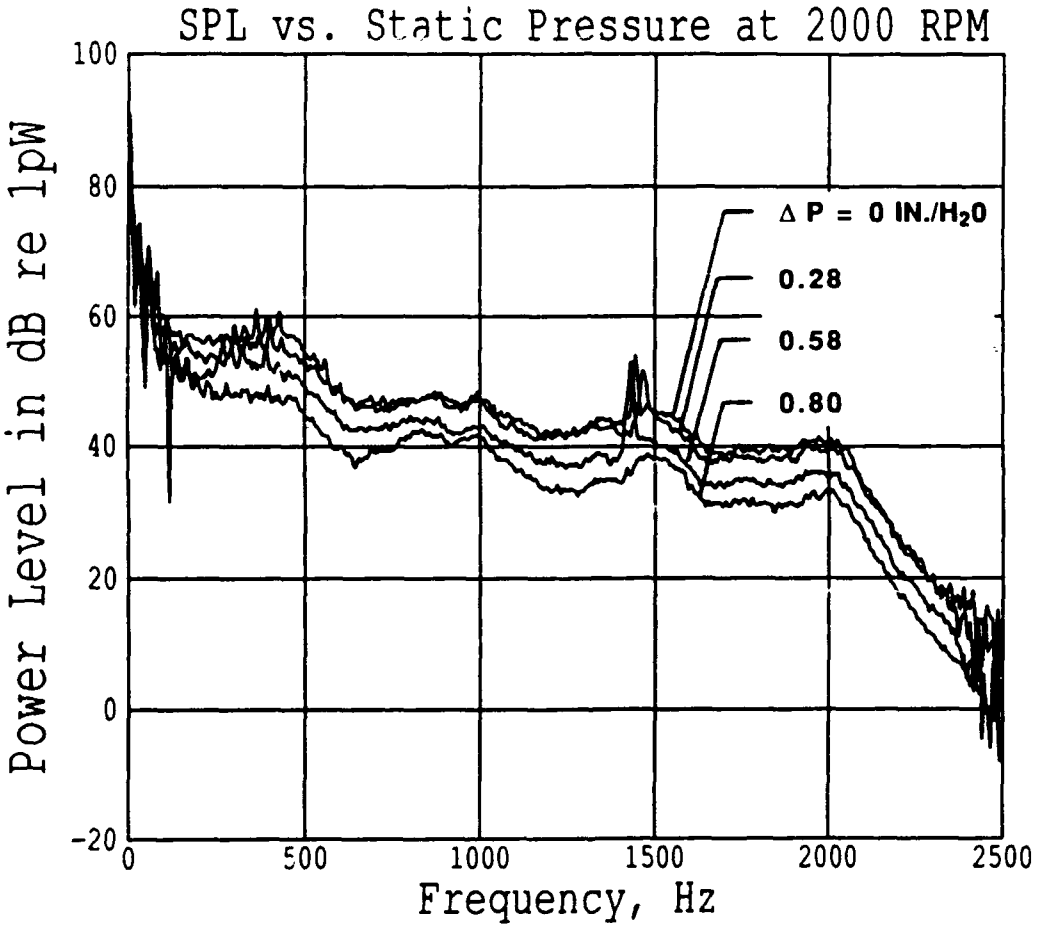

Figure 52. Sound Power Measurements of the Blower at 2000 RPM

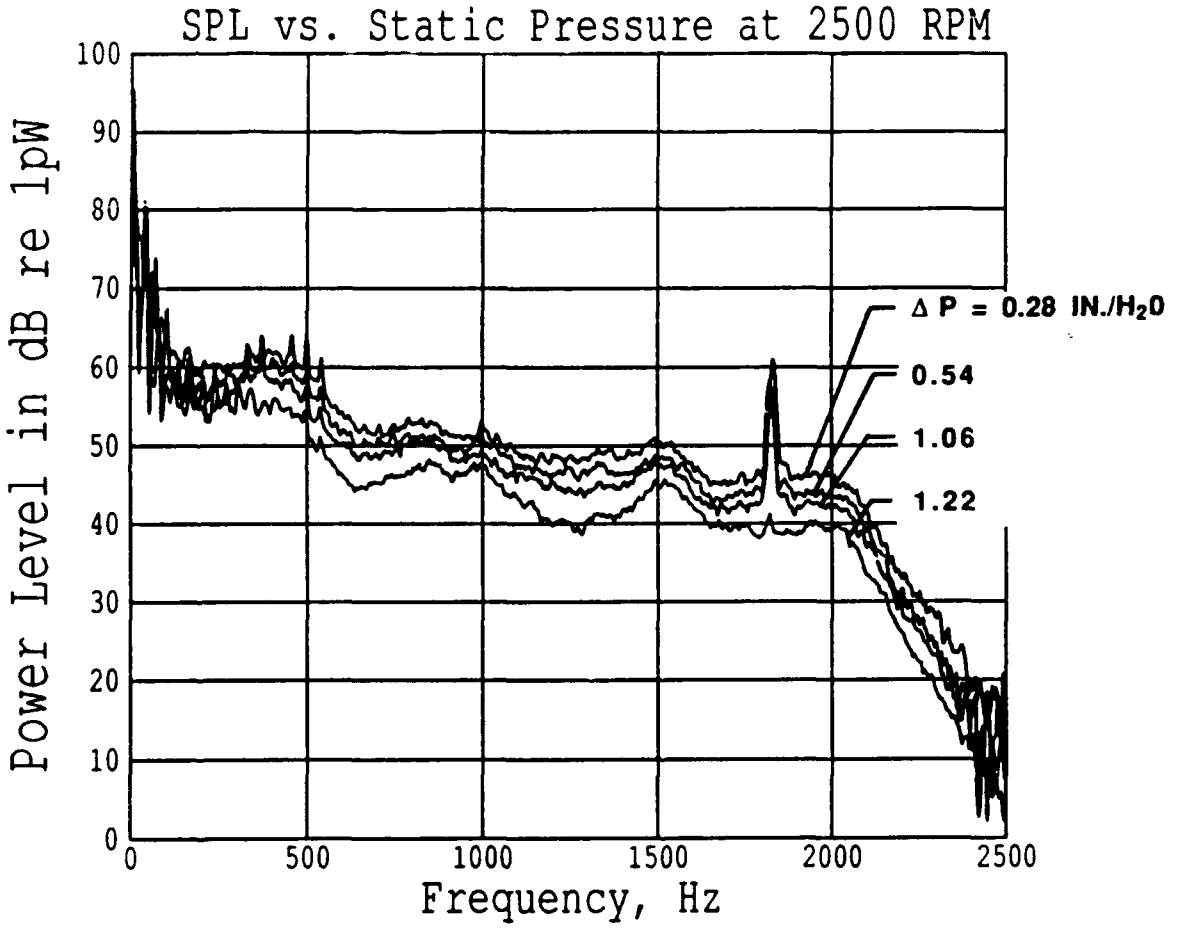

Figure 53. Sound Power Measurements of the Blower at 2500 RPM

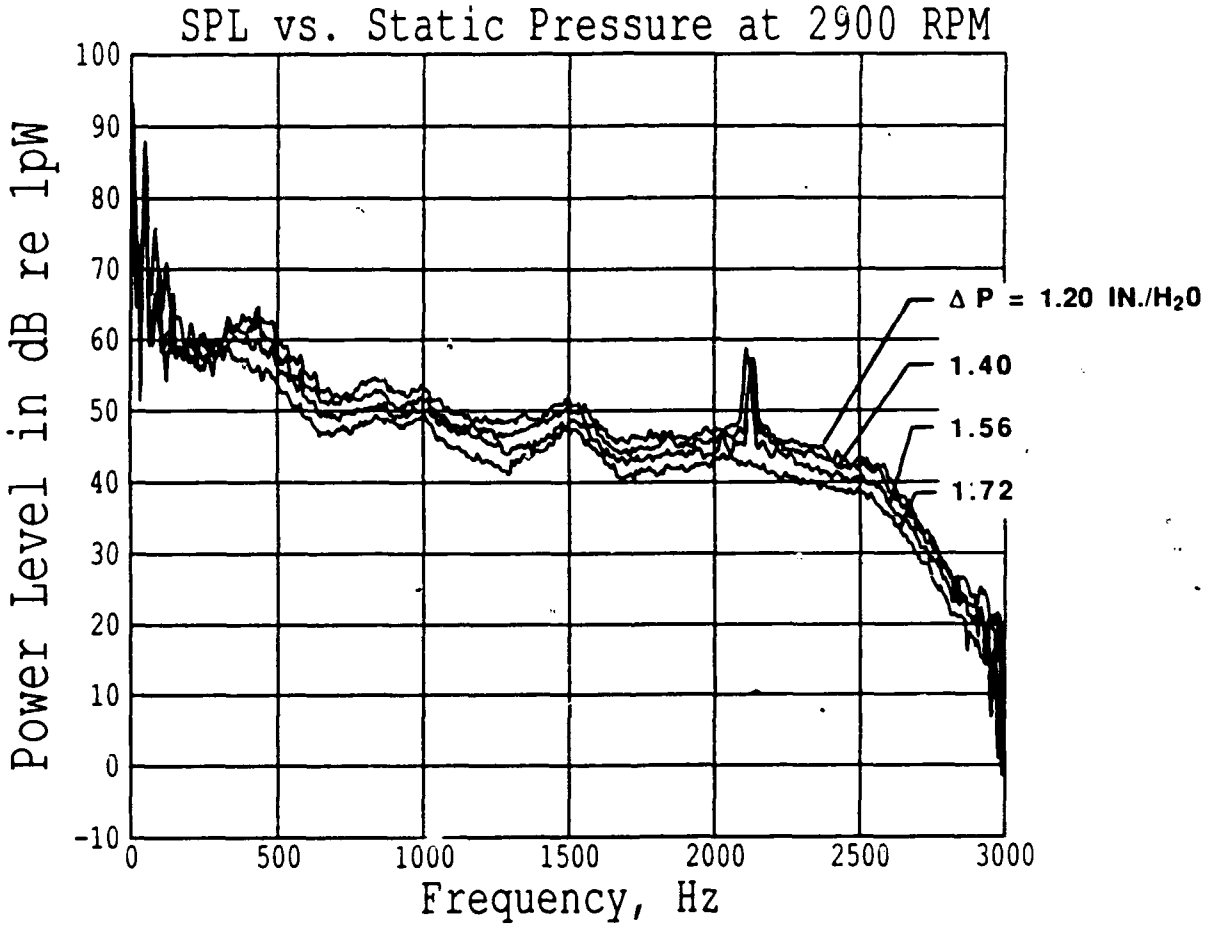

Figure 54. Sound Power Measurements of the Blower at 2900 RPM

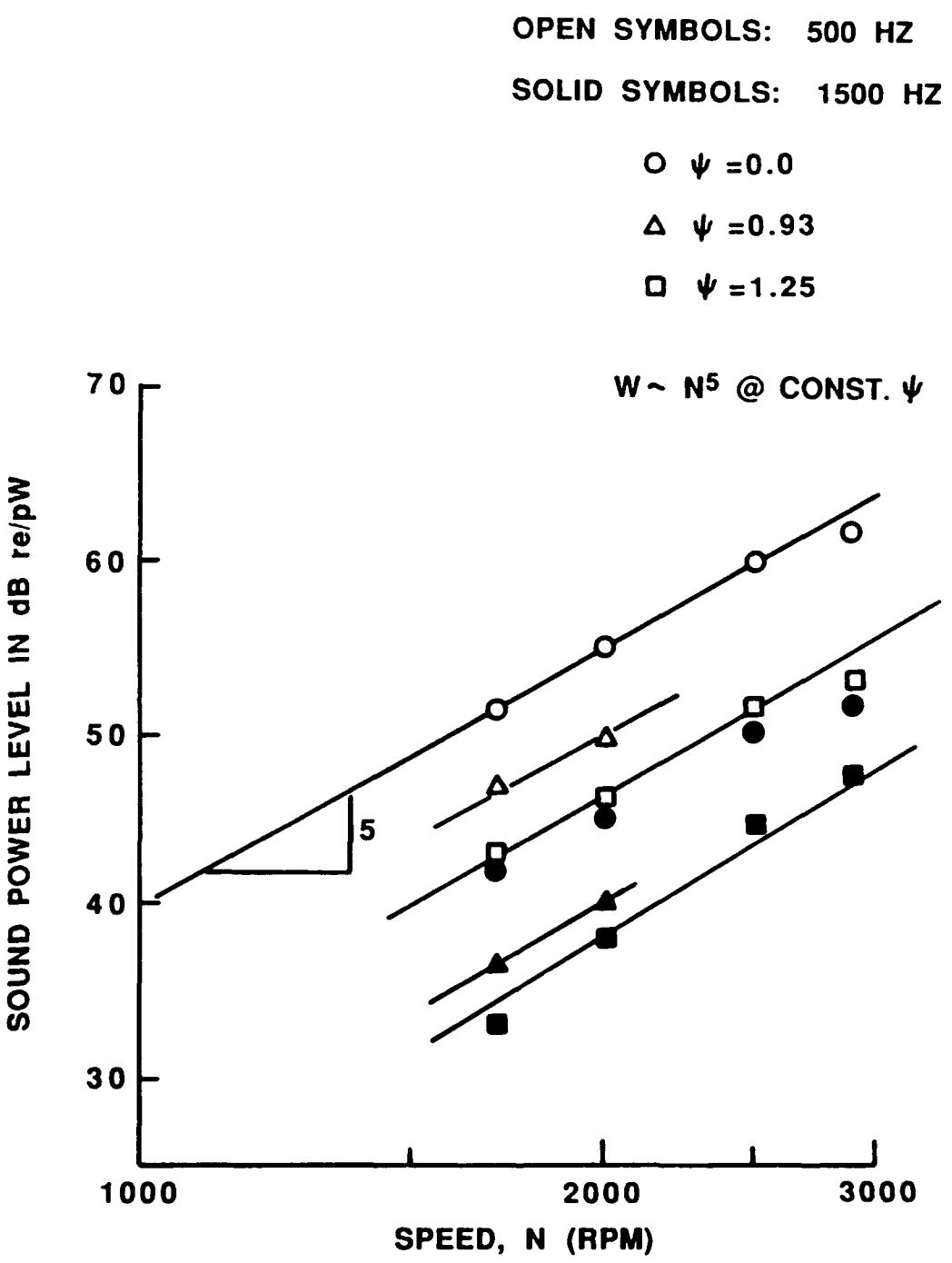

Figure 55. Sound Power Level as a Function of Wheel Speed at Constant Pressure Coefficient

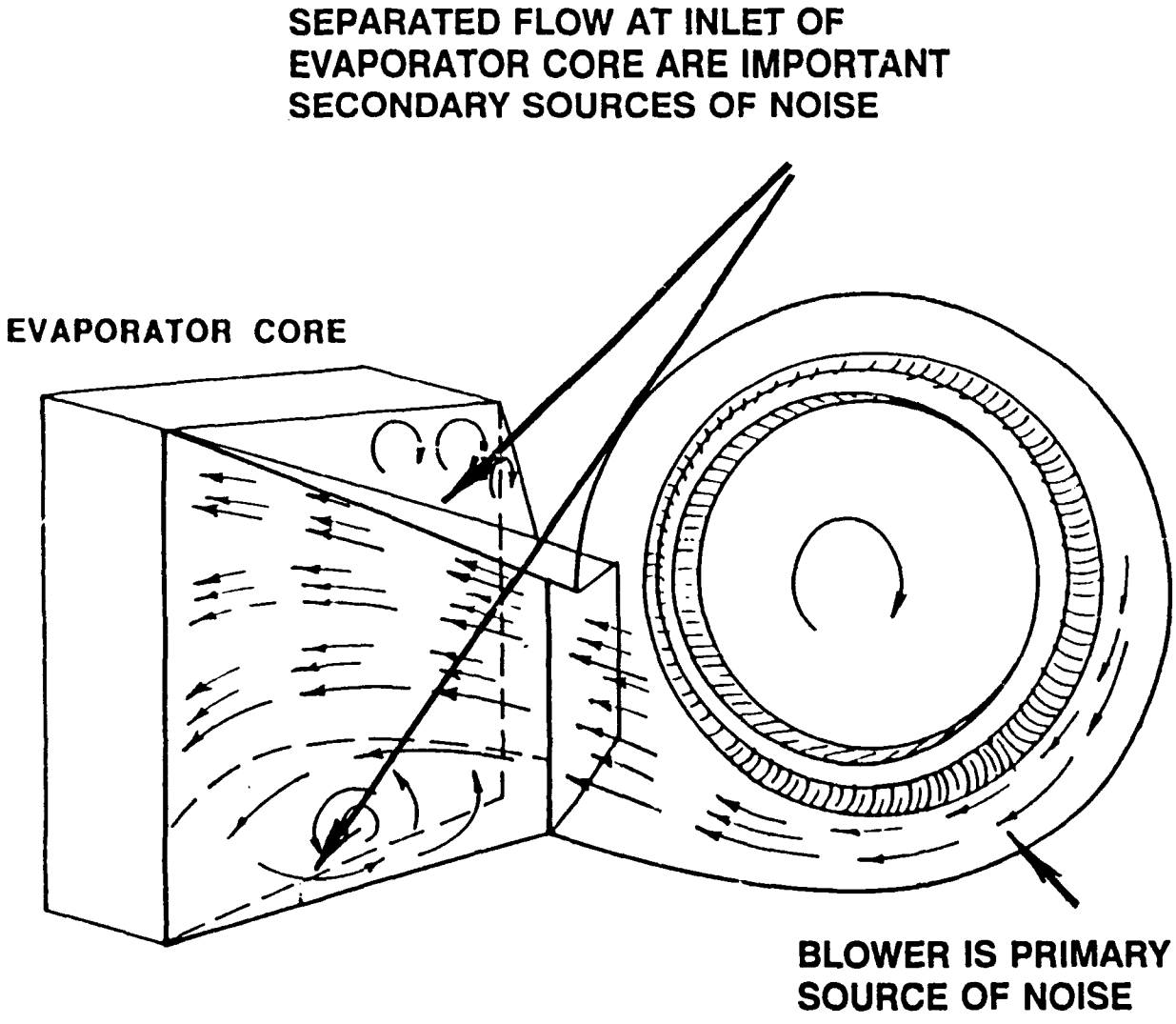

Figure 56. Flow Visualization in the Exit Region of the Blower

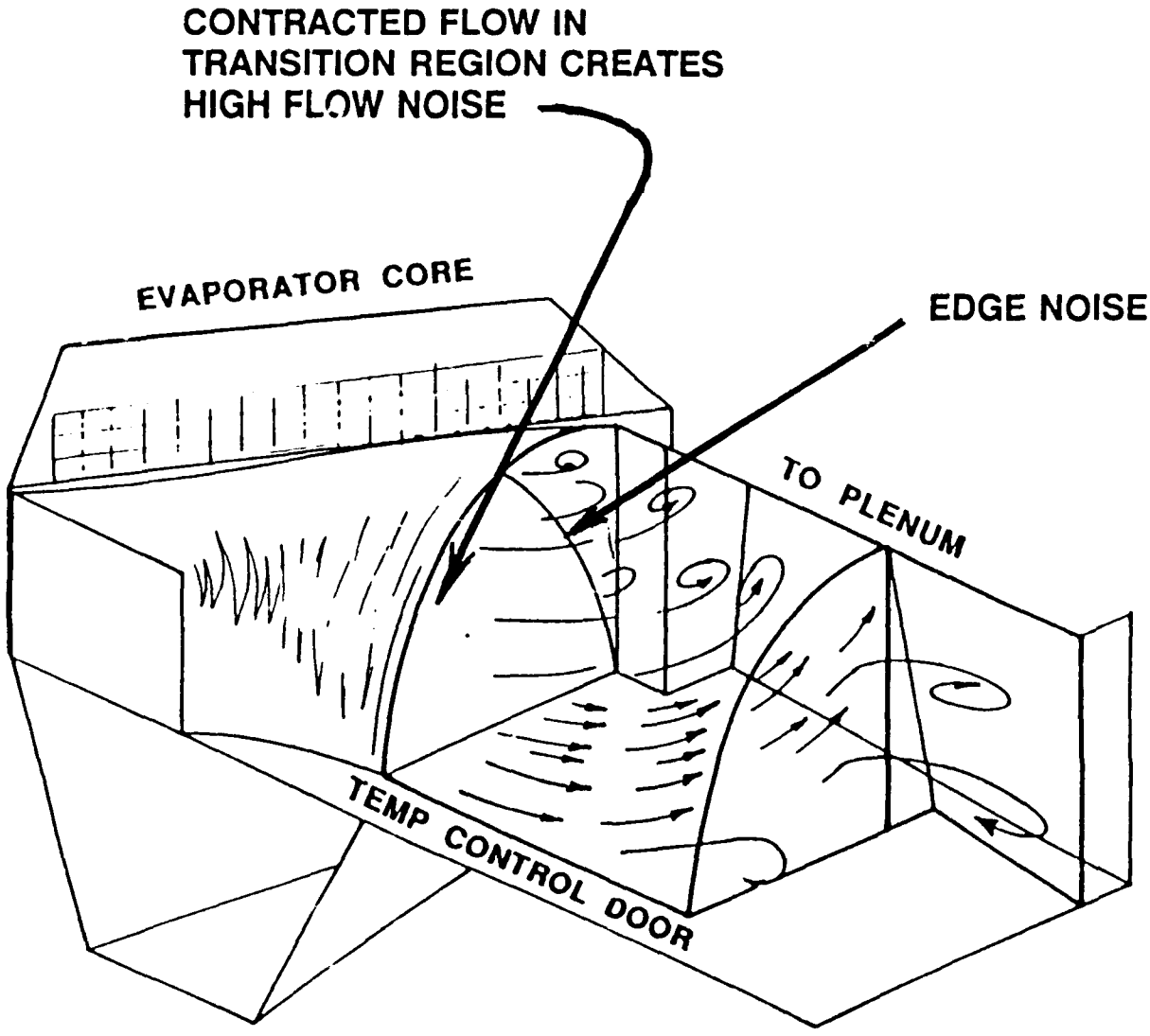

Figure 57. Flow Visualization in the Transition Region Between the Evaporator Core and Plenum Section

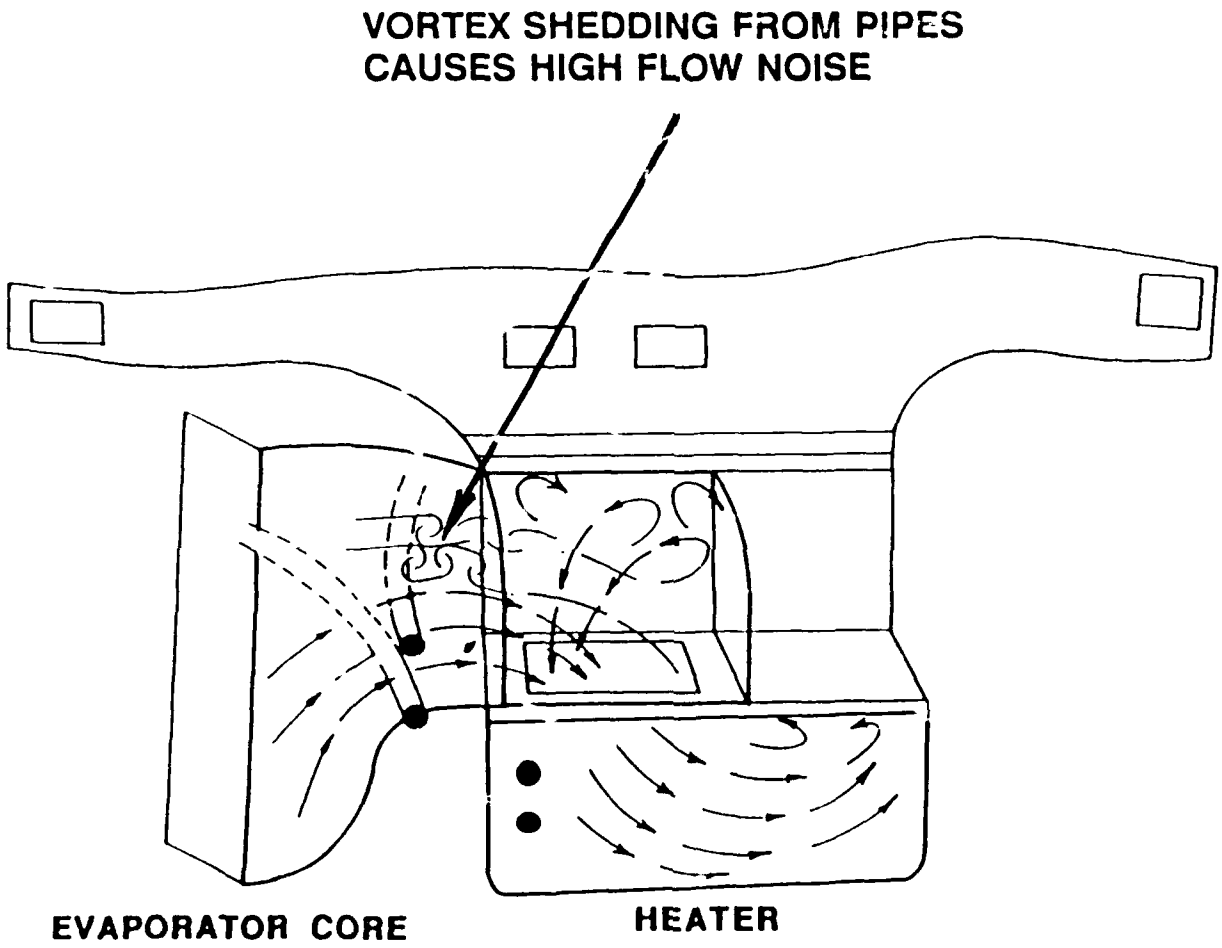

Figure 58. Flow Visualization Upstream of Heater Core and Distribution Ducts

APPENDIX 1

HVAC System Noise Reduction Using Resonators

Measurements of the sound power radiated by the HVAC system operating in its maximum AC condition showed a tone at the blade passage frequency (BPF) to be several dB above the surrounding broadband noise. The BPF tone is also one of the most irritating components of the overall spectrum and becomes increasingly noticeable as the total pressure rise across the blower is reduced. Therefore, if the system losses and wheel speed are decreased, the BPF tone may become an even more significant problem. Following Neise and Koopmann (1980), the use of a quarter-wavelength resonator to reduce the BPF noise was investigated. Figure 1.1 shows the concept employed. The body of the resonator was fabricated from sheet stainless steel and the piston was teflon. The perforated area at the scroll cutoff was very fine metal screen. The polypropylene throat on a production blower was cut out and replaced with the resonator. Tests were conducted in the INCE plenum box, but only the sound pressure level at a few spatial locations was measured. The results were found to be independent of microphone position. Shown in Figure 1.2 are typical experimental results for the blower operating under free-delivery conditions. The resonator was set (tuned) to cancel pure tone energy at 1460 Hz. The fan speed was varied such that the BPF occurs at frequencies both above and below this tuned frequency. The results show, quite dramatically, the effectiveness of the resonator. The tonal is reduced by up to 10 dB, almost to the point

where it is of the same level as the broadband noise. Further testing with the resonator has not been pursued because system losses must be reduced before such noise control devices warrant serious consideration.

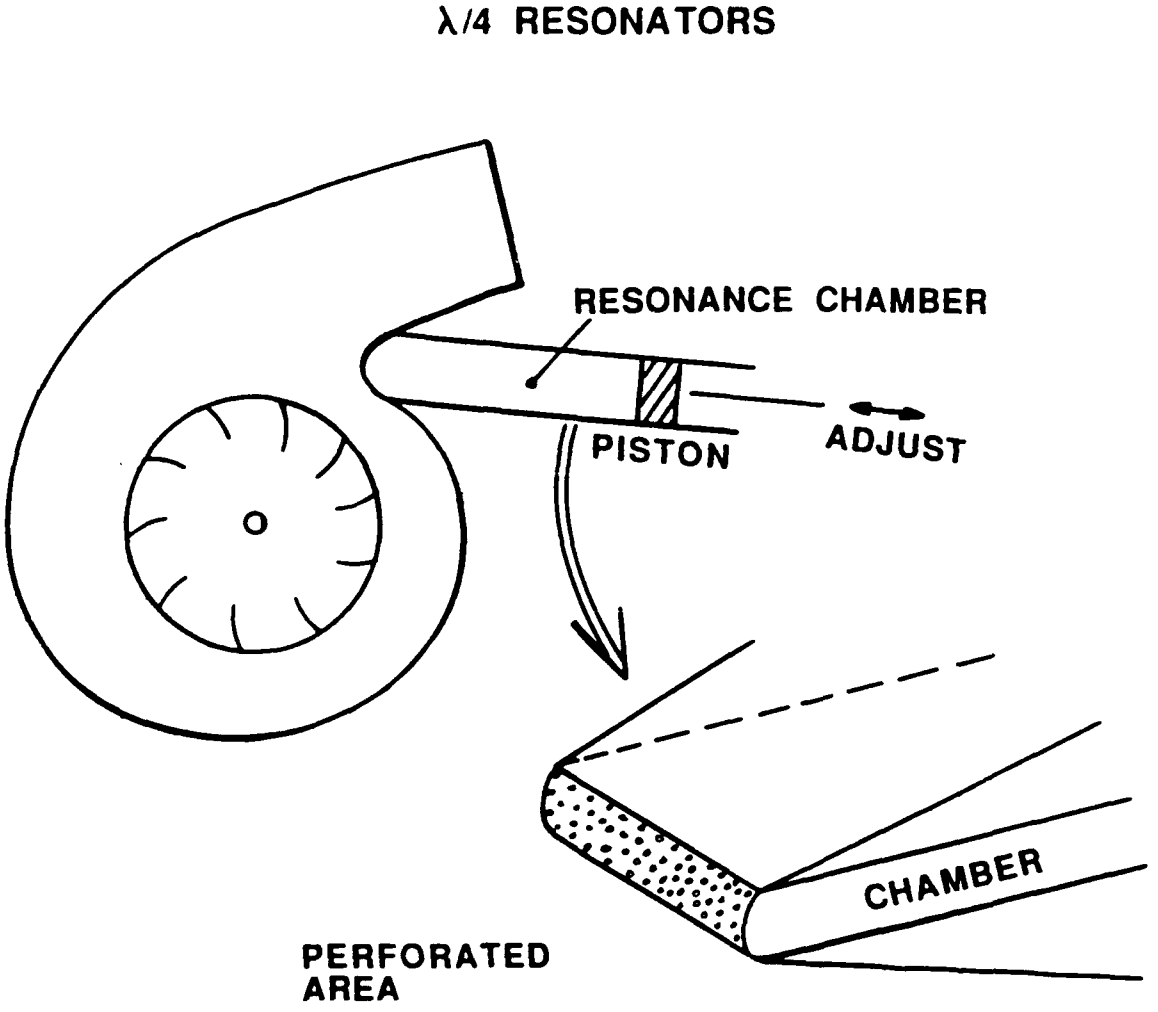

Figure 1.1 The 1/4 Wavelength Resonator Concept

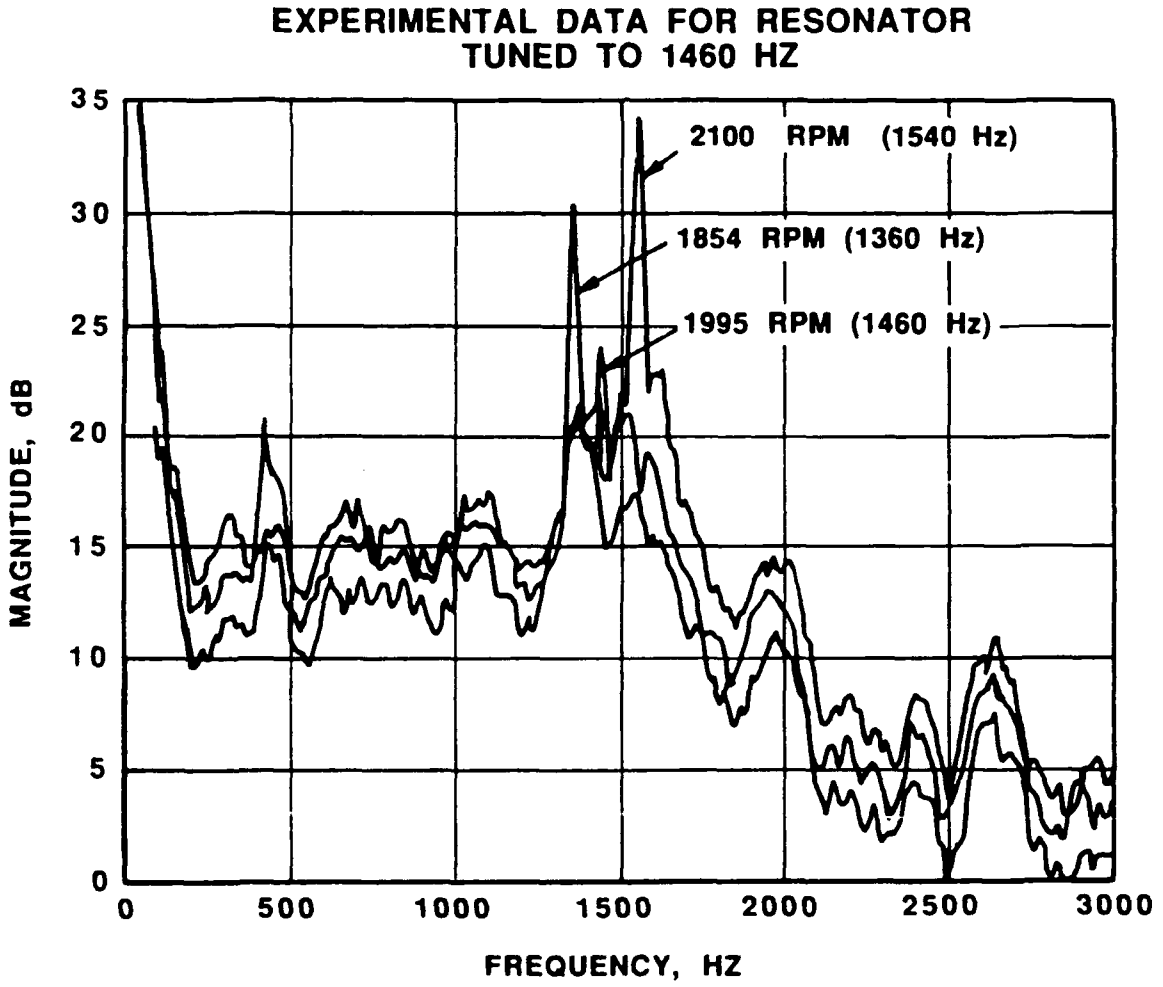

Figure 1.2 Experimental Data Showing the Effectiveness of the 1/4 Wavelength Resonator

APPENDIX 2

Register Noise

Acoustic intensity measurements performed in Plane 2 showed the HVAC system registers to be significant local sources of noise. Although their contribution to the total sound power radiated by the system is small, their proximity to the vehicle's occupants justifies giving them additional attention. A simple experiment was conducted which gives further insight into the noise generating mechanisms of registers. Noise measurements were performed on the HVAC system operating with all registers open, and with the middle two registers closed. Closing the middle two registers results in an approximate 40% decrease in the mass flow rate through the system and an approximate 20% increase in the flow velocity from the two remaining registers. Both the acoustic intensity and sound pressure level (SPL) were measured approximately 18 inches in front of the middle registers. The SPL measurements were performed in addition to the intensity measurements because of interest in frequencies higher than the 3 kHz limit of the intensity system and in order to help verify the results. Airflow equivalent to the throughput when operating in its maximum AC condition (when all vents are open) was supplied to the HVAC system through a dryer hose connected to the ARL Penn State quiet airflow facility.

Figure 2.1 shows relative intensity levels measured with all vents open and with the middle vents closed. Table 2.1 presents the SPL results. The SPL data show a 13 dB noise decrease at 125 Hz and a 5 dB noise increase at 8 kHz when the two middle vents are closed. When the middle vents are closed, the high-frequency noise radiated from the

outer vents increases very noticeably. This is interesting in that although the mass flow rate through the system decreases by approximately 40%; the higher frequency noise still increases. The velocity through the outer vents is increased under these conditions and a dipole source mechanism is known to exist at the trailing edges of the louvers. Such sources have a radiation efficiency that increases as the sixth power of velocity. Thus, the high-velocity airflow over the louvers appears to be an important noise source with the magnitude and location of spectral peaks dependent on the flow velocity. The louvers act as little airfoils in a high-velocity airflow and radiate sound from their trailing edges.

In order to help verify the register noise hypothesis, a 30 ft. section of dryer hose was connected to a blower located in an acoustically isolated box, and a stock register and insert (to hold the register) were placed on the exit end. Sound pressure level measurements were performed when the register directed the airflow straight out, and when the airflow was directed at a rather sharp angle (louvers set at approximately 45°). The airflow rate was approximately equal to that through a given register when the HVAC system is operated in its maximum AC condition. For comparison purposes, SPL measurements were also obtained for the noise emitted by the airflow exiting the hose without a register or insert present. The measurements were performed approximately 1 ft. to the side of the hose exit and are depicted schematically in Figure 2.2. The measurement results are summarized in Table 2.2 and show that, compared to the open jet, the louvers are very significant high-frequency noise sources, particularly when the airflow is directed at a sharp angle.

Table 2.1 Octave Band SPL for HVAC System with Air Supplied by an Auxiliary Quiet Airflow Source

Octave Band Frequency (kHz)	Measured SPL All Vents Open (dB re. 20 μPa)	Measured SPL Middle Vents Closed (dB re. 20 μPa)
0.125	65.0	52.0
0.250	62.8	57.5
0.500	60.2	57.2
1.000	58.3	58.0
2.000	56.4	57.7
4.000	55.8	58.3
8.000	53.3	58.3

Table 2.2 Octave Band SPL Measurements of Register Noise

Octave Band Frequency	Open Jet No Register	Register Louvers at 0°	Register Louvers at 45°
0.125	46.5	48.0	47.0
0.250	39.5	43.0	43.5
0.500	34.0	41.5	44.5
1.000	29.0	43.0	47.0
2.000	24.0	42.0	45.5
4.000	<20.0	40.0	44.0

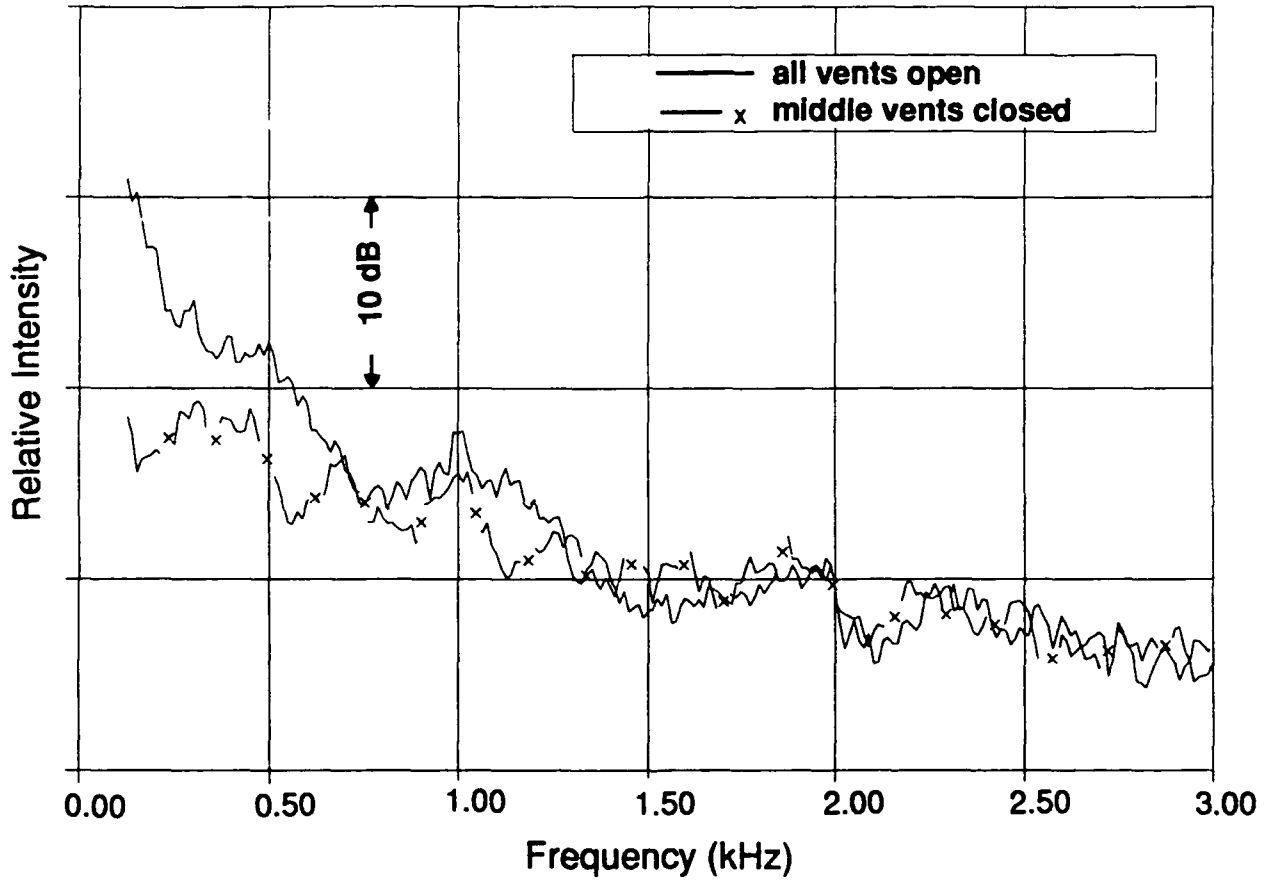

Figure 2.1 Relative Intensity Levels Measured With All Vents Open and With the Middle Vents Closed

BASELINE MEASUREMENT - OPEN JET, NO REGISTER OR INSERT

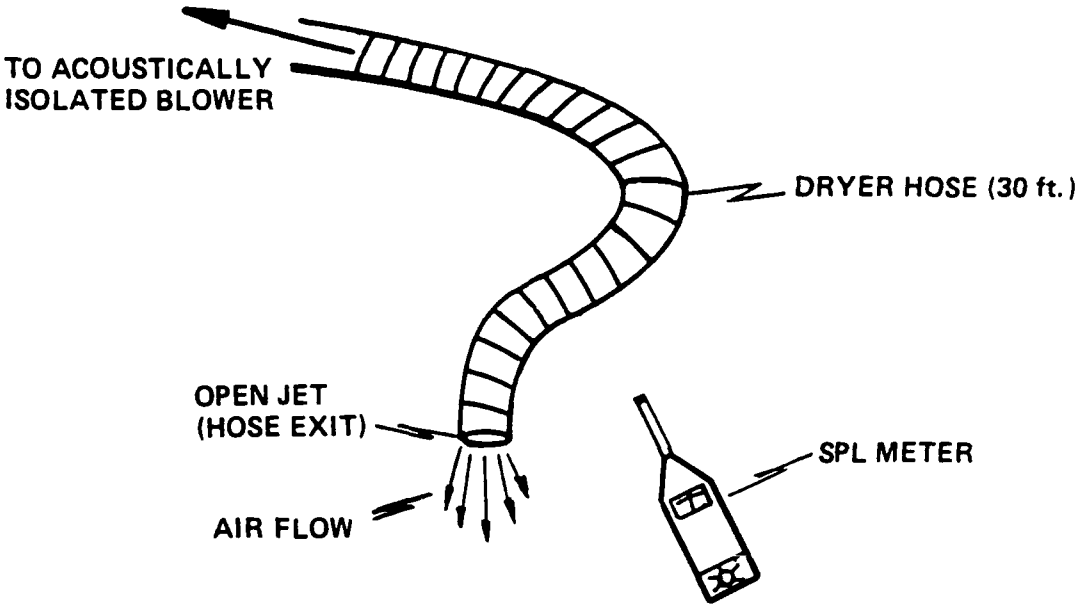

MEASUREMENT WITH REGISTER AND INSERT

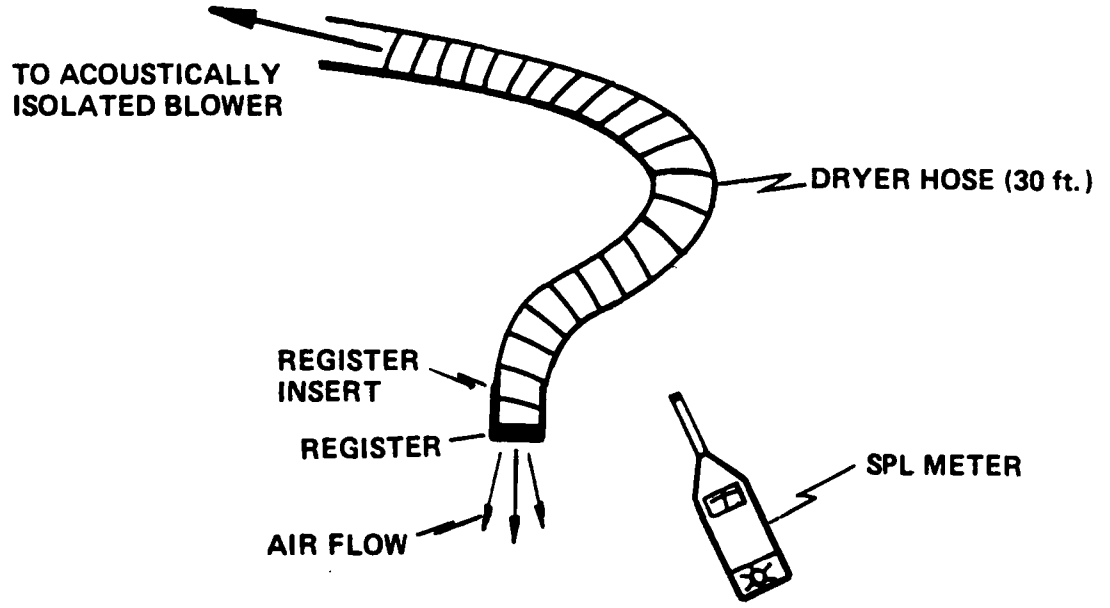

Figure 2.2 Schematic of the Register Noise Measurements